# D4.1 Classification of building materials, characterization of their main physical features and determination of their decay forms and products

| | |
|---|---|
| Deliverable number | D4.1 |
| Deliverable title | **Classification of building materials, characterization of their main physical features and determination of their decay forms and products** |
| Nature[1] | **R** |
| Dissemination Level [2] | **PU** |
| Author (email)<br>Institution | **Rebecca Piovesan (r.piovesan@iuav.it)**<br>**IUAV** |
| Editor (email)<br>Institution | **Fabrizio Antonelli (fabrizio.antonelli@iuav.it)**<br>**IUAV** |
| Leading partner | **IUAV** |
| Participating partners | **IUAV – UNIPD – UGR – OSLOMET** |
| Official submission date: | **31/05/2021** |
| Actual submission date: | |

[1] **R**=Document, report; **DEM**=Demonstrator, pilot, prototype; **DEC**=website, patent fillings, videos, etc.; **OTHER**=other

[2] **PU**=Public, **CO**=Confidential, only for members of the consortium (including the Commission Services), **CI**=Classified, as referred to in Commission Decision 2001/844/EC

## Modifications Index

| Date | Version |
|---|---|
| 03/05/2021 | 0.1 First draft |
| 12/05/2021 | 0.2 First draft verified by IUAV |
| 26/05/2021 | 0.3 First draft verified by WP leader |
| 24/06/2021 | 0.4 Input of the main contents from IUAV, UNIPD and UGR |
| 28/06/2021 | 0.5 Input of the main contents from all partners |
| 30/06/2021 | 0.6 Final version |

This work is a part of the HYPERION project. HYPERION has received funding from the European Union's Horizon 2020 research and innovation programme under grant agreement no 821054.

Content reflects only the authors' view and European Commission is not responsible for any use that may be made of the information it contains.

# ACRONYMS AND ABBREVIATIONS

| | |
|---|---|
| BL | Botticino Limestone |
| CC | Climate Change |
| CH | Cultural Heritage |
| CM | Carrara Marble |
| CoA | Colorimetric analysis |
| CS | Costozza Stone |
| d-HAM | dynamic- Heat Air and Moisture |
| EDS | Energy-dispersive X-ray spectroscopy |
| ETr | Euganean Hills Trachyte |
| FTIR | Fourier Transform Infrared Spectroscopy |
| GSP | Granada Santa Pudia Limestone |
| IC | Ion Chromatography analysis |
| IS | Istrian Stone |
| LS | Lartios Stone |
| MIP | Mercury Intrusion Porosimetry |
| MM | Macael Marble |
| OM | Optical microscopy |
| PLOM | Polarized-light optical microscopy |
| RLM | Reflected light microscopy |
| RV | Red Verona Limestone |
| SEM | Scanning Electron Microscopy |
| SS | Sfouggaria Stone |
| TDI | Total Decay Index |
| TLM | Transmitted light microscopy |
| TRh | Tønsberg Latite |
| TSy | Tønsberg Monzonite/ Tønsbergite |
| WP | Work Package |
| XRPD | X-Ray Powder Diffraction |

# Table of Contents

# Table of Figures

# Table of Tables

# Executive Summary

The deliverable D4.1 entitled as "**Classification of building materials, characterization of their main physical features and determination of their decay forms and products**", reports on the results obtained in task 4.1 "Identification, classification and characterization of the building materials and their d-HAM properties" during the first two years of the project.

This deliverable contains information about the building materials, their deterioration pattern and the decay products. Data derive from: i) on-site investigation performed on the Tier 1 buildings in Venice, Rhodes, Granada, and Tønsberg; ii) analyses performed in laboratory on a set of samples collected directly from the Venetian Tier 1; iii) analyses performed in laboratory on 12 rock types selected as representative of the building and decorative stones historically used in Venice, Rhodes, Granada, and Tønsberg as well as on two wood types widely used in Tønsberg.

Tier 1 of the various cities underwent different characterization protocols, since travel limitations due to the sanitary contingencies prevented on-site survey on those monuments composed of stone and lithoid materials by UNIPD and IUAV teams. For this reason, a complete characterization approach was performed only for Tier 1 in Venice and in Tønsberg, the latter formed mainly of wood and analyzed by OSLOMET. For Tier 1 in Granada and Rhodes, which show only one type of building stone, the decay was evaluated on some representative portions of the constructions based on photographs, photogrammetric and laser scanner survey, therefore according to a remote-based work.

All the high-resolution map files are stored in the Dataset_D4.1.zip file.

# 1. Introduction

## 1.1. Background

The deliverable D4.1 "**Classification of building materials, characterization of their main physical features and determination of their decay forms and products**" is an important document reporting all data acquired through the characterization of the materials constituting the Tier 1 of the various sites, as well as natural materials (stones and wood) representing the main varieties locally used, although not necessarily constituting the Tier 1 buildings. Materials were selected in such a way to comprise a wide range of petrographic and/or textural features, which eventually control the response of the material to environmental forcing. The idea was to provide constraints on materials vulnerability, which could be applied also to materials other than those here considered. The deliverable arises from an intense debate on the most suitable stone and timber materials to be tested, and an accurate on-site survey to define the sampling strategy in order to characterize the building materials and their deterioration products. Due to travel limitation for the sanitary contingencies, this was possible only for Venice and Tønsberg Tier 1 buildings.

All the information here reported will be stored in the HRAP system.

## 1.2. Purpose of the document

This deliverable is aimed to provide the significant petrographic, and chemical properties of the studied building materials as well as to describe and characterize their typical deterioration patterns and products.

The data produced will be also used to evaluate the effect of micro-climate conditions on deterioration of the different building materials and to quantify their surface recession rate.

## 1.3. Position in the HYPERION Ecosystem

The HYPERION high-level logical architecture is presented in Figure 1, as defined in Deliverable D2.3 "Architecture Specification". The yellow rectangle shows the position of the WP4 in the HYPERION Ecosystem. The data on classification and characterization of the building materials as results of Task 4.1 will implement the integrated HT simulator and the HRAP system.

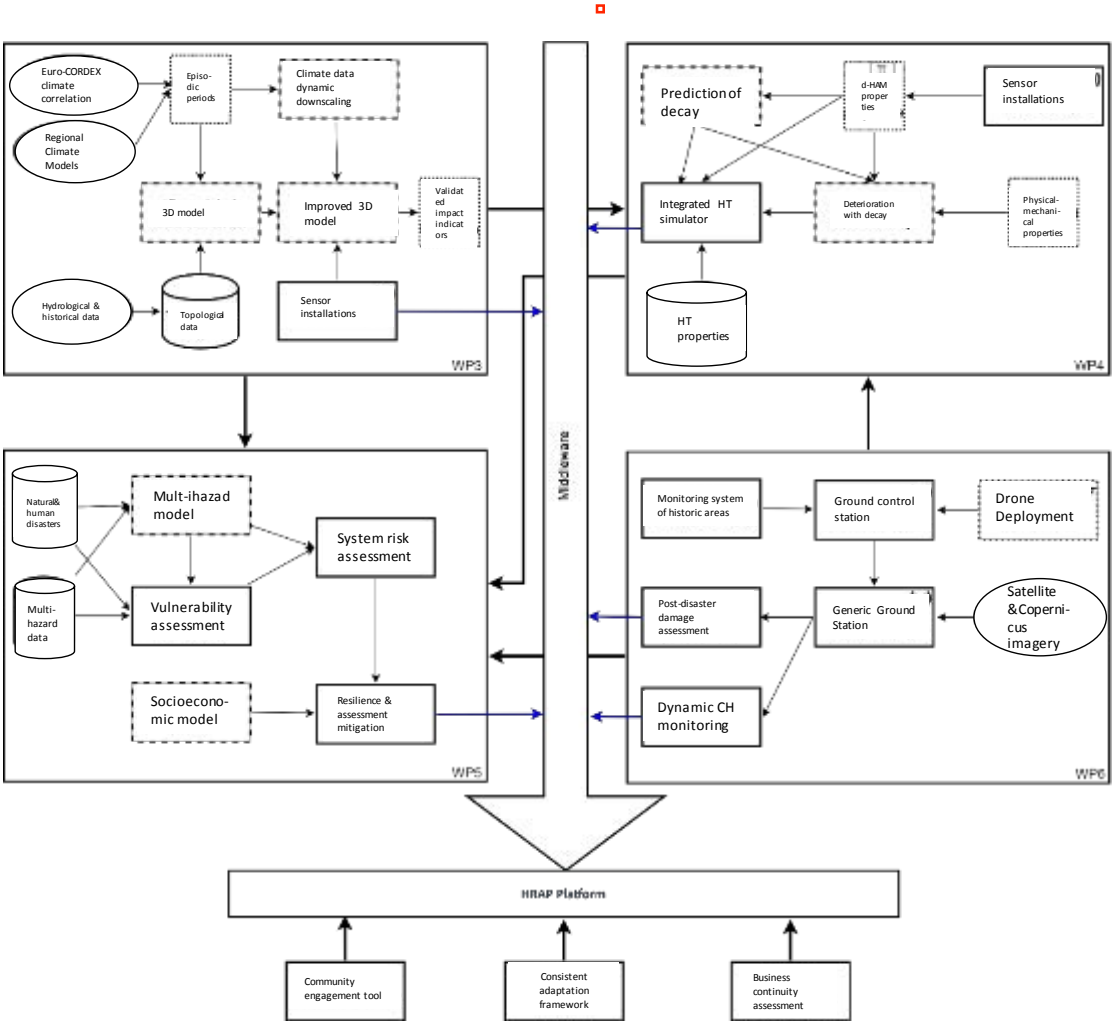


Figure 1: Position of the WP4 within the HYPERION Ecosystem

# 2. Approach

## 2.1. Sampling approach

### 2.1.1. Stones

#### *Rock types selected for laboratory tests*

For the experimental studies, two rock types from the region of each Pilot Sites were selected, with the exception of Venice for which, due to the well-known richness of this city in terms of "ancient marbles" (*sensu lato*, in architectural terms, comprising all rock types that can be polished, used in antiquity), six different stones (magmatic, metamorphic and sedimentary) were chosen. The twelve stones selected for laboratory tests considered for this study are listed in Table 1.

Table 1: List of the rock types selected for laboratory tests

| Provenience | | Lithology | Label | Petrographic group | Main composition |
|---|---|---|---|---|---|
| Norway | Tønsberg | **Monzonite/ Tønsbergite** | TSy | Magmatic, intrusive | Silicatic |

| | | | | | |
|---|---|---|---|---|---|
| | Tønsberg | **Latite** | TRh | Magmatic, effusive | Silicatic |
| Spain | Macael | **Macael Marble** | MM | Metamorphic - Marble | Carbonatic |
| | Granada | **Santa Pudia Limestone** | GSP | Sedimentary - Limestone | Carbonatic |
| Rhodes | Rhodes | **Sfouggaria Stone** | SS | Sedimentary - Limestone | Carbonatic |
| | Lardos | **Lartios Stone** | LS | Sedimentary - sandstone | Carbonatic and silicatic |
| Italy | Botticino (Brescia) | **Botticino Limestone** | BL | Sedimentary - Limestone | Carbonatic |
| | Carrara (Massa Carrara) | **Carrara Marble** | CM | Metamorphic - Marble | Carbonatic |
| | Verona | **Red Verona Limestone** | RV | Sedimentary - Limestone | Carbonatic |
| | Costozza (Vicenza) | **Costozza Stone** | CS | Sedimentary - Limestone | Carbonatic |
| | Euganean Hills (Padova) | **Trachyte** | ETr | Magmatic, effusive | Silicatic |
| Croatia | Istrian peninsula | **Istrian Stone** | IS | Sedimentary - Limestone | Carbonatic |

For every rock type a sets of 20 cubes (5x5x5 cm), 30 slabs (7x7x2 cm), and 12 cylinders (length: 7 cm; diameter: 4 cm) were produced. The majority of the samples were used in ageing tests and physical-mechanical analyses pertaining to Tasks 4.2 and 4.3; a cube and a slab for each sample were addressed to petrographic studies.

### *Samples collected in-situ*

Thirty micro-samples of original stones were collected in-situ from the Clock Tower of Venice after approval of the sampling plan by the *Soprintendenza Archeologia, belle arti e paesaggio per il Comune di Venezia e Laguna.* The sampling was performed following these guiding lines:

A. maximize the variability of the sampled rock types and deterioration products;
B. preserve the macroscopic appearance of the element/artifact avoiding the damage of the sound surfaces;
C. restrict sampling operations to already damaged surfaces;
D. adjust the sample size to the needs of the planed analyses.

On these samples, petrographic, chemical and biological analyses were performed in order to correctly classify and characterize both the lithology and the deterioration products. The list of the samples and their positions on the building is reported in Annex 1A.

## 2.1.2. Bricks

### *The Santa Maria dei Servi Church (Venice)_Tier 2 building*

The Church of Santa Maria dei Servi (XIV century) was selected as Tier 2 building in Venice (Figure 2) in order to study the differential material loss in relation to the properties of the bricks. Bricks, indeed, being artificial materials have high variability in aesthetic qualities and intrinsic properties depending by the firing process adopted (in particular the reached temperature) and the raw materials used.

Figure 2: Photos of Santa Maria dei Servi façade in Venice

### *On-site sample collection*

Twenty-three samples were collected from the main façade (ANNEX 1B). Samples were collected (Figure 3) for performing the petrographic characterisation (XRPD, POM, SEM-BSE and hyperspectral analysis).


Figure 3: Samples collection on the main façade

### *Commercial bricks*

Commercial bricks (GP, RSS, RS and R6) used in restoration of historic building constructions were analyzed in order to assess their petro-chemical and aesthetical compatibility with the historic venetian brick masonries. These bricks are produced by a traditional molding method and fired at the temperatures reported in Table 2.

Table 2: List of samples of commercial bricks

| Label | Firing temperature (ºC) | Sample image |
|---|---|---|
| **GP** | 1050 |  |
| **RSS** | 950 | 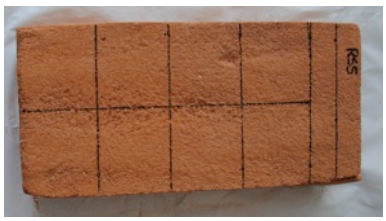 |
| **R6** | 600 |  |
| **RS** | 980 |  |

## 2.1.3. Timber

The Fadum storehouse, the Heierstad loft, the residential building Bentegården and the ruins of the Western Tower were selected as Tier 1 buildings in Tønsberg, Norway. The first three are timber buildings. The focus was to select proper material properties for the first two buildings and to investigate the fungal colonization on them. Regarding the wood species, no differences are expected for the building of Bentegården compared to the Fadum storehouse and Heierstad loft. The building elements of the examined constructions are made of different types of timber and have a different age. For that reason, the building components were grouped into homogeneous categories (Figure 4). The Fadum storehouse and the ground level of the Heierstad loft -highlighted with different shades of brown in Figure 4- are made of Norway Spruce (*Picea abies*), while the upper level of the Heierstad loft -highlighted with orange color in Figure 4- is made of Scotch pine (*Pinus sylvestris*) [1].

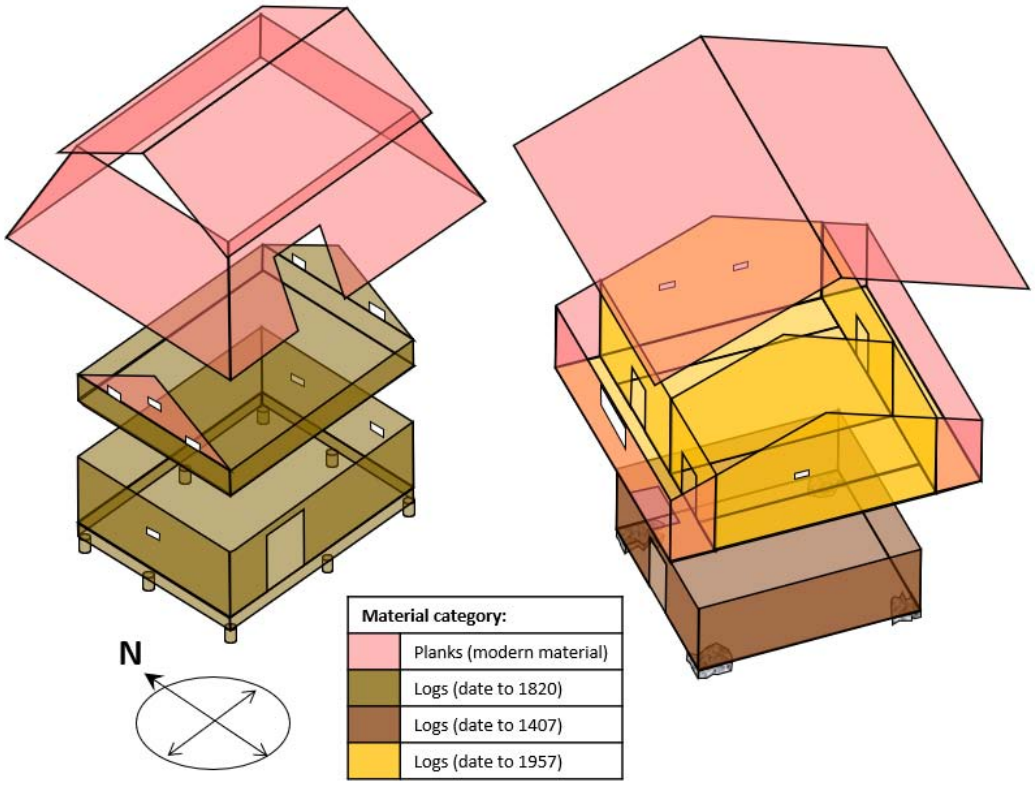


Figure 4: The building components have been grouped in four homogeneous categories, highlighted with different colors, based on the type and age of wood that they are made of

## 2.2. Analytical approach

Various features were analyzed in order to characterize both the compositional and physical properties of the materials and their deterioration patterns and products, using a multi-analytical approach. In the case of materials from historical buildings, non-invasive analyses were initially carried out through mapping both the building and decorative materials employed and deterioration patterns, as macroscopically detected. Only few micro-samples were then collected to verify the macroscopic identification of building materials and their deterioration products.

### 2.2.1. Stones, bricks and their deterioration products

For the study and the characterization of both stones and their deterioration products, the following analytical approach and instrumentations were adopted.

#### *Polarized-light optical microscopy (PLOM)*

The petrographic and textural characteristics of thin sections were examined under a polarized-light optical microscope. Samples were prepared as 30 μm-thick thin sections.

#### *Optical microscopy (OM)*

Biological colonization was observed using an optical microscope. In order to identify and discern the different (micro)organisms, fresh slides were prepared [2].

### *X-Ray powder diffraction (XRPD)*

Mineralogical analyses were performed on samples prepared as fine-grained powder in a hand mortar by X-ray powder diffraction using a:

- Panalytical Empyrean diffractometer, for the stone samples,
- and a X'Pert PRO diffractometer, for the brick samples,

both operating in Bragg-Brentano reflection geometry equipped with CuKα radiation (operating at 40 kV and 40 mA) and an X'Celerator detector.

Qualitative analysis of diffraction data was carried out with X'Pert HighScore Plus® software (PANalytical) and the PDF-2 database.

### *Scanning Electron Microscopy and energy-dispersive X-ray spectroscopy*

Micro-morphological and textural investigations were done using a:

- ZEISS EVO15 scanning electron microscope (SEM) equipped with a $LaB_6$ cathode coupled with an X Flash 6160 BRUKER energy-dispersive X-ray spectroscopy (EDS) system, for the Clock Tower samples.
- CamScan MX-2500 microscope, coupled with an EDS Sapphire Si(Li) detector (LEAP+Si(Li) crystal), equipped with a $LaB_6$ cathode, for the brick samples.

Samples were prepared as polished thick stratigraphic cross-sections or studied as such after been gold or graphite-coated.

### *Fourier-transform infrared spectroscopy (μFTIR)*

Organic compounds identification was performed by the mean of a ThermoFisher Scientific iN10 Infrared Microscope. A little amount of powder was sampled from the stone surface, using a needle, deposited and pressed on a standard KBr pellet, then analyzed in transmittance mode.

### *Chromatography analysis (IC)*

Chemical analyses of the main ions couponing salts were performed by the mean of a ThermoFisher Scientific Dionex Aquion Ion Chromatography System. Samples were prepared as fine-grained powder, weighed, dispersed in pure water and the solutions analyzed after filtration. Standards were also analyzed to verify the accuracy of the results.

### *Spectrophotometry Colorimetric analysis (CoA)*

Color measurements were made in the CIEL*a*b* color space, where L* is the lightness (positive and negative values), while a* and b* are the chromaticity coordinates (the red-green and the yellow-blue direction, respectively). Color data were acquired, on the stones for laboratory tests, with a CM-2600d Konica Minolta portable spectrophotometer with a D65 illuminant and 10° standard observer. To maximize the statistical data an average of 10 points with 3 scans each was acquired for each sample. On the dried and wet fired bricks it was assayed on a 3nh spectrophotometer.

### 2.2.2. Timber

Fungal growth was detected on some building components of the Fadum storehouse and the Heierstad loft and, thus, it was decided to examine it thoroughly. Fungal colonization, both in aerosol and on the surface of the building elements, was investigated. Active sampling was performed outdoors, in the ground, and in the upper level of the two buildings in order to detect fungal cells and spores. A portable Surface Air System (SAS) sampler with a flow rate of 180 L/min was used for active sampling. In all sampling positions, both malt and dichloran glycerol (DG-18 without hyphen) agar were used as the growth media in the plates. The fungal colonies were counted three days after the sample collection and the fungal identification took place ten days after the sample collection. Regarding the fungal colonies on the building material surfaces, samples were collected in malt agar plates by using a pocketknife and the fungal species on them were identified in the laboratory ten days later. The morphology of fungi isolated colonies was observed by an optical microscope. In particular, conidiophores and conidia fungal structures were examined after methylene blue staining.

## 2.3. Mapping approach

The distribution maps of both the rock types and deterioration products (the latter represented in function of their intensity) were produced according to the following protocol:

A. Execution of the technical drawing of the building, reporting in details every single element and architectural structure;
B. First draft of the maps based on the analysis of high-resolution images of the building;
C. On-site survey of the building for the production of detailed maps of all the building and decorative materials and deterioration morphologies;
D. Sampling and analysis of the most representative materials and deterioration products;
E. Revision of the detailed maps on the basis of both the results of the analytical investigations performed on the micro-samples of the *in situ* original materials and on-site mapping.

Each step of this protocol adopted for the pilot sites is reported as follows:

#### *Venice*

The complete protocol from step A to E were adopted only on the Venice Tier 1 building, the Clock Tower, which acts as standard model for the Hyperion Approach.

#### *Rhodes*

Step A and B were performed on portions of the Naillac Pier and the St. Nikolaos Fort representing two of the Tier 1 buildings of Rhodes, the same portions were investigated also by WP6 by photogrammetric and hyperspectral surveys.

*Granada*

A probabilistic Bayesian method is proposed [3] to identify the most plausible degradation pattern using photogrammetry data. The methodology is applied to the San Jerónimo Monastery, a CH Tier 1 building in Granada (Spain), and in the CH Puerta Elvira in Granada (Spain), classified as Tier 2 in the Hyperion Project.

*Tønsberg*

Instead of steps A, B and C, a 3-dimenssional representation of the two case studies was produced by leveraging data from laser scanning and on-site surveys. The focus was to depict the geometry of the building without reporting in detail every single element and architectural structure. Step D was also followed.

# 3. Characterization and mapping of building materials

## 3.1. Stones

### 3.1.1. Selected Stones for laboratory tests

#### *Minero-petrographic classification*

**Monzonite/Tønsbergite (TSy)**

Figure 5: Cubic specimen of the Monzonite TSy

*Texture*: phanerocrystalline, coarse-grained, holocrystalline, equigranular, hypidiomorphic. There are myrmekites and perthites.

*Components:*

Table 3: Rock-forming minerals listed in order of their relative abundance in the Monzonite TSy

| Essential minerals (in descending order of abundance) | Accessory minerals | Secondary minerals |
|---|---|---|

| | | |
|---|---|---|
| Plagioclase (oligoclase) | Opaque minerals | Kaolinite |
| K-feldspar (orthoclase) | Hematite | Sericite |
| Biotite | Apatite | |
| Clinopyroxene | Calcite | |
| Quartz | | |

*Rock classification* [4]*:* Monzonite

*Origin:* Tønsberg – Norway

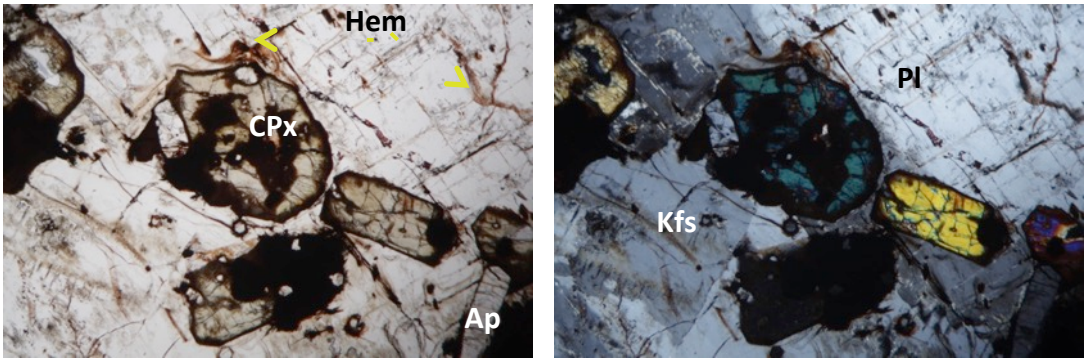


Figure 6: Photomicrographs of representative thin sections of the Monzonite TSy

Plain (left) and crossed (right) polarized light; long side of the pictures is 3.4 mm. Labels: Apatite (Ap); Clinopyroxene (Cpx); Hematite (Hem); K-feldspar (Kfs); Plagioclase (Pl) [5].

## Latite (TRh)

Figure 7: Cubic specimen of the Latite TRh

*Texture:* aphanitic, hypo-crystalline, inequigranular, hiatal.

*Components:*

Table 4: Rock-forming minerals listed in order of their relative abundance in the Latite TRh

| Essential minerals (in descending order of abundance) | Accessory minerals | Secondary minerals |
|---|---|---|
| K-feld**spar** | Hematite | Kaolinite |
| Plagioclase | Opaque minerals | Sericite |
| Clinopyroxene | Apatite | |
| Quartz | Calcite | |

*Rock classification* [4]*:* Latite

*Origin:* Tønsberg - Norway

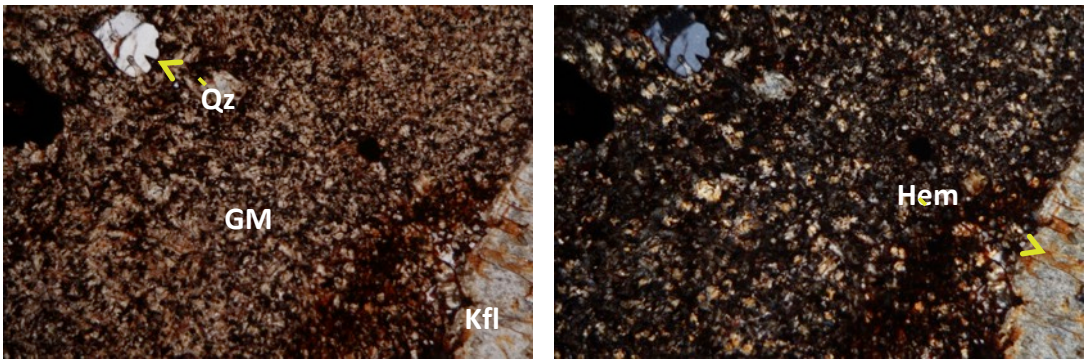


Figure 8: Photomicrographs of representative thin sections of the Latite TRh

Plain (left) and crossed (right) polarized light; long side of the pictures is 3,4 mm. Labels: Groundmass (GM); Hematite (Hem); K-feldspar (Kfs); Quartz (Qz).

## Macael Marble (MM)

Figure 9: Cubic specimen of the Macael marble MM

*Texture:* granofelsic, heteroblastic, hiatal.

*Microstructure features:* Mosaic, heteroblastic, with 120° triple junctions. Crystal's boundaries are mainly curved and secondarily straight. It is medium grained with Maximum Grain Sizes (MGS) 1.57 mm.

*Components:*

Table 5: Rock-forming minerals listed in order of their relative abundance in the Macael marble MM

| Essential minerals (in descending order of abundance) | Accessory minerals | Secondary minerals |
|---|---|---|
| Calcite | Mica | |
| | Quartz | |
| | Epidote | |
| | Opaque minerals | |

*Rock classification* [6]*:* Marble

*Origin:* Macael - Spain

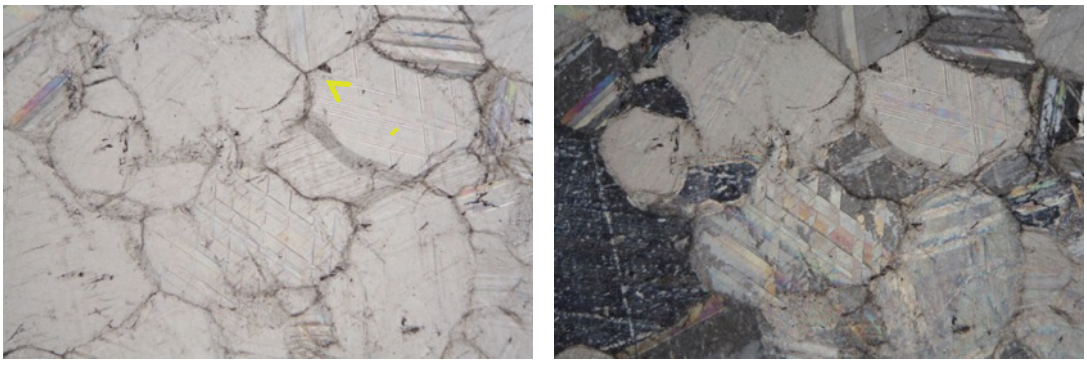

Figure 10: Photomicrographs of representative thin sections of the Macael marble MM

Plain (left) and crossed (right) polarized light; long side of the pictures is 3,4 mm. The yellow arrow shows a triple point.

## Santa Pudia Limestone (GSP)

Figure 11: Cubic specimen of the Santa Pudia limestone GSP

*Description:* Fossiliferous sedimentary rock consisting of micritic calcite and limited spathic cement. Allochems are essentially bioclasts constituted by bryozoans, articulated coralline algae, echinoderms, and mollusks. The cement is present as filling of fossils voids and substitution of shells.

It is worth noting the presence of iron oxides and hydroxides of a limonitic-hematitic nature that give the sample a yellowish-pale color.

*Binder:* spathic intragranular cement.

*Components:*

Table 6: Components listed in order of their relative abundance in the Santa Pudia limestone GSP

| **Allochems (in descending order of abundance)** | **Minerals** |
|---|---|
| Bryozoans | Calcite |
| Articulated coralline algae | Quartz |
| Echinoderms | Limonite-Hematite |
| Mollusks | |
| Intraclasts | |

*Rock classification:*

*Folk* [7]*:* Packed Biomicrite

*Dunham* [8] - *Embry & Klovan* [9]*:* Packstone

*Origin:* Tortonian deposits of the Guadalquivir Basin (Post-Orogenic Neogene Basins of the Betic Chains) [10]

*Age:* Miocene (Tortoniense medium-Messieniense) [11]

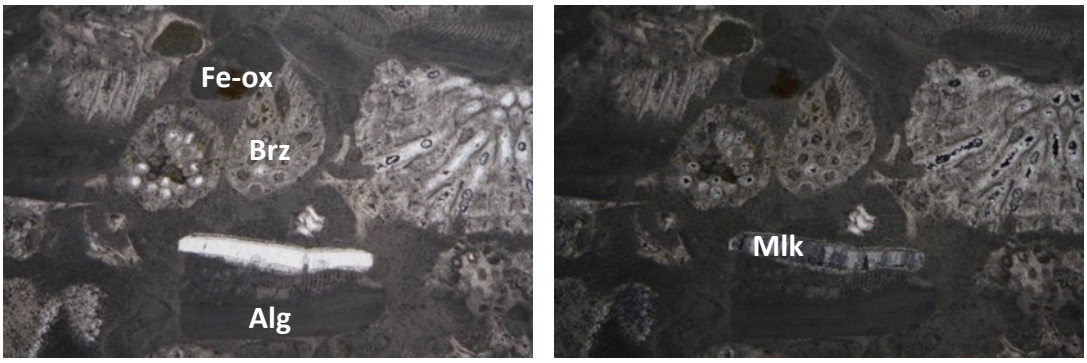


Figure 12: Photomicrographs of representative thin sections of the Santa Pudia limestone GSP

Plain (left) and crossed (right) polarized light; long side of the pictures is 3,4 mm. Labels: Algae (Alg); Bryozoans (Brz); Fe oxides (Fe-ox); Mollusks (Mlk).

## Sfouggaria Stone (SS)

Figure 13: Cubic specimen of the Sfouggaria stone SS

*Description:* Sedimentary fossiliferous rock consisting of a limestone mainly composed of calcareous algae scattered in spathic cement; micrite is limited to filling bioclasts. Main allochems constituents are articulated coralline algae, planktonic foraminifera (Numulites), bryozoans, echinoderms and intraclasts.

It is worth noting the presence of iron hydroxides-oxides of a limonitic-hematitic nature that give the sample its characteristic yellow-pale color. Chert and glauconite grains are also present as singenetic minerals.

*Binder:* spathic cement.

*Components:*

Table 7: Components listed in order of their relative abundance in the Sfouggaria stone SS

| **Allochems (in descending order of abundance)** | **Minerals** |
|---|---|
| Articulated coralline algae | Calcite |
| Intraclasts | Limonite-Hematite |
| Bryozoans | Chert |
| Echinoderms | Glauconite |
| Planktonic foraminifera (Numulites) | |

*Rock classification:*

*Folk* [7]*:* Biosparite rich in iron oxide and hydroxide

*Dunham* [8] - *Embry & Klovan* [9]*:* Grainstone rich in iron oxides and hydroxides

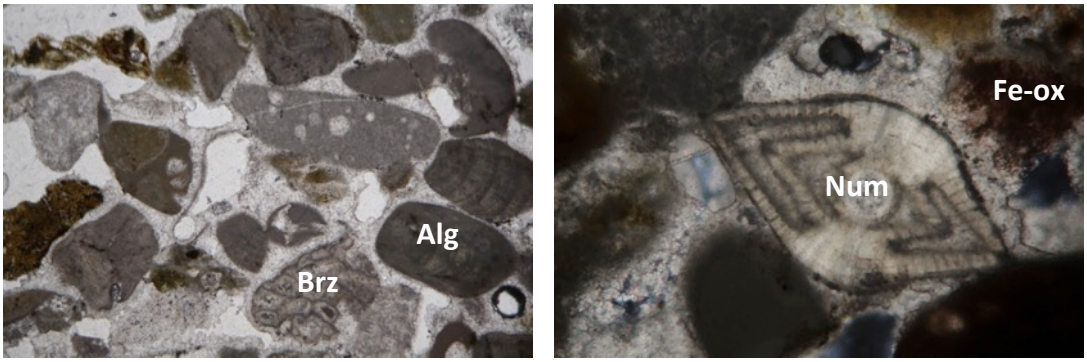


Figure 14: Photomicrographs of representative thin sections of the Sfouggaria stone SS

Plain (left) and crossed (right) polarized light; long side of the pictures is 3,4 mm (left), 1,4 mm (right). Labels: Algae (Alg); Bryozoans (Brz); Fe oxides (Fe-ox); Numulites (Num).

## Lartios Stone (LS)

Figure 15: Cubic specimen of the Lartios stone LS

*Description:* Sedimentary rock consisting of sandstone composed mainly of quartz, feldspar, chlorite, clasts of lavas and metamorphic rocks as well as a few bioclasts, bound only by spathic calcite.

*Binder:* spathic cement.

*Components:*

Table 8: Components listed in order of their relative abundance in the Lartios stone LS

| **Allochems (in descending order of abundance)** | **Minerals** |
|---|---|
| Planktonic foraminifera (Miliolids) | Calcite |
| Articulated coralline algae | Quartz |
| Echinoderms | Feldspar |
| Articulated coralline algae | Chlorite |

| | |
|---|---|
| | Effusive magmatic rocks (basic, hyalocrystalline) |
| | Metamorphic rocks (gneiss, schist often chlorite-bearing) |

*Rock classification:* Hybrid arenites with both carbonate and non-carbonate intrabacinal clasts

*Zuffa* [12]*:* Hybrid arenites

*Origin:* Lardos (Rhodes)

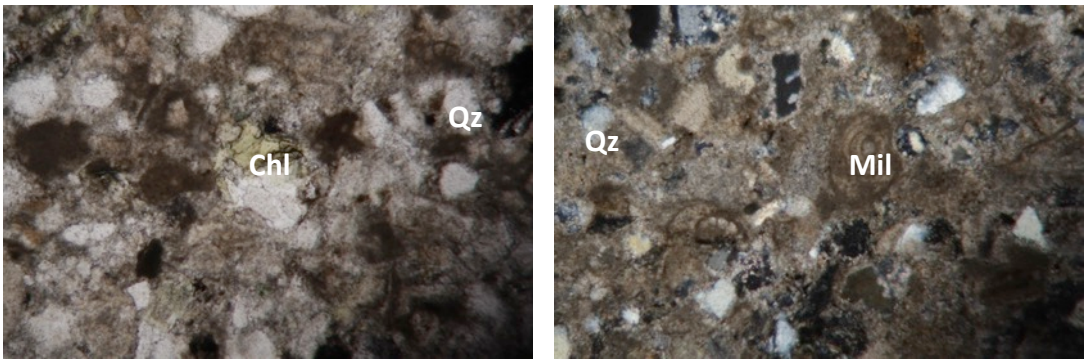


Figure 16: Photomicrographs of representative thin sections of the Lartios stone LS

Plain (left) and crossed (right) polarized light; long side of the pictures is 1,4 mm. Labels: Quartz (Qz); Chlorite (Chl); Milliolids (Mil).

## Botticino Limestone (BL)

Figure 17: Cubic specimen of the Botticino limestone BL

*Description:* Compact sedimentary rock corresponding to a micritic limestone made of very fine-grained calcite crystals (<4 μm) and abundant spathic dolomite crystals mainly gathered in iso-oriented veins. Stylolites are frequent, with small deposits of clay minerals often occurring along them.

*Binder:* micritic matrix and spathic cement.

*Components:*

Table 9: Components listed in order of their relative abundance in the Botticino limestone BL

| **Allochems** (in descending order of abundance) | **Minerals** |
|---|---|
| Globigerinoides | Calcite |
| | Clay minerals |

*Rock classification:* Micrite

*Folk* [7]*:* Micrite

*Dunham* [8] - *Embry & Klovan* [9]*:* Mudstone

*Origin:* Corna Formation - Brescia Italy

*Age:* Upper Triassic (Upper Raethian)

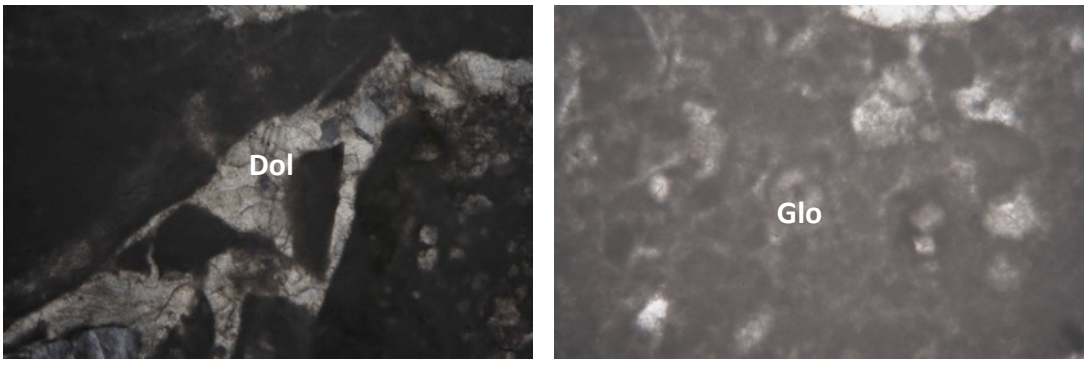


Figure 18: Photomicrographs of representative thin sections of the Botticino limestone BL

Plain (left) and crossed (right) polarized light; long side of the pictures is 3,4 mm (left), 1,4 mm (right). Labels: Globigerinoides (Glo); Dolomite (Dol).

## Carrara Marble (CM)

Figure 19: Cubic specimen of the Carrara marble CM

*Texture:* granofelsic, homeoblastic.

*Microstructure features:* Mosaic, with rare 120° triple junctions, mainly homeoblastic, locally partially heteroblastic. Crystals' boundaries are mainly curved and rarely straight. It is fine grained with Maximum Grain Sizes (MGS) 0.66 mm.

*Components:*

Table 10: Rock-forming minerals listed in order of their relative abundance in the Carrara marble CM

| Essential minerals (in descending order of abundance) | Accessory minerals | Secondary minerals |
|---|---|---|
| Calcite | Fe oxides | |

*Rock classification* [6]*:* Marble

*Origin:* Carrara - Italy

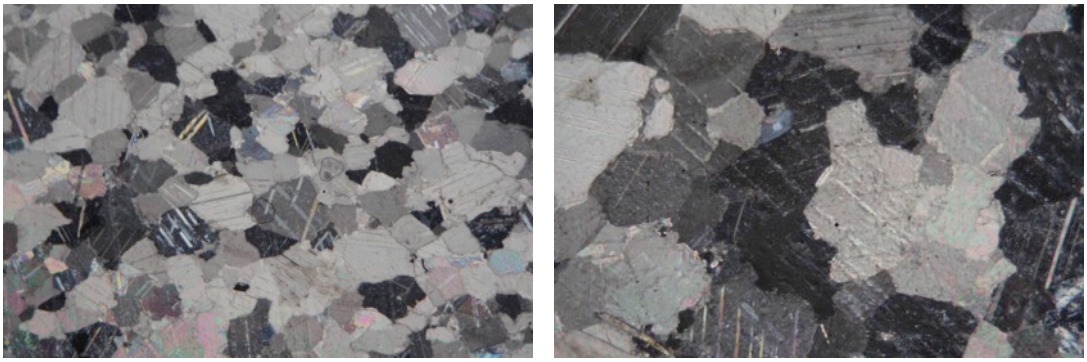

Figure 20: Photomicrographs of representative thin sections of the Carrara marble CM

Crossed (right) polarized light; long side of the pictures is 3,4 mm (left), 1,4 mm (right).

## Red Verona Limestone (RV)

Figure 21: Cubic specimen of the Red Verona limestone RV

*Description:* Carbonate sedimentary rock corresponding to a nodular limestone with abundant bioclasts within a micritic mud and rare spathic cement. The allochem constituents are ammonites (macroscopic), fragments of bivalves (pelagic

lamellibranchs), planktonic micro-foraminifera and echinoderms. There are also opaque minerals (hematite) responsible for the stone's pinkish color.

*Binder:* micritic mud and rare spathic cement.

*Components:*

Table 11: Components listed in order of their relative abundance in the Red Verona limestone RV

| **Allochems** (in descending order of abundance) | **Minerals** |
|---|---|
| Ammonites | Calcite |
| Pelagic lamellibranchs bivalves | Hematite |
| Micro planktonic foraminifera | |
| Echinoderms | |

*Rock classification:*

*Folk* [7]*:* Biomicrite with clay levels and nodular texture

*Dunham* [8] - *Embry & Klovan* [9]*:* Mudstone with nodular texture

*Origin:* *Rosso Ammonitico* formation - Verona Italy

*Age:* Middle and Upper Jurassic

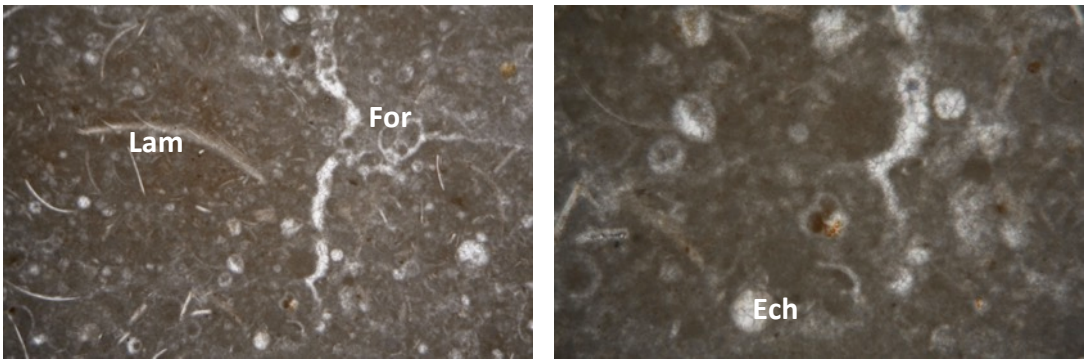


Figure 22: Photomicrographs of representative thin sections of the Red Verona limestone RV

Plain (left) and crossed (right) polarized light; long side of the pictures is 3,4 mm (left), 1,4 mm (right). Labels: Echinoderms (Ech); Foraminifera (For); Lamellibranchs (Lam).

## Costozza Stone (CS)

Figure 23: Cubic specimen of the Costozza stone CS

*Description:* Sedimentary carbonate rock corresponding to a grain-supported fossiliferous limestone made of poor spathic cement and subordinate micritic mud. Allochems constituents are articulated coralline algae, benthic foraminifera (main Miliolids and Nummulites), bryozoans, echinoderms and mollusks.

It is worth noting the presence of iron hydroxides of a limonitic-goethitic nature that give the sample its characteristic yellowish color.

*Binder:* spathic cement and rare micritic mud**.**

*Components:*

Table 12: Components listed in order of their relative abundance in the Costozza stone CS

| **Allochems** **(in descending order of abundance)** | **Minerals** |
|---|---|
| Articulated coralline algae | Calcite |
| Benthonic foraminifera (Miliolids, Nummulites) | Limonite-Goethite |
| Bryozoans | |
| Echinoderms | |
| Mollusks | |

*Rock classification:*

*Folk* [7]*:* Packed Biosparite rich in iron hydroxide

*Dunham* [8] - *Embry & Klovan* [9]*:* Packstone to grainstone rich in iron hydroxide

*Origin: Calcareniti di Castelgomberto* formation – Costozza (Vicenza) Italy

*Age:* Oligocene

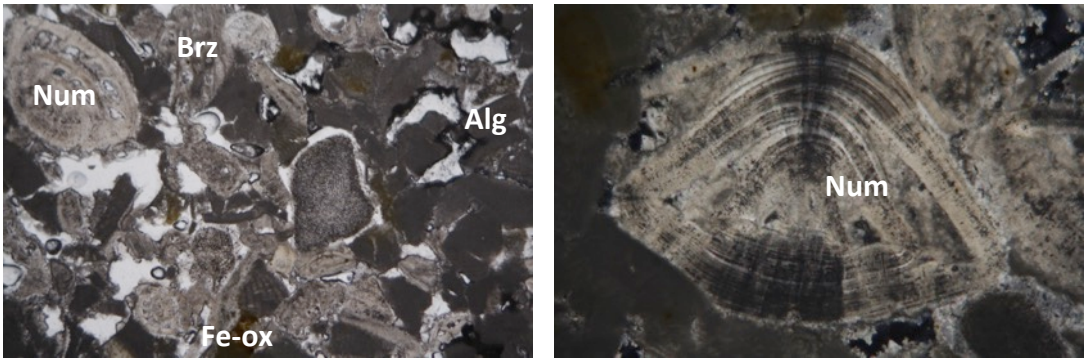


Figure 24: Photomicrographs of representative thin sections of the Costozza stone CS

Plain (left) and crossed (right) polarized light; long side of the pictures is 3,4 mm (left), 1,4 mm (right). Labels: Algae (Alg); Bryozoans (Brz); Fe oxides (Fe-ox); Numulites (Num).

## Trachyte (Eth)

Figure 25: Cubic specimen of the trachyte Etr

*Texture:* aphanitic, holocrystalline, microcristalline, glomeroporphyritic, microlitic, pilotaxitic.

*Components:*

Table 13: Rock-forming minerals listed in order of their relative abundance in the trachyte Etr

| Essential minerals (in descending order of abundance) | Accessory minerals | Secondary minerals |
|---|---|---|
| Plagioclase | Apatite | |
| Anorthoclase | Zircon | |
| K-feldspar (sanidine) | Magnetite | |
| Biotite | Opaque minerals | |
| Clinopyroxene (augite) | Rutile | |

Amphibole (kaersutite)

*Rock classification* [4]*:* Trachyte

*Origin:* Euganean Hills – Padova Italy

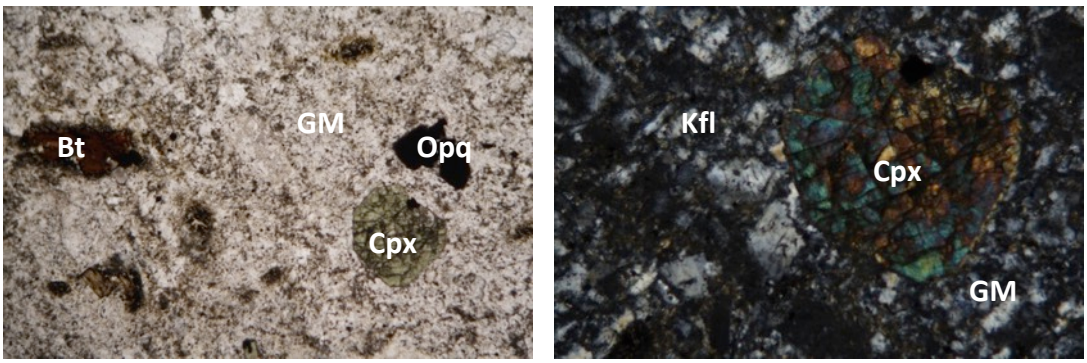


Figure 26: Photomicrographs of representative thin sections of the trachyte Etr

Plain (left) and crossed (right) polarized light; long side of the pictures is 3,4 mm (left), 1,4 mm (right). Labels: Biotite (Bt); Clinopyroxene (Cpx); Groundmass (GM); K-feldspar (Kfs); Opaque minerals (Opq).

## Istrian Stone (IS)

Figure 27: Cubic specimen of the Istrian stone IS

*Description:* Compact sedimentary rock corresponding to a marine limestone made of very fine-grained calcite crystals (<4 micrometers). The texture frequently features iso-oriented veins and small nuclei or cavities filled with secondary spathic calcite. Stylolites, as well as sedimentary joints, are frequent, with small deposits of clay minerals and iron oxides and hydroxides (Hematite-Limonite) often occurring along them, colored by red or yellow-ochre

*Binder:* micritic mud.

*Components:*

Table 14: Components listed in order of their relative abundance in the Istrian stone IS

| Allochems (in descending order of abundance) | Minerals |
|---|---|
| Bivalves or featureless fossil fragments | Calcite |
| | Hematite-Limonite |

*Rock classification:* Micritic Limestone

*Folk* [7]*:* Micrite

*Dunham* [8] - *Embry & Klovan* [9]*:* Mudstone

*Origin:* Istrian peninsula (Unity of the External Dinarides)

*Age:* Jurassic (Upper Tithonian)

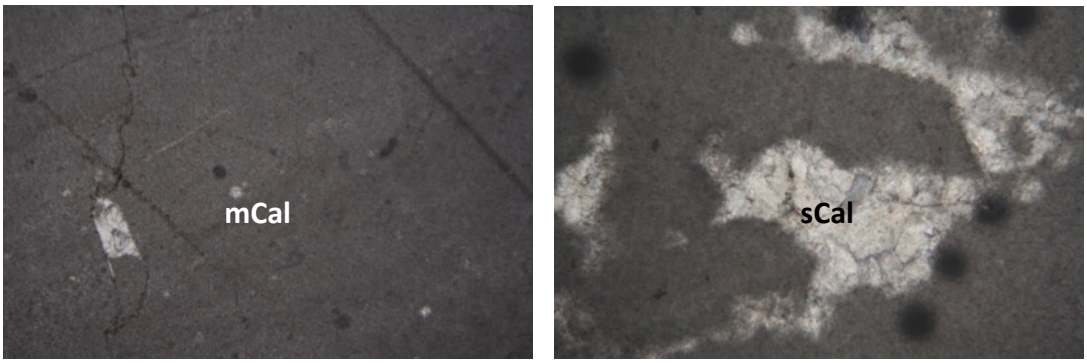


Figure 28: Photomicrographs of representative thin sections of the Istrian stone IS

Plain (left) and crossed (right) polarized light; long side of the pictures is 3,4 mm (left), 1,4 mm (right). Labels: micritic Calcite (mCal); spathic Calcite (sCal).

## *X-Ray powder diffraction (XRPD)*

Table 15: Semi-quantitative mineral composition of the twelve rock types selected for laboratory tests

| Minerals / Lithology | Cal | MgCal | Dol | Qz | Pl | K-Fs | Ano | Bt | Chl | WM | Cpx | Amp |
|---|---|---|---|---|---|---|---|---|---|---|---|---|
| **TSy** | | | | | xxx | x | | ** | | | ** | |
| **TRh** | | | | | xxx | x | | ** | | | ** | |
| **MM** | xxx | ** | | | | | | | | x | | |
| **GSP** | xxx | | | ** | | | | | | | | |
| **SS** | xxx | | | x | | | | | | | | |
| **LS** | xx | | | xx | x | | | | x | x | | |
| **BL** | xxx | | xx | | | | | | | | | |
| **CM** | xxx | | x | ** | | | | | | | | |
| **RV** | xxx | | | ** | | | | | | | | |
| **CS** | xxx | | | | | | | | | | | |
| **Etr** | | | | x | xx | x | xx | ** | | | x | x |

| | |
|---|---|
| **IS** | xxx |

Mineral abbreviations mainly after [5]: Amp = Amphibole; Ano = Anortoclase; Bt = Biotite; Cal = calcite; Chl = clhorite; Cpx = Clinopyroxene; Dol = dolomite; Kfs = K-feldspar; MgCal = Magnesium-calcite; Qz = quartz; Pl = Plagioclase; WM = white mica. Relative quantity: xxx = very abundant; xx = abundant; x = medium; ** = scarce; * = rare.

### *Colorimetric analysis (CoA)*

Table 16: Colorimetric measurements of the twelve selected rock types for laboratory tests

| Lithology | L* | a* | b* |
|---|---|---|---|
| Monzonite/ Tønsbergite | 58.78 | 5.47 | 6.74 |
| Latite | 53.75 | 5.54 | 7.94 |
| Macael Marble | 77.00 | -0.88 | -1.22 |
| Santa Pudia Limestone | 88.52 | 0.67 | 8.23 |
| Sfouggaria Stone | 69.60 | 3.27 | 12.06 |
| Lartios Stone | 56.17 | -0.73 | -0.23 |
| Botticino Limestone | 81.25 | 1.13 | 4.58 |
| Carrara Marble | 82.95 | -0.34 | 2.68 |
| Red Verona Limestone | 72.58 | 6.90 | 11.12 |
| Costozza Stone | 87.81 | 1.68 | 10.68 |
| Trachyte | 66.87 | -0.42 | 4.61 |
| Istrian Stone | 82.69 | 0.40 | 3.04 |

## 3.1.2. Venice Tier 1 building materials

### *Petrographic classification*

The petrography of thirteen over thirty of the micro-samples collected at the Clock Tower was studied to define their lithological nature. Five different rock types were detected. Table 17 reported below lists all micro-sample and their affiliation to the recognized rock types.

Table 17: Petrographic affiliation of the thirteen micro-samples investigated under the polarizing microscope

| Sample<br>Rock types | 1E | 2E | 3E | 4E | 5E | 1N | 2N | 3N | 4N | 1S | 1W | 5W | 8W |
|---|---|---|---|---|---|---|---|---|---|---|---|---|---|
| **White marble Carrara** | | X | | | | | | | | X | | | |
| **White marble Proconnesian** | | | | X | | | | | | | | | |

| | | | | | | | | | | | | |
|---|---|---|---|---|---|---|---|---|---|---|---|---|
| **Red Verona** | | | | | | | X | | X | | | | |
| **Istrian Stone** | | | X | | X | | | | | | | X | X |
| ***Scaglia Rossa*** | X | | | | | X | | X | | | X | | |

In addition to these stone types, three others were recognized in the South façade by means of macroscopic study and recognition only.

## **White marble (Carrara)** [13]

*Texture:* granofelsic, homeoblastic, hiatal.

*Microstructure features:* Polygonal, with triple points, sometimes purely mosaic and homeoblastic. Crystal's boundaries are mainly straight. Crystals maximum grain size (MGS) 0.60 mm (TdO_2E); 0.58 mm (TdO_1S).

*Components:*

Table 18: Rock-forming minerals listed in order of their relative abundance in the micro-samples of Carrara marble

| Essential minerals (in descending order of abundance) | Accessory minerals | Secondary minerals |
|---|---|---|
| Calcite | Pyrite | |
| | Quartz | |
| | Graphite | |

*Rock classification* [6]*:* Marble


Figure 29: Sampling points of Carrara marble (sample TdO_2E, left and TdO_1S)

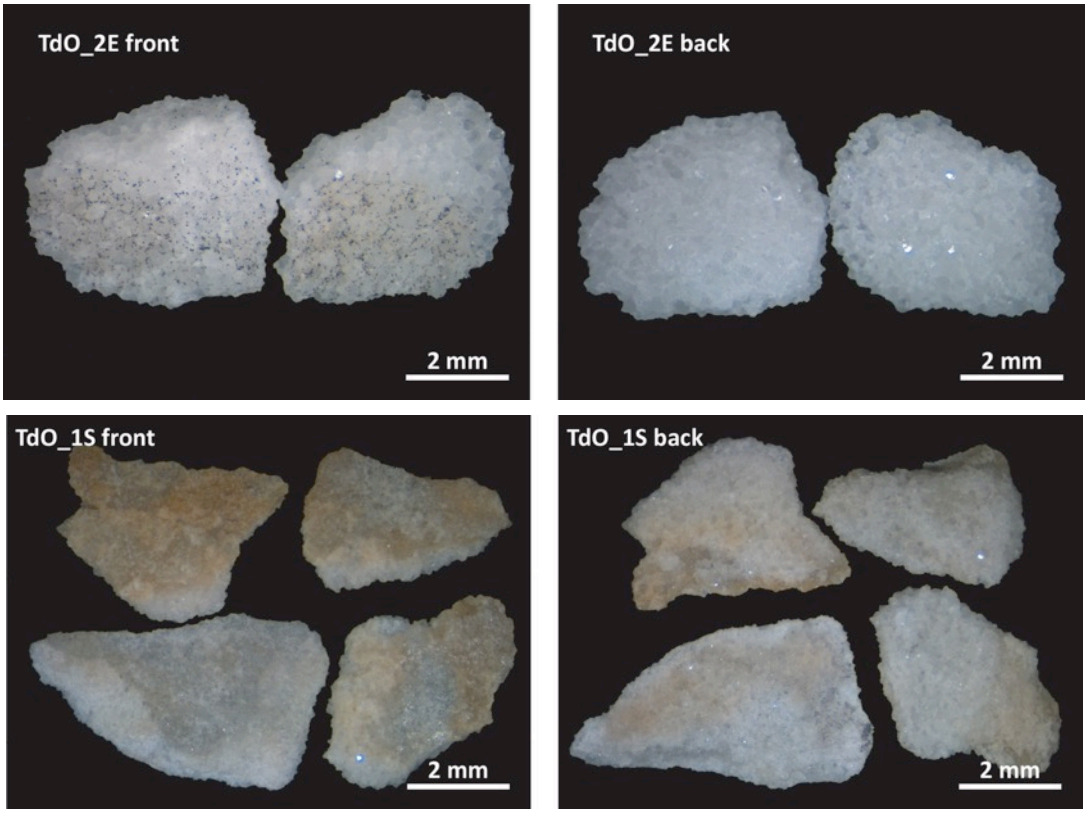


Figure 30: Stereomicroscope photos of Carrara marble samples TdO_2E and TdO_1S

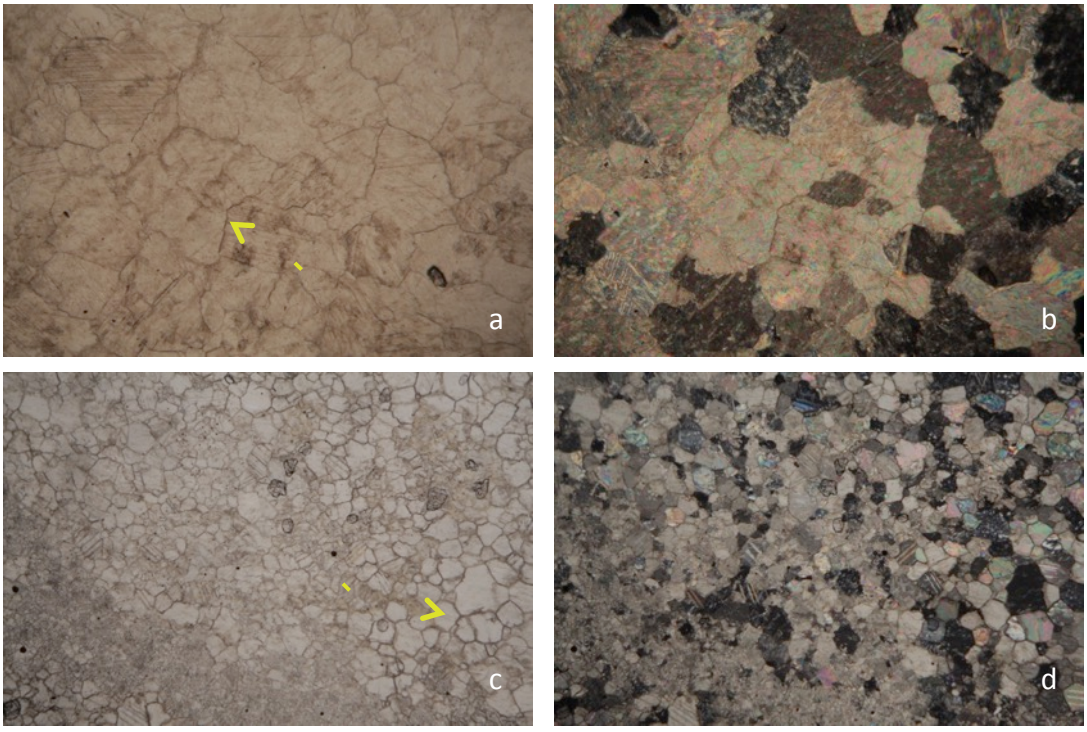


Figure 31: Transmitted light optic microscopy microphotographs of sample TdO_2E (a, b) and TdO_1S (c, d), Carrara marble

Plain (left) and crossed (right) polarized light; long side of the pictures is 3,4 mm. The yellow arrows show a triple points.

## White marble (Proconnesos) [13]

*Texture:* granofelsic, heteroblastic, hiatal.

*Microstructure features:* Polygonal, with triple points, sometimes purely mosaic and heteroblastic. Crystal's boundaries are mainly straight e secondarily curved. Crystals maximum grain size (MGS) 1.09 mm.

*Components:*

Table 19: Rock-forming minerals listed in order of their relative abundance in the micro-samples of Proconnesian marble

| Essential minerals (in descending order of abundance) | Accessory minerals | Secondary minerals |
|---|---|---|
| Calcite | | |

*Rock classification* [6]*:* Marble


Figure 32: Sampling point of Proconnesian marble (sample TdO_4E)

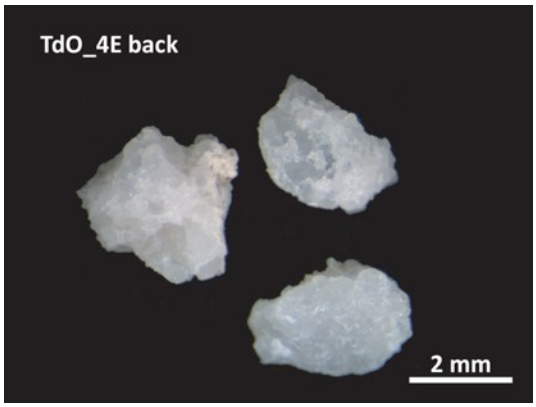


Figure 33: Stereomicroscope photos of Proconnesian marble (samples TdO_4E)

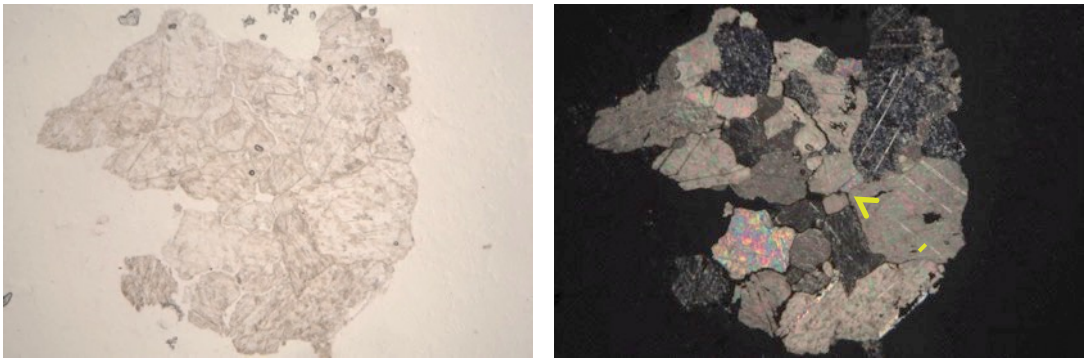

Figure 34: Transmitted light optic microscopy microphotographs of sample TdO_4E, Proconnesian marble

Plain (left) and crossed (right) polarized light; long side of the pictures is 3,4 mm. The yellow arrow shows a triple point.

## Istrian stone

*Description:* Compact sedimentary rock corresponding to a marine limestone made of very fine-grained calcite crystals (<4 micrometers). Very rare fragments of unidentifiable shells define the allochem constituents. Stylolites, as well as sedimentary joints, are frequent, with small deposits of clay minerals and iron oxides and hydroxides (Hematite-Limonite) often occurring along them, colored by red or yellow-ochre

*Binder:* micritic mud.

*Components:*

Table 20: Components listed in order of their relative abundance in the Istrian samples

| **Allochems** **(in descending order of abundance)** | **Minerals** |
|---|---|
| Fossil fragments | Calcite |
| | Hematite-Limonite |

*Rock classification:*

*Folk* [7]*:* Micrite

*Dunham* [8] - *Embry & Klovan* [9]*:* Mudstone

*Origin:* Istrian peninsula (Unity of the External Dinarides)

*Age:* Jurassic (Upper Tithonian)


Figure 35: Sampling points of Istrian stone (sample TdO_E3 and TdO_5E)

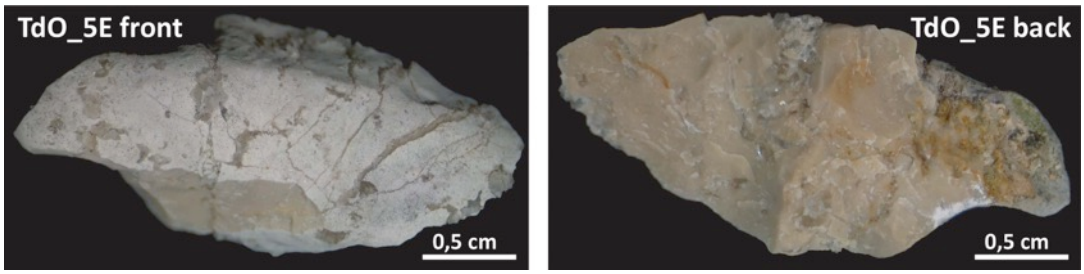


Figure 36: Stereomicroscope photos of Istrian stone (samples TdO_5E)

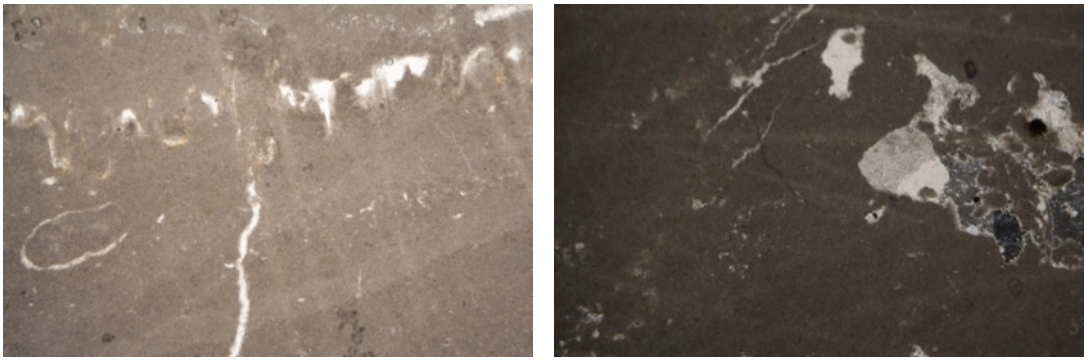

Figure 37: Transmitted light optic microscopy microphotographs of samples TdO_3E (left) and TdO_5E (right), Istrian stone

Plain (left) and crossed (right) polarized light; long side of the pictures is 3,4 mm.

## **Red Verona** *(Rosso di Verona)*

*Description:* Carbonate sedimentary rock corresponding to a nodular limestone with abundant bioclasts within a micritic mud and rare spathic cement. The allochem constituents are ammonites (macroscopic), fragments of bivalves (pelagic lamellibranchs), planktonic micro-foraminifera and echinoderms. There are also opaque minerals (hematite) responsible for the stone's pinkish color.

### *Components:*

Table 21: Components listed in order of their relative abundance in the Red Verona samples

| Allochems | Minerals |
|---|---|

| (in descending order of abundance) | |
|---|---|
| Pelagic lamellibranchs | Calcite |
| Planktonic micro-foraminifera | Hematite-Limonite |
| Echinoidea | |

*Rock classification:*

*Folk* [7]*:* Biomicrite with clay levels and nodular texture

*Dunham* [8] - *Embry & Klovan* [9]*:* Wackestone with nodular texture

*Origin: Rosso Ammonitico* formation - Verona Italy

*Age:* Middle and Upper Jurassic


Figure 38: Sampling points of Red Verona limestone (samples TdO_2N and TdO_4N)

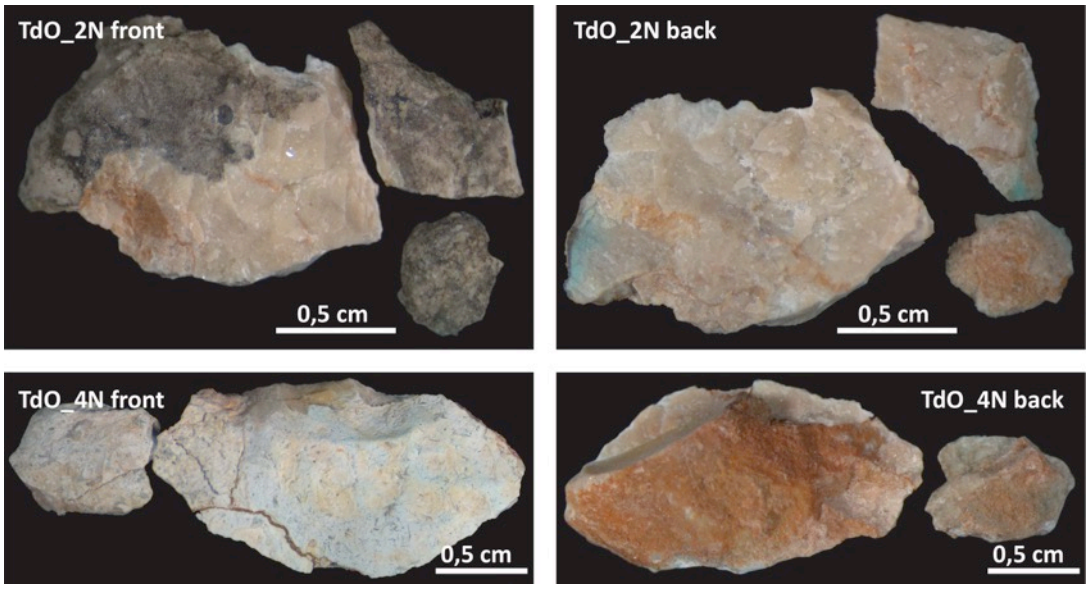


Figure 39: Stereomicroscope photos of Red Verona limestone (samples TdO_2N and TdO_4N)

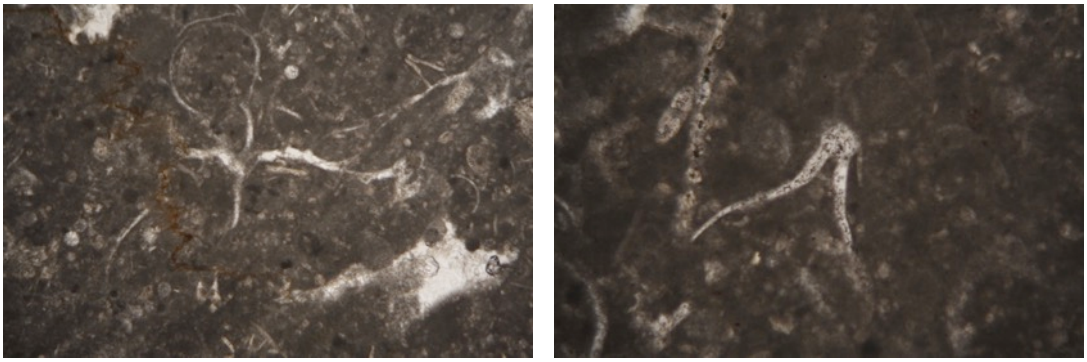

Figure 40: Transmitted light optic microscopy microphotographs of sample TdO_2N, Red Verona Plain (left) and crossed (right) polarized light; long side of the pictures is 3,4 mm (left), 1,4 mm (right).

### ***Pietra di Prun*** *(Scaglia Rossa)*

*Description:* Carbonate sedimentary rock consisting of micritic mud and, subordinately, of spatic cement, sparite is limited as filler of fossil footprints. Allochem constituents are planton microforaminifera, globotruncane, globigerinides. White variety: rock type locally known as "*Pietra di Prun"* or "*Pietra di Lessina"* or also "*lastame*".

*Binder:* micritic mud and spathic cement.

*Components:*

Table 22: Components listed in order of their relative abundance in the *Pietra di Prun* samples

| **Allochems (in descending order of abundance)** | **Minerals** |
|---|---|
| *Calpionellidae (Phitonella ovalis)* | Calcite |
| *Globotruncanidae (Marginotruncana)* | Hematite-Limonite |
| *Calcispherula innominata* | |
| *Biserial Heterohelicidae* | |
| *"Stomiosphaera" sphaerica* | |
| *Globigerinidae* | |

*Rock classification:* Micritic Limestone

*Folk* [7]*:* Biomicrite

*Dunham* [8] - *Embry & Klovan* [9]*:* Wackestone

*Origin:* *Scaglia Rossa Veronese* formation

*Age:* Upper Cretaceous


Figure 41: Sampling points of *Pietra di Prun* limestone (samples TdO_1E and TdO_3N)

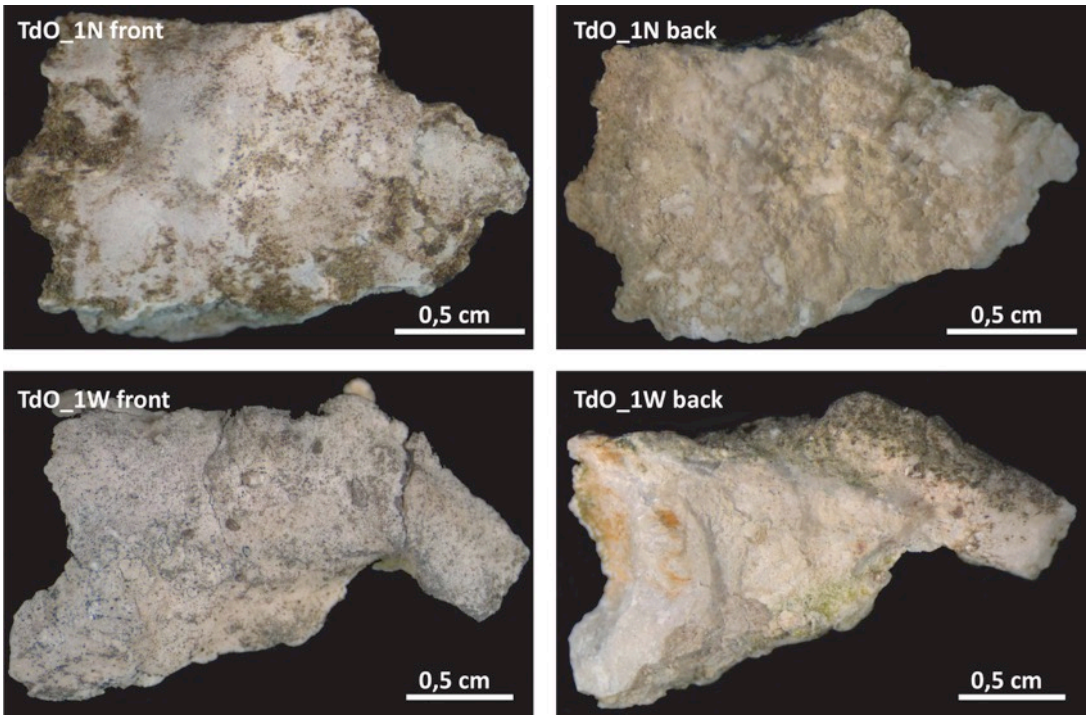


Figure 42: Stereomicroscope photos of *Pietra di Prun* limestone (samples TdO_1N and TdO_1W)

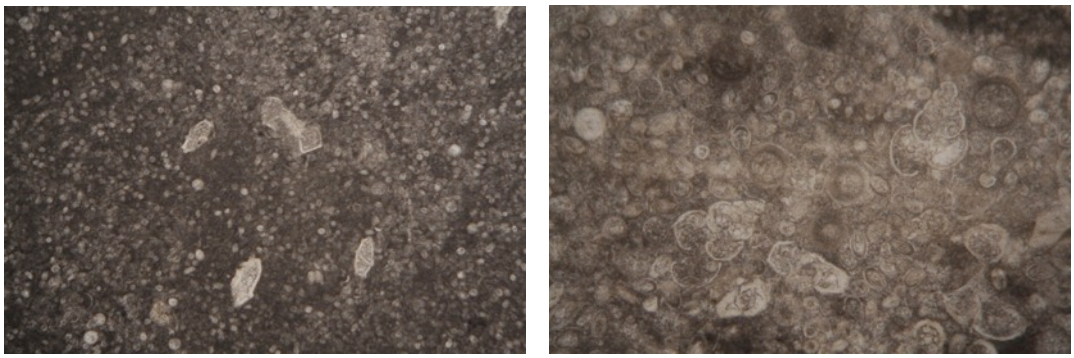

Figure 43: Transmitted light optic microscopy microphotographs of sample TdO_1N and TdO_1E, *Pietra di Prun*

Plain polarized light; long side of the pictures is 3,4 mm (left), 1,4 mm (right). In the left figure: *Globotruncanidae* and *Calpionellidae*, in the right ones: *Biserial Heterohelicidae, Calpionellidae* and *Globotruncanidae*

## *Other rock types recognized only on a macroscopic base*

### Imperial porphyry, porfido rosso antico

*Macroscopic description:* effusive igneous rock showing porphyric structure: pink phenocrysts of plagioclase floating in a purple groundmass. The red-purple color is due to trace of piemontite, the manganese member of the epidote group, and indicates a degree of metamorphism.

*Rock classification:* Andesite-Dacite

Figure 44: Circular decoration in Imperial porphyry

### Pavonazzetto Toscano Marble

*Macroscopic description:* Brecciated calcite marble with dark purple hematite-rich matrix.

*Rock classification:* Marble

Figure 45: Shaped slabs of Pavonazzetto Toscano Marble

### Hematitic cataclastic limestone (Rosso di Eretria or Rosso di Francia)

*Macroscopic description:* Shattered and deformed light-pink to red cataclastic hematitic limestone.

*Rock classification:* Cataclastic Limestone

Figure 46: Circular decoration in hematitic cataclastic limestone

### *Lithological mapping of Clock Tower*

Observations on the use of stone types in relation to the types of architectural elements revealed a thoughtful use of different stone types. In particular, the most valuable are located on the proper tower while the most common are more abundant on the two wings of the building. In particular, most of the columns and buttresses are made of Istrian stone, except for those on the ground floor, where the more precious Carrara marble is used. The decorative elements that stand out are the Imperial porphyry in the two rose windows in the center of the façade and, of course, the precious design created by the Tuscan Pavonazzetto marble around the clock. The Red Verona seems to be limited to the base of the two Moors. The lithological map is available in ANNEX 2.

## 3.2. Bricks

### 3.3.1 X-ray diffraction

Samples of twenty-three historical bricks collected on the façade of Santa Maria dei Servi (Tier 2 building in Venice, XIV century) were analyzed. The bulk XRPD analyses show a relative abundance of primary minerals (i.e. calcite and dolomite) and secondary firing minerals (i.e. diopside and gehlenite) suggesting a certain homogeneity in raw materials used. Presence of carbonates and new Ca- and Mg-silicate phases provide indications of the different temperatures reached during firing. Diopside and gehlenite occur at firing temperatures above 800 °C [14], but the persistence of peaks of calcite and dolomite indicate that temperature do not exceed the 750-800 °C [15]. Gypsum and mirabilite are often present as weathering products due to the salt decay process that affects Venice and the lagoonal environment [16] [17].

Table 23: XRDP results: mineralogical assemblages in historical bricks from Santa Maria dei Servi

| | Qz | K-fs | Pl | Cal | Dol | Di | Geh | Gyp | Mir | Ill | Hem |
|---|---|---|---|---|---|---|---|---|---|---|---|
| **A1** | xxx | x | x | | x | xx | | * | | | * |
| **A2** | xxx | | | | | x | * | | | | * |
| **A3** | xxx | x | | x | | | | * | | | * |

| | | | | | | | | | | | | |
|---|---|---|---|---|---|---|---|---|---|---|---|---|
| **A4** | x | | xx | xx | | xxx | | * | x | | * |
| **A5** | xxx | x | x | x | | | | * | | * | * |
| **A6** | xxx | x | x | xx | | | | * | | * | * |
| **A7** | xx | x | x | xx | | xx | | ** | * | | * |
| **A8** | xx | x | x | xx | | xxx | | ** | xx | | * |
| **A9** | xxx | x | xx | | | xx | | | | | * |
| **A10** | xx | x | xx | x | | xxx | | * | x | | * |
| **A11** | xx | x | xx | x | | xxx | | ** | xx | | * |
| **A13** | xxx | x | xx | x | | xx | | xx | * | | * |
| **B2** | x | * | xx | | | xxx | | x | x | | * |
| **B3** | xxx | x | x | | x | x | | | | | * |
| **B5** | xxx | * | | xx | x | | | ** | | * | * |
| **B6** | xx | xx | xx | xx | | xxx | | x | x | | * |
| **B7** | xxx | | x | | * | | | * | | * | * |
| **B8** | xxx | | xx | | x | xx | | * | * | | * |
| **B9** | xxx | x | xx | | x | xx | | x | * | | * |
| **B10** | xxx | | xx | * | ** | xx | | xxx | | | * |
| **B11** | xxx | x | xx | | | xx | | xx | * | | * |
| **C2** | **x** | | xx | | | xxx | * | xxx | xx | | |
| **C3** | xxx | x | x | xx | | | | x | * | | |

Mineral abbreviations after [5]: Qz = quartz; Ill = illite; Kfs = K-felspar; Pl = Plagioclase; Cal = calcite; Dol = dolomite; Hem = Hematite; Di = diopside; Gh = gehlenite; Gyp = gypsum; Mir = mirabilite. Relative quantity: xxx = very abundant; xx = abundant; x = medium; ** = scarce; * = rare.

The mineral composition of commercial bricks determined by XRPD analysis (Table 24) showed that are mainly composed by of quartz, gehlenite, anorthite, sanidine and diopside, matching the high temperatures these samples reached during firing [18] [14]. The new phases were less abundant in RSS than in the other samples. Peaks of illite and chlorite were still present in R6 because of its low firing temperature (600°C), due to weak reaction processes which were either very slight or did not take place at all. The diffractograms of GP showed higher amorphous phase (Am; Table 24) according to the highest temperature reached.

Table 24: XRDP results: mineralogical assemblages in fired bricks

| | Qz | Ill | Chl | K-fs | Pl | Cal | Dol | Hem | Wo | Di | Gh | Bst | Am |
|---|---|---|---|---|---|---|---|---|---|---|---|---|---|
| **GP** | xxx | | | xx | x | | | ** | x | xx | xx | | x |
| **RS** | xxx | | | x | x | | | ** | x | x | x | | |
| **RSS** | xxx | | | x | x | | | ** | x | x | x | | |
| **R6** | xxx | xx | xx | x | xx | x | x | ** | | | | | |

Mineral abbreviations after [5]: Qz = quartz; Ill = illite; Chl = clhorite; Kfs = K-felspar; Pl = Plagioclase; Cal = calcite; Dol = dolomite; Hem = Hematite; Wo = wollastonite; Di = diopside; Gh = gehlenite; Am = amorphous. Relative quantity: xxx = very abundant; xx = abundant; x = medium; ** = scarce; * = rare.

Under optical microscopy the matrix of sample GP was the lightest, suggesting the higher content of carbonate in the raw materials (Figure 47 left), brownish Fe oxides were observed dispersed in the matrix (Figure 47 right, and Figure 48), causing the

red color in samples RSS, RS and R6, probably hematite, as the XRPD results suggest. Phyllosilicates are still present in R6 (Figure 48 left).

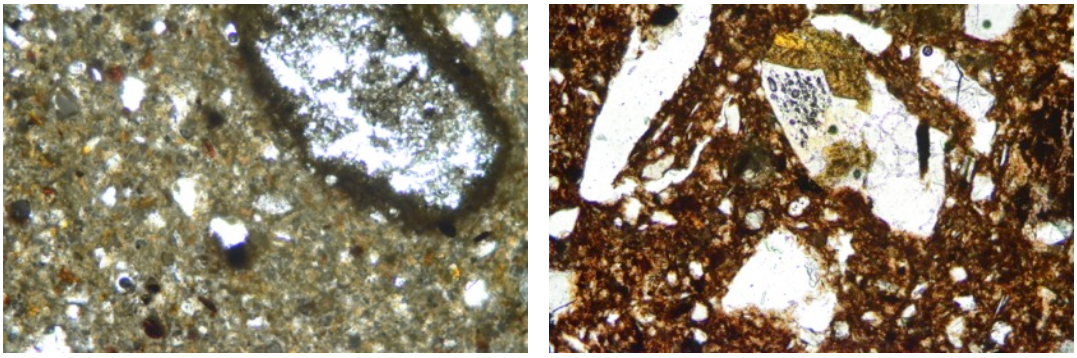

Figure 47: Photomicrographs (plain polars) of fired commercial bricks (10 x): brick GP (left); brick RSS (right)

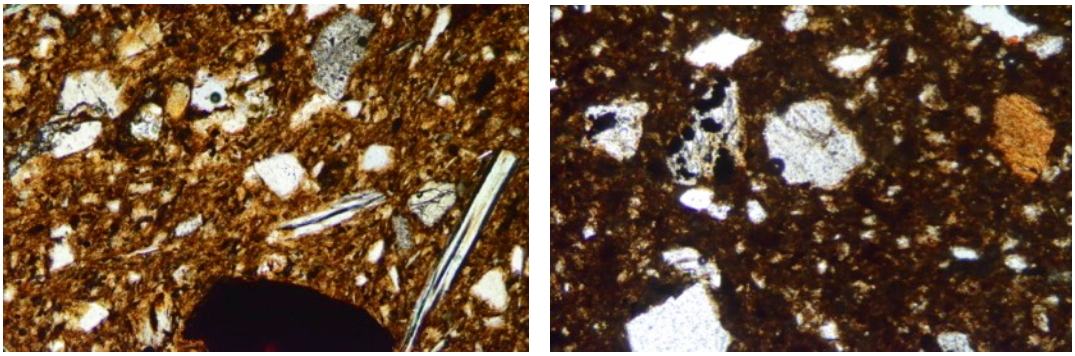

Figure 48: Photomicrographs (plain polars) of fired commercial bricks (10 x): brick R6 (left); brick RS (right)

SEM analysis allowed detailed study of reaction rims suraunding quartz and K-feldspar grains (Figure 49 left). Brick GP (fired at 1050°C) showed a partially vitreous groundmass and well-developed reaction bridges, especially along quartz and feldspar borders. Brick RSS, fired at 950°C, and RS, fired at 980°C, have similar mineralogical patterns: carbonates were completely decomposed and new phases had formed. In brick R6, fired at 600°C, only incipient dehydroxylation and decarbonation were observed.

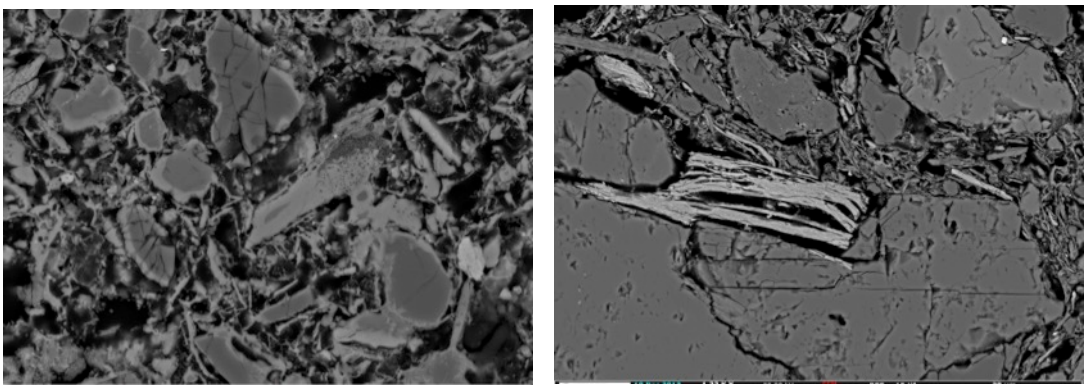

Figure 49: SEM-BSE images of fired commercial bricks: brick GP (left); brick RSS (right); C) brick R6; d) brick RS

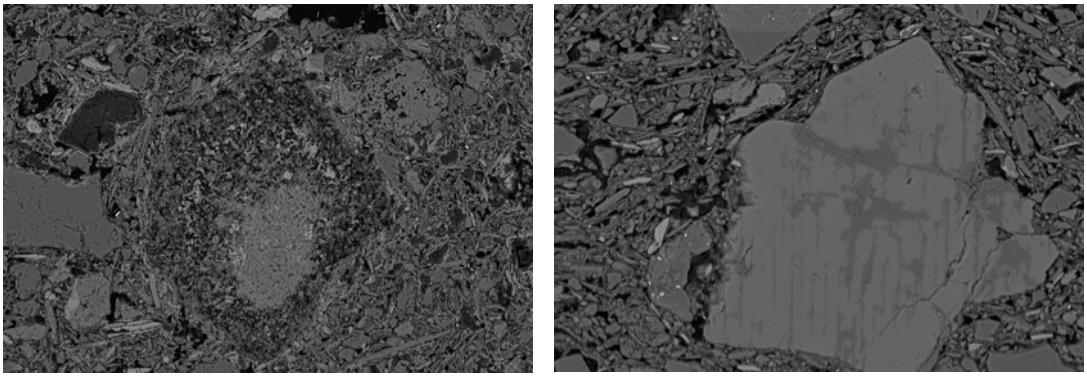

Figure 50: SEM-BSE images of fired commercial bricks: brick R6 (left); brick RS (right)

Color of historical and commercial bricks were analyzed in assisting the aesthetical compatibility in choice of bricks replacement in case of restoration interventions.

Table 25: Color measurements (Lab) of historic and commercial bricks

| **Historical bricks** | | | | | | | | | | | |
|---|---|---|---|---|---|---|---|---|---|---|---|
| **side a** | | | | **side b** | | | | **side c** | | | |
| **sample** | **L*** | **a*** | **b*** | **sample** | **L*** | **a*** | **b*** | **sample** | **L*** | **a*** | **b*** |
| **A1** | 61.4 | 11.64 | 23.4 | **B1** | 76.8 | 1.55 | 8.79 | **C1-W** | 78.21 | -1.08 | 10.68 |
| **A2** | 62.28 | 7.89 | 20.95 | **B2** | 59.67 | 4.06 | 21.1 | **C1-R** | 68.81 | 7.82 | 21.34 |
| **A3** | 56.59 | 11.7 | 22.65 | **B3** | 62.12 | 12.56 | 23.58 | **C2** | 63.74 | 2.36 | 27.99 |
| **A4** | 52.44 | 18.04 | 25.84 | **B4** | 62.28 | 5.63 | 7.77 | **C3** | 61.13 | 8.16 | 15.05 |
| **A5** | 59 | 13.35 | 24.33 | **B5** | 58.68 | 12.54 | 22.27 | | | | |
| **A6** | 67.07 | 8.28 | 23.24 | **B6** | 64.49 | 3.08 | 18.15 | **Commercial bricks** | | | |
| **A7** | 60.95 | 8.64 | 20.76 | **B7** | 50.2 | 18.17 | 23.96 | **sample** | **L*** | **a*** | **b*** |
| **A8** | 66.25 | 8.33 | 23.07 | **B8** | 58.99 | 12.66 | 22.31 | **GP** | 70.42 | 6.89 | 24.28 |
| **A9** | 66.33 | 5.21 | 23.16 | **B9** | 64.79 | 6.89 | 19.06 | **RS** | 60.23 | 16.41 | 25.86 |
| **A10** | 70.42 | 5.24 | 18.96 | **B10** | 60.38 | 8.17 | 20.34 | **RSS** | 56.51 | 19.05 | 25.4 |
| **A11** | 67.25 | 9.63 | 19.89 | **B11-Y** | 57.65 | 5.13 | 19.13 | **R6** | 53.51 | 9.35 | 20.01 |
| **A12** | 53.81 | 12.98 | 23.72 | **B11-B** | 36.65 | 3.4 | 9.15 | | | | |
| **A13** | 45.23 | 12.6 | 25.05 | | | | | | | | |

## 3.3. Timber

The material properties for the building components of the two constructions were derived from the database of WUFI® Pro 5.3 [19] and they are presented in Table 26. The following properties were chosen based on the validation of the numerical model in WUFI by experimental data, i.e. measurement of moisture content in timber [1].

Table 26: Selected material properties for the building elements in the two case studies

| Building components | Material from the WUFI Pro database | $\rho$ [kg/m$^3$] | $c$ [J/kgK] | $\lambda$ [W/mK] |
|---|---|---|---|---|
| Planks in the Fadum storehouse and the Heierstad loft | Softwood (by Fraunhofer Institute for Building Physics, Germany) | 400 | 1400 | 0.09 |
| Logs forming the walls and floors of the Fadum storehouse | Spruce, tangential (by LTH Lund University, Sweden) | 430 | 1600 | 0.14 |
| Logs forming the walls and floors of the ground level of the Heierstad loft | Scandinavian spruce transverse direction (by Norwegian University of Science and Technology 'NTNU') | 420 | 1600 | 0.13 |
| Logs forming the walls and floors of the upper level of the Heierstad loft | Pine transverse direction (by NTNU). | 510 | 1600 | 0.13 |

# 4. Identification and mapping of deterioration patterns and characterization of decay products

Maps reporting the deterioration patterns and the evaluation of their intensity were realized following the guide lines of the "ICOMOS-ISCS: Illustrated glossary on stone deterioration patterns" [20] combined with Fitzner and Heinrichs [21] indications. The two joined approaches allowed us to properly classify the decay morphologies as well as assign the level (intensity) of deterioration, here expressed in the range between 0 to 5, with 0 corresponding to the absence of deterioration and 5 to the maximum intensity of it (Table 27). In the maps, each pattern refers to a specific intensity, whereas different color to different deterioration forms (e.g. alveolization, black crust, crack). Taking into account all the deterioration patterns, which can be observed contemporaneously also on the same elements/ashlar/point/portion of the building, a total decay index (TDI) was calculated considering the higher value among the observed deterioration types.

Table 27: Decay values, intensity and patterns

| Deterioration level (DL) | Deterioration intensity description | Pattern | Total decay index (TDI) |
|---|---|---|---|
| **0** | no visible | | 0 |

| | | | |
|---|---|---|---|
| **1** | very slight |  | 1 |
| **2** | slight |  | 2 |
| **3** | moderate |  | 3 |
| **4** | severe |  | 4 |
| **5** | very severe |  | 5 |

## 4.1. Venice (Clock Tower)

Following all the steps reported in Section 2.3, the deterioration morphologies impacting the Clock Tower (Tier 1 of Venice) were mapped in detail (as reported in the paragraphs below) and the decay products carefully characterized through several analytical techniques as reported in Section 2.2. The total decay index (TDI) map is reported in ANNEX3F.

### 4.1.1. Crack & deformation

The mapping indicated that the main morphologies belonging to this group are:

- **cracks,** more specifically fractures (Figure 51), with the intensity between 1 and 2 (very slight to slight), the façade more concerned by this phenomenon is the South one (ANNEX 3Aa).
- **deformations** mainly as bowing phenomenon (i.e. a convex deformation involving especially the median section (Figure 52) of the marble panels and showing very slight or slight intensity. This decay pattern is more evident in the East façade (ANNEX 3Ab). A more intense deformation (DL 3) involves the extreme NE pilaster strip (lesana) where one stone block appears to be slightly tilted (Figure 52 right).

Figure 51: Fractures on the arch above a door (left) and on a pilaster strip base (right)

Figure 52: Slight bowing of a marble panel (left) and deformation on the NE lesena of the South façade (right)

### 4.1.2. Detachment

The mapping revealed that the main morphologies belonging to this group are:

- **blistering** (Figure 53) with the intensity between 1 and 2 (very slight to slight), involving only the South façade were the salts crystallization and black crusts are more intense (ANNEX 3Ba).
- **disintegration** (Figure 54) of limestone and crystalline marbles (sugaring) panels, in the last case probably due to thermal shock. These morphologies are more common on the side façades (ANNEX 3Bb, 3Bc) showing intensity of 1 or 2 (very slight to slight).

Figure 53: Blistering involving both stone substrate and superficial black crusts

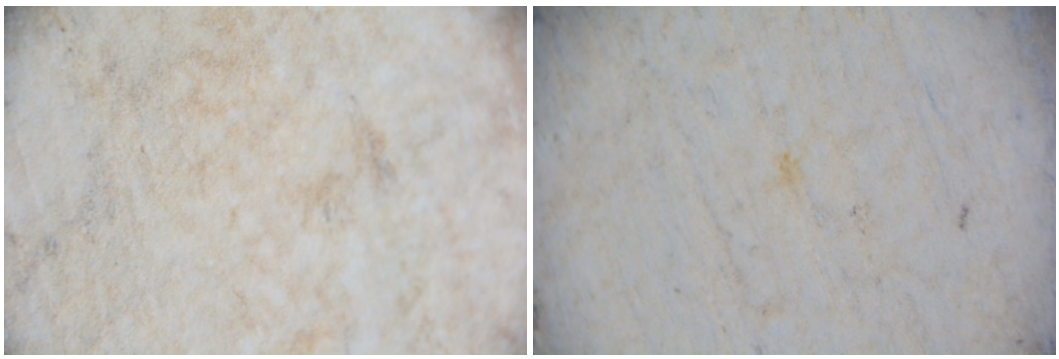

Figure 54: Details of sugaring on crystalline marble panels

### 4.1.3. Features induced by material loss

The mapping revealed that the main morphologies belonging to this group are:

- **differential erosion** with the intensity between 1 and 2 (very slight to slight), in particular as a consequence of a major recession rate (due to dissolution effect) of the fine-grained calcite portions of limestone (Figure 55) with respect to those with average-to-coarse grained carbonate. This decay morphology is more common in the East and West façades (ANNEX 3Cb, 3Cc).
- **microkarst** (Figure 56) of slight intensity (DL 2) interesting all the Istrian Stone small columns of all the balustrades (ANNEX 3C).
- **missing part** with the intensity widely varying between very slight and very severe (DL 1 to 5). In particular, some *rotae* of *hematitic cataclastic limestone* are partially or completely missing (ANNEX 3C).

Figure 55: Differential matrix erosion on *Scaglia Rossa* slabs

Figure 56: Microkarst on the small columns of the balustrade

### 4.1.4. Discoloration & deposit

The mapping shows that the main morphologies belonging to this group are:

- **black crusts** are quite frequent, mainly in the western side of the ground floor of the South façade (ANNEX 3Da), heavily afflicting the Corinthian

capitals (Figure 57). The intensity of these alteration morphology covers all the range from 1 to 5 (very slight to very severe).

- **discoloration** is represented by **bleaching** and **staining** (ANNEX 3D). In the former case, red limestones (i.e. *Rosso di Verona* and *Pietra di Prun*), due to weather process, altered and loss their hematitic pigments from the surface layers and change their colors to lighter ones. This pattern is more present in the two side façades, ranging in intensity from 1 to 4 (very slight to severe). Staining, instead, creates greenish and reddish localized halos due respectively to the dispersion of copper (Figure 57 right) and iron products deriving from the weathering of metallic elements. The intensity of this decay product range from 1 to 3 (very slight to moderate).
- **efflorescence** mainly appear as whisker-like crystals (Figure 58 left) of very slight and slight intensity (corresponding to DL 1 and 2) on the surface of the small columns of the balustrades (ANNEX 3D).
- **patinas**, resulting from ageing of ancient treatments, appear as a yellowish layer (Figure 58 right) mainly on crystalline marble slabs and columns/pilasters (ANNEX 3D). The intensity of this decay product range from 1 to 3 (very slight to moderate).
- **soiling** is the most widespread decay morphology in the whole building (ANNEX 3D). It appears as a tenuous blackish-gray layer (intensity between 1 and 4, very slight to severe) that confers a dirty appearance to the stone (Figure 59).

Figure 57: Black crusts on a Corinthian capital (left), copper-based oxides staining (right)

Figure 58: Efflorescence on a small column of the balustrade (left), yellowish patina (right)

Figure 59: Marble panels showing yellowish patinas and soiling (left), detail of the soling deposit (right)

### 4.1.5. Biological colonization

- **lichens** and **fungi** colonization (intensity between 1 and 2: very slight to slight; Figure 60) mainly developed on Istrian stone in a homogeneous way in the three façades (ANNEX 3E).
- **moss** were rarely identified but when present are visually impactful (Figure 61); they were found mainly in the walkways between the balustrades of the two wings of the building and therefore they cannot be mapped on the elevations.

Figure 60: Lichens (left) and fungi (right) on the stone balustrade

Figure 61: Moss on the Istrian-stone flooring of the side walkways

### 4.1.6. Study of the deterioration products and morphologies

Several analyses of the different kind of deterioration products were performed on micro-samples collected from the building. The results acquired with each analytical methodology are reported below.

#### *X-Ray powder diffraction (XRPD)*

XRPD investigation on twenty-one of the collected micro-samples were performed to identify mineral compositions of the rocks and possible deterioration products. The analyses, which results are listed in Table 28, confirmed the carbonate (mainly calcite) composition of all the stone substrates that are constituted by Istrian stone, *Rosso di Verona*, *Pietra di Prun* and crystalline marbles (*Carrara* and *Proconnesian*). Analyses on black crusts (TdO_4S_b, and TdO_5S-b) showed very abundant gypsum beside medium quantities of quartz and oxalate (weddellite).

Table 28: Semi-quantitative and qualitative mineral composition of the decay products micro-samples

| Minerals / Sample | Cal | MgCal | Dol | Gp | Qz | Cu-compound | We | WM |
|---|---|---|---|---|---|---|---|---|
| **1E** | xxx | | | | ** | | | |
| **1N** | xxx | | | | * | | | |
| **1S** | xxx | x | | | ** | * | | |
| **1W** | xxx | | | | ** | | | * |
| **2N** | xxx | | | | * | | | |
| **2S** | xxx | xx | | | | * | | |
| **3E** | xxx | | | | | | | |
| **3N** | xxx | | | | ** | | | |
| **4E** | xxx | | | | * | | | |
| **4N** | xxx | | | | ** | | | |
| **4S_b** | | | | xxx | x | | x | |
| **4W** | xxx | | | | ** | | | |
| **5E** | xxx | | ** | | ** | | | |
| **5S_a** | xxx | | | x | ** | | | |
| **5S-b** | | | | xxx | x | | x | x |
| **5W** | xxx | | | | ** | | | |
| **6E** | xxx | | | | | | | |
| **7E** | xxx | | | | * | | | |
| **7W** | xxx | | | | * | | | |
| **8E** | xxx | | | | ** | | | |
| **8W** | xxx | | | | ** | | | |

Mineral abbreviations mainly after [5]: Cal = calcite; Dol = dolomite; Gp = Gypsum; Qz = quartz; We = weddellite; WM = white mica. Relative quantity: xxx = very abundant; xx = abundant; x = medium; ** = scarce; * = rare.

#### *Scanning Electron Microscopy and energy-dispersive X-ray spectroscopy (SEM-EDS)*

SEM-EDS investigation performed on fourteen samples shows traces of previous treatments as well as evidences of deterioration morphologies and products.

### Disintegration, microkarst, erosion and bleaching

Backscattered electrons images (BEI) shown in several samples evidence of a thin layer (some dozens μm high) of decoese rock (Figure 62). This micro-feature can be linked to decay morphologies such as disintegration, differential erosion, and microkarts. In few cases the same layers are characterized by the loss of coloring minerals (i.e. iron oxides) macroscopically detectable as bleaching (discoloration) phenomena (Figure 63).

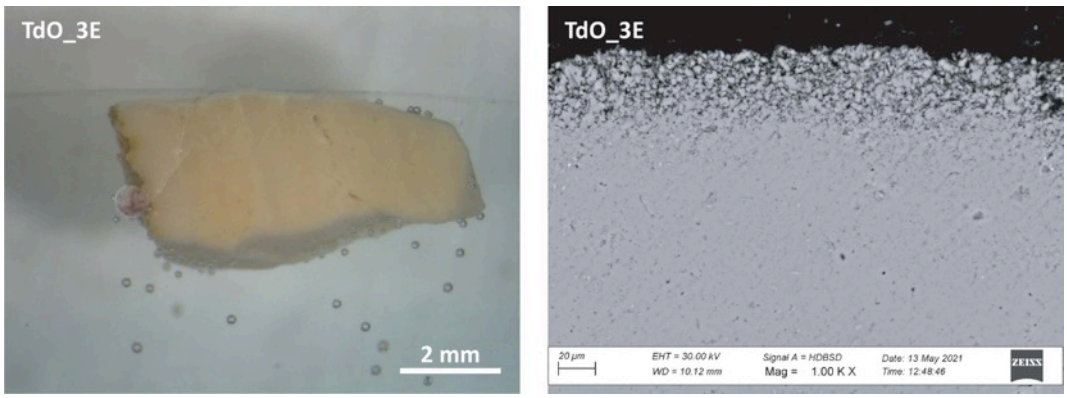


Figure 62: Sample TdO_3E: stereomicroscope photos of the polished transversal section (left), BEI of the surface of the sample (right)

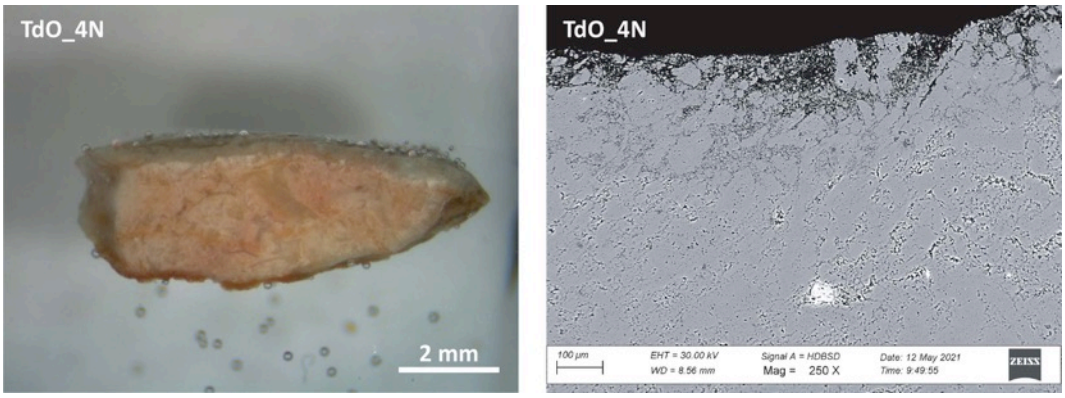


Figure 63: Sample TdO_4N: stereomicroscope photos of the polished transversal section (left), BEI of the surface of the sample (right); sparkling white particles in the BEI image

### Deposits

Several samples showed superficial deposits, from very thin layer of "dirt" - mainly of silicate nature - to fully formed black crusts of some hundred μm thickness typically composed by gypsum, marked by the element sulfur, incorporating atmospheric particulates indicated, among others, by the element silicon (Figure 64). In some cases under the black crust also subflorescence are testified by the present of a deposit, between the stone and the crust itself (Figure 64), characterized by high values of Chlorine (Cl) and Sodium (Na) and indicating a recrystallization of Halite (NaCl).

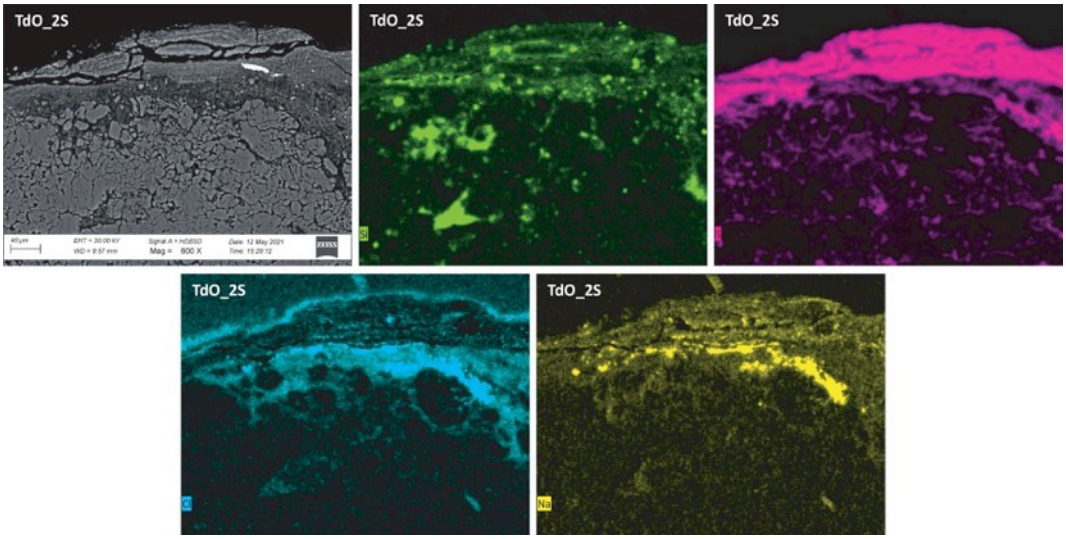


Figure 64: Sample TdO_2S from the up left: BEI of the black crust, elemental distribution map of Si (Silicon, green), and S (Sulfur, pink), Chlorine (Cl, light blue), and Sodium (Na, yellow)

On the surface of samples showing macroscopic staining morphologies induced by dispersion of copper from metallic element (e.g. Moors statue) EDS analysis confirmed the presence of Cu-based products (Figure 65).

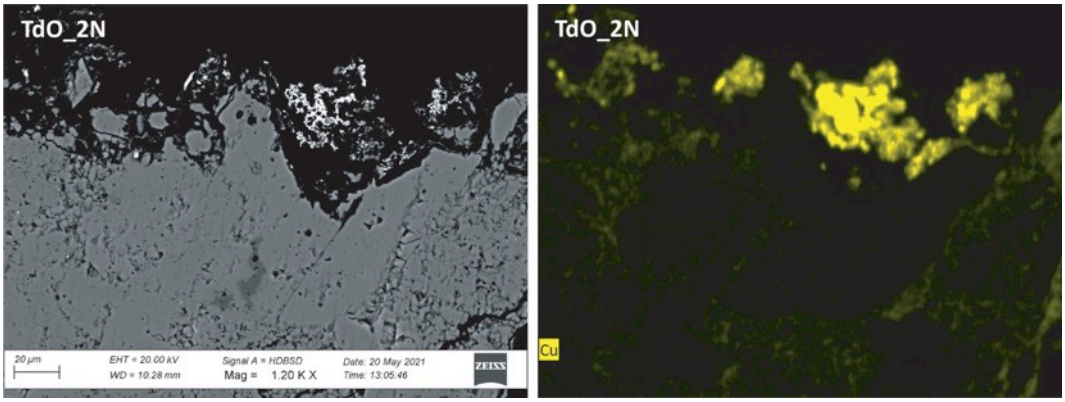


Figure 65: Sample TdO_2N from the left: BEI of the Cu-bearing deposit, elemental distribution map of Copper (Cu, yellow)

### Ancient treatments

In some samples artificial superficial layers were detected. They were identified as past treatments. In particular in samples TdO_1S and TdO_5S, both from the columns of the ground floor, the abundance of the element Fluorine (F) in the layer suggested the employ of a fluosilicates (Figure 67) as consolidating agent, component also confirmed by the FTIR analyzes.

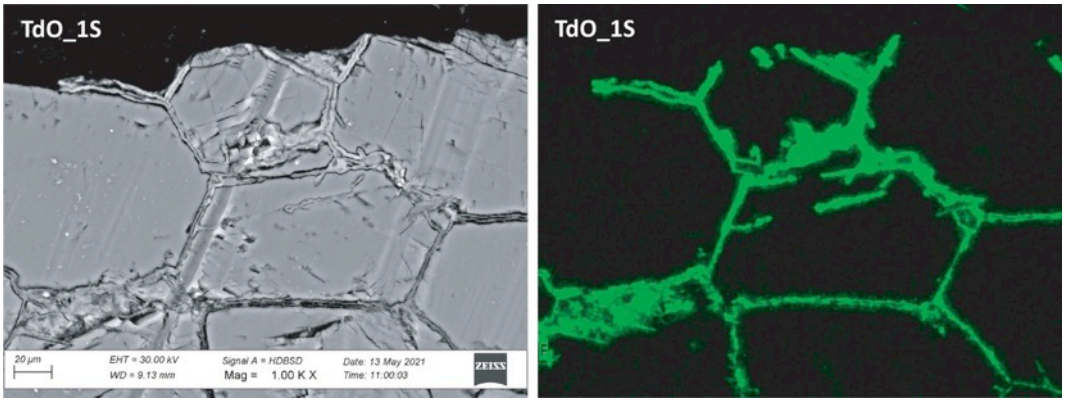


Figure 66: Sample TdO_1S from the left: BEI of the treatment deposit into the micro-cracks of the sample, elemental distribution map of Fluorine (F, green)

**Micro damages**

The most superficial calcite crystals in the crystalline marble from the ground floor, when observed through SEM (BEI images) showed peculiar damages clearly referred to a cleavage process (Figure 67). Studies on conservation procedures [22] revealed that this damage could be an unintentional secondary effect of the laser cleaning procedure performed on the stone surface to remove deposits. This technique induces the calcite crystals to break following the natural cleavage directions.

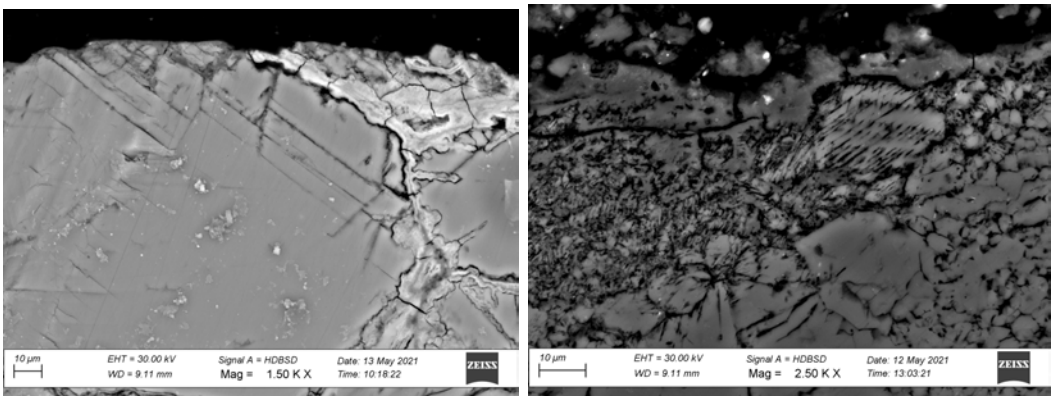

Figure 67: Sample TdO_1S (left) and TdO_4S (right): BEI of the surface of the sample showing the characteristic cleavage of calcite

## *Fourier-transform infrared spectroscopy (FTIR)*

Some micro-fragments revealed the presence of aged treatments applied in the past, probably as strengthening agents, during not documented restoration.

The study of µFTIR spectra of TdO_1S and TdO_3S samples allowed to suppose the use of fluosilicates (Figure 68) for the consolidation and protection of stone surfaces, whereas sample TdO_6E suggested the use of acrylic-silicone compounds (Figure 69). In some cases, such as sample TdO_4W, it has been detected the characteristic pecks of calcium oxalate dehydrate (weddellite), as product of mineralization process of organic compounds.

Table 29: Identified compounds in the examined samples using µFTIR

| Sample / Identified components | 1S | 3S | 4W | 6E | 7W |
|---|---|---|---|---|---|
| **Calcite** | x | x | x | x | x |
| **Weddellite** | x | x | x | | |
| **Fluosilicates** | x | x | | | |
| **Silicates** | | | x | x | |
| **Acrylic** | | | | x | |

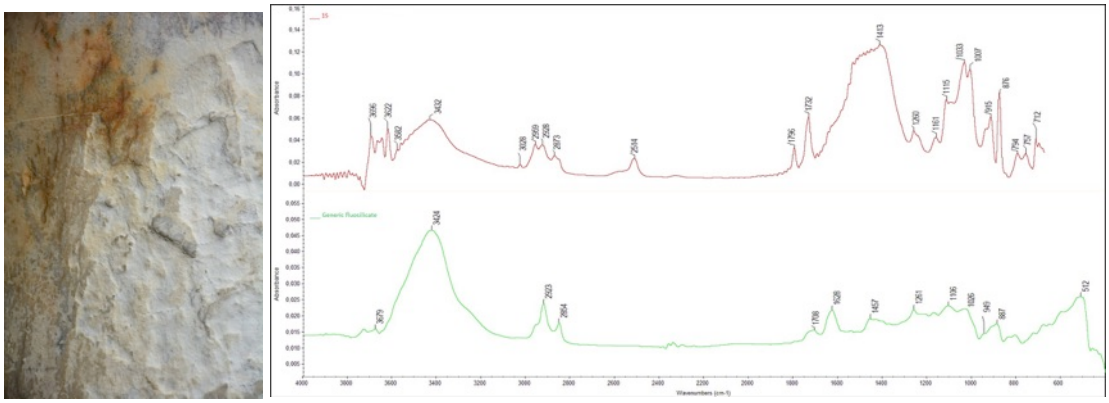

Figure 68: Comparison between µFTIR spectra of sample TdO_1S (sampling point on the left) and a general fluosilicate

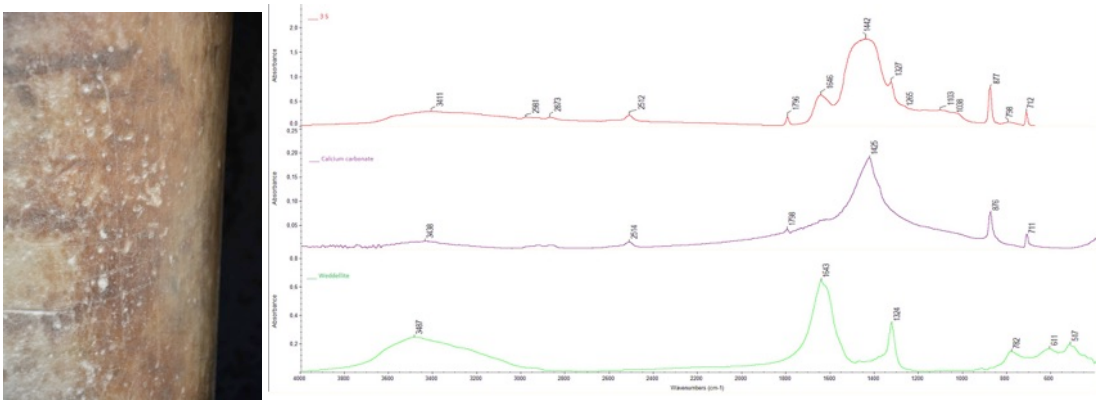

Figure 69: Comparison between µFTIR spectra of sample TdO_3S (sampling point on the left), weddellite and calcite

## *Ion Chromatography analysis (IC)*

Five samples of efflorescence and stone powders were studied to reveal the possible presence, nature and quantity of deliquescent salts deriving from degradation reactions and certainly harmful to the stone material. Table 30 shows a quantitative evaluation of the anions that identify these salts. The samples were tested for all the following anions: Fluorides, Chlorides, Nitrites, Bromides, Nitrates, Phosphates, Sulphates, however in Table 30 are reported only the detected ones.

Table 30: Anions and their relative % obtained by ICA

| Sample / Anions | 2S | 5S | 5W | 7E | 8E |
|---|---|---|---|---|---|
| **Fluorides** | 0,007 | 0,006 | - | - | - |
| **Chlorides** | 0,133 | 0,067 | 0,051 | 0,044 | 0,036 |
| **Nitrates** | 0,050 | 0,036 | 0,058 | 0,028 | 0,035 |
| **Sulphates** | 1,086 | 0,676 | 0,132 | 0,046 | 0,033 |

The main contents are of chlorides and sulphates anions, composition coherent with Halite (NaCl) and Gypsum ($CaSO4 \cdot H2O$) recrystallizations.

### *Biological analysis*

Biological investigations on eight out of the thirty of the micro-samples collected at the Clock Tower were performed to define the nature of the various types of biological colonization. Five different vegetal organisms were detected. Table 31 reported below lists the recognized organisms for each micro-sample.

Table 31: Biodeteriogens observed and studied in the eight micro-samples

| Sample / Biodeteriogens | 9E | 10E | 11E | 12E | 1N | 1W | 2W | 3W |
|---|---|---|---|---|---|---|---|---|
| ***Caloplaca saxicola* (Hoffm.) Nordin** | X | X | | | | | X | |
| ***Candelariella aurella* (Hoffm.) Zahlbr** | | | X | | | | | |
| **Meristematic fungi** | | | X | | X | X | X | X |
| **Moss** | | | | X | | | | |
| **Green algae** | | | | | X | X | X | X |
| **Cyanobacteria** | | | | | | X | | |

### *Caloplaca saxicola*

*Description:* Crusty lichen with lecanorine apothecia with bright orange disc and slightly lighter margins (Figure 70, and Figure 71). The thallus is placodomorphic and pale yellow in color. The chemical test with potassium hydroxide (KOH) solution gives a positive result (K+).

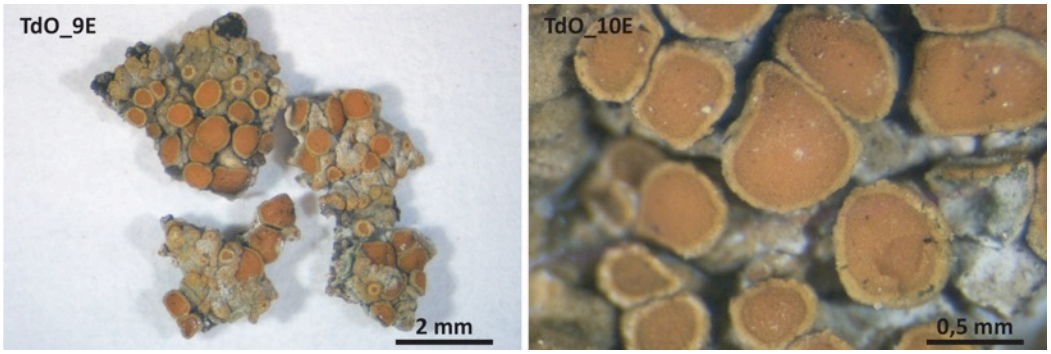


Figure 70: Crusty lichens with orange apothecia and pale yellow placodiomorphic thallus. Samples TdO_9E and TdO_10E

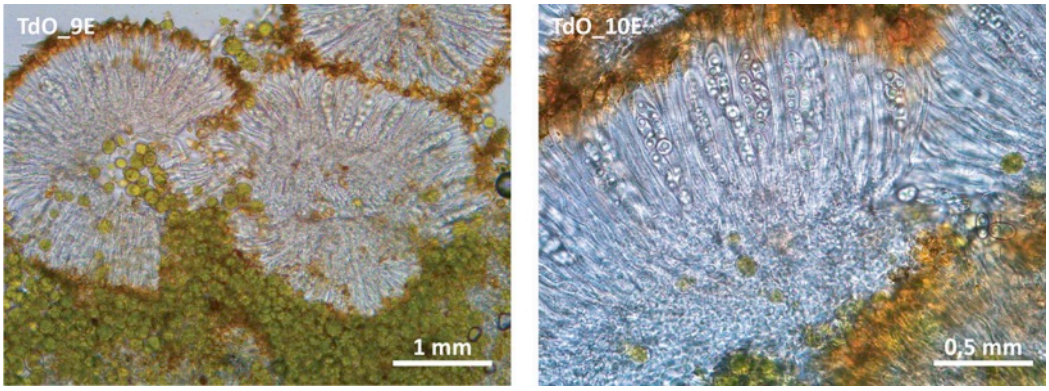


Figure 71: Micrographs of fresh slides under OM. Samples TdO_9E and TdO_10E

Apothecia in cross-section (left), detail of the asci containing eight spores (right).

*Classification:* *Caloplaca saxicola* (Hoffm.) Nordin [23]

### *Candelariella aurella*

*Description:* Crusty lichen with yellow apothecia and blurred thallus. Some apothecia are covered with a blackish patina (Figure 72, and Figure 73), while others have brownish branching. Chemical test with potassium hydroxide solution (KOH) gives negative result (K-).

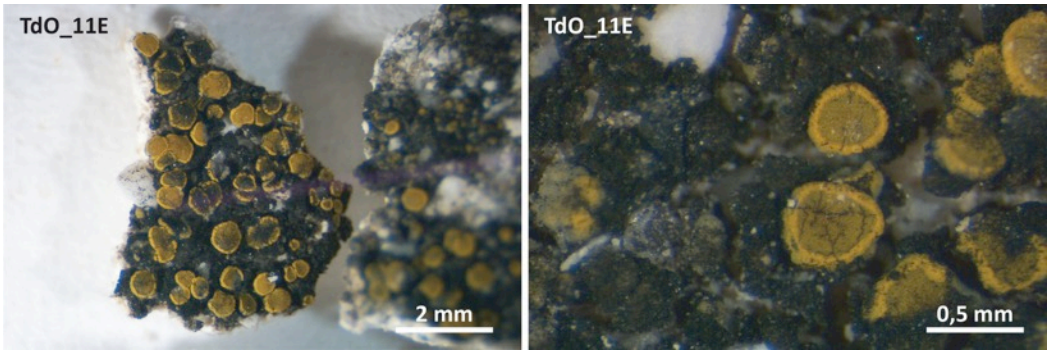


Figure 72: Crusty lichens with yellow apothecia and blurred thallus. Sample TdO_11E

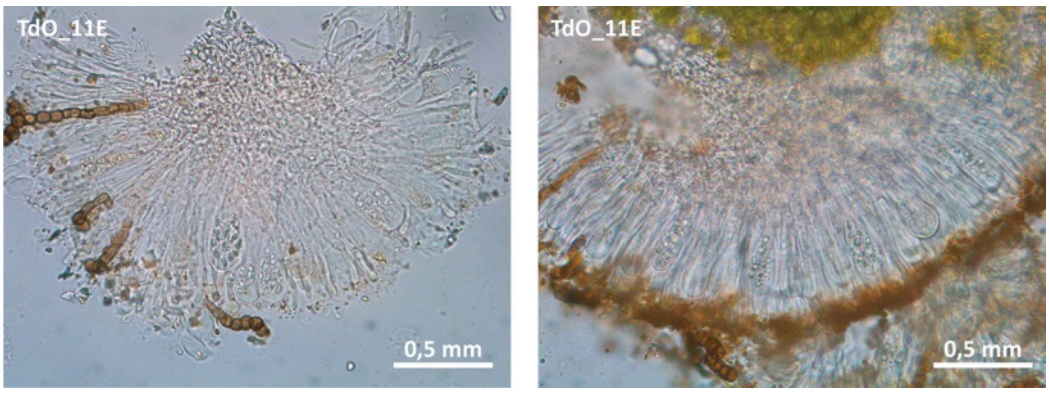


Figure 73: Micrographs of fresh slides under OM. Sample TdO_11E

Apothecia in cross-section (left), detail of the asci containing eight ellipsoidal bicellular spores (right).

*Classification:* *Candelariella aurella* (Hoffm.) Zahlbr [23]

## Meristematic fungi

*Description:* blackish patina (Figure 74) and brownish branching due to meristematic fungi whose fungal hyphae are arranged in a chain and whose brown coloration indicates the presence of melanin. This biological material often appears in combination with lichens and algae (Figure 75).

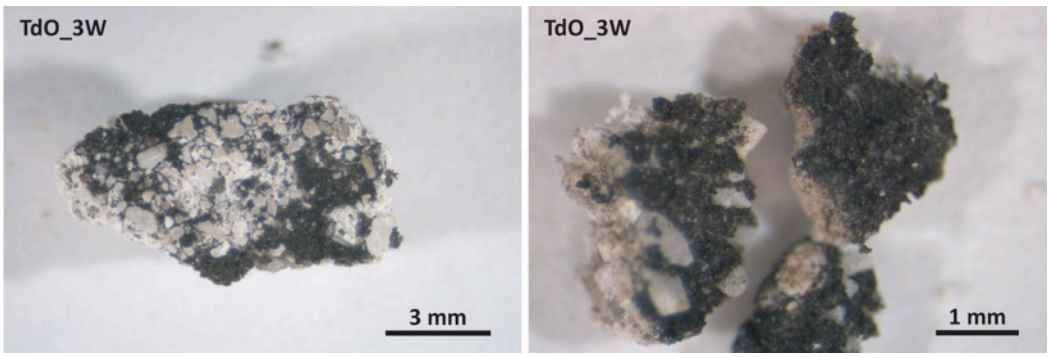


Figure 74: Blackish patina of biological material on the stone surface. Sample TdO_3W

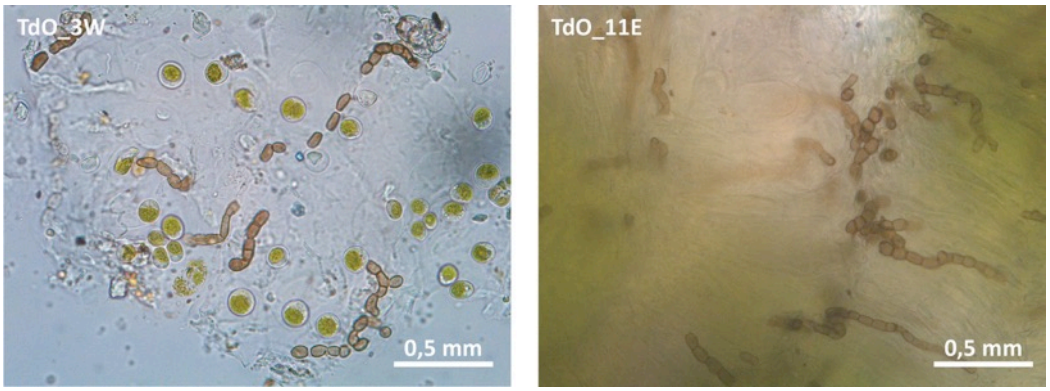


Figure 75: Micrographs of fresh slides under OM. Samples TdO_3W and TdO_11E

Hyphae of meristematic fungi and cells of green algae (left), meristematic fungal hyphae arranged on the surface of an apothecium (right).

*Classification:* meristematic fungi

## Moss

*Description:* plant belonging to the bryophyte division and more specifically to the class of mosses (Figure 76 left). Under the stereomicroscope we can see the gametophyte, i.e. the green part of the moss consisting of leaflets, and the sporophyte of which we can see the capsules, or urns, containing the spores, which are carried on top by filaments known as setae (Figure 76 right).

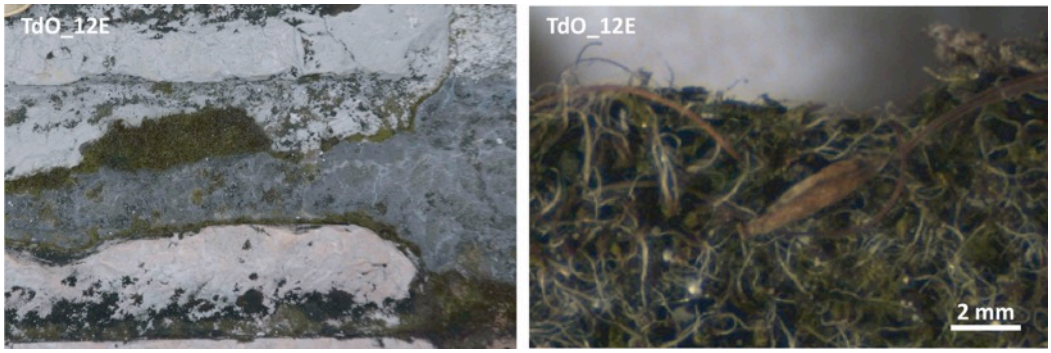


Figure 76: Sampling point of moss from the Istrian-stone flooring of the wings walkway (left), details of the sporophyte with the capsule and setae (right). Sample TdO_12E

*Classification:* moss

***Green Algae***

*Description:* Investigation of greenish patinas identified green algae cells combined with cyanobacteria colonies and a few fungal hyphae (Figure 77).

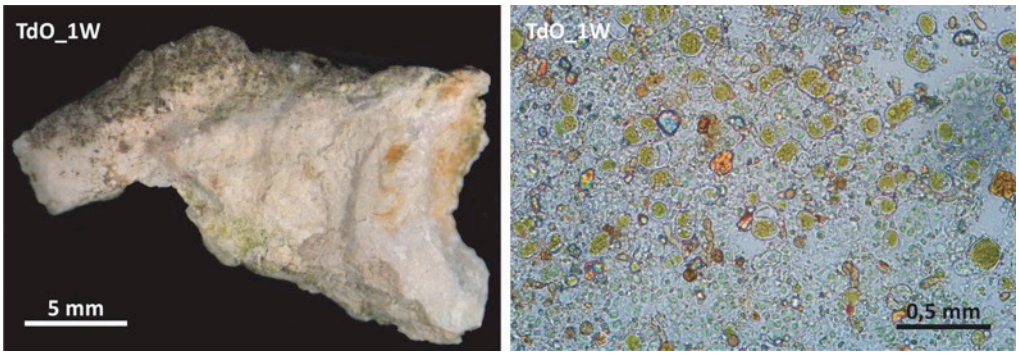


Figure 77: Faint greenish patina and black particles on the stone (left). Green algae cells, cyanobacteria colonies and a few fungal hyphae (right). Sample TdO_1W

*Classification:* Green algae

## 4.2. Rhodes (Nailac Pier and Saint Nikolas lighthouse and fort)

Following the steps A and B reported in Section 2.3, the deterioration morphologies impacting the Nailac Pier and Sant Nikolas (Tier 1 of Rhodes) were mapped on selected areas.

### 4.2.1. Material loss

The only morphologies detectable from the high-resolution images received were those connected to the loss of material. In particular, both the buildings, that are mainly constituted by a porous calcarenite (Sfouggaria Stone) blocks, are affected by severe alveolizations and, subordinately, by erosion and missing parts (Figure 78). An example of alveolizations and its map is reported in Figure 79. All mappings concerning the Rhodian buildings investigated are reported in Annex 4.

Figure 78: Example of Material loss morphologies in Nailac Pier and Saint Nikolas. From the left: alveolizations, erosion and missing part, missing parts

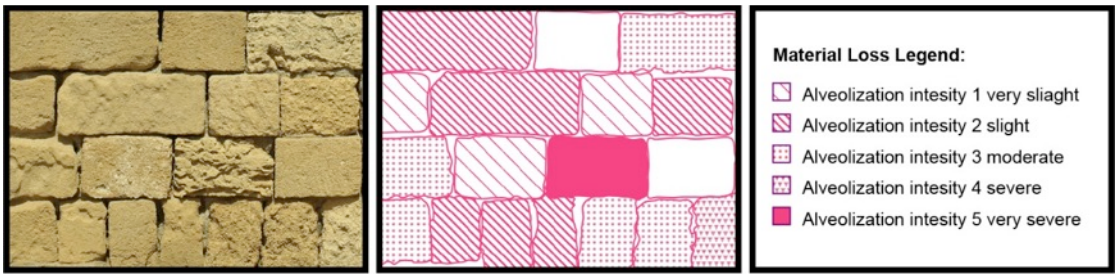


Figure 79: Example of a mapped area on Nailac Pier. From the left: high-resolution image, material loss map, and patterns legend

## 4.3. Granada (S. Jerónimo Monastery, Puerta Elvira)

In Granada the deterioration patterns of loss material were analysed following the methodology of Jalón et al. 2021 [3]. The masonry stone has been analysed in San Jerónimo Monastery, classified as Tier 1, the degradation patterns of the bricks have been identified in the CH Puerta Elvira.

### 4.3.1. Material loss

#### *S. Jerónimo Monastery*

As an example, the main façade is analyzed (Figure 80). In Figure 81, the measured deterioration profiles (S1, S2) of the main facade and its location are presented.

Figure 80: Main facade of San Jerónimo Monastery


Figure 81: Measured deterioration profiles (S1, S2) and its location [3]

Next, different deterioration patterns are considered: Bilinear, Triangular, and Square, and the relative likelihood of the candidate deterioration patterns are computed following the methodology explained in Jalón et al. (2021) [3]. The results are shown in Figure 82. Note that the Triangular Model was found to be the most suitable (P=0.518) to estimate the degradation of the main facade.

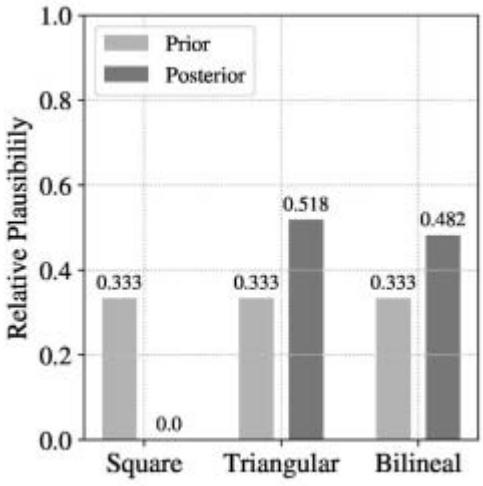


Figure 82: Degradation patterns ranking [3]

Figure 83 represents the measured deterioration profiles (S1, S2), the posterior mean deterioration pattern, and the confidence intervals (P5, P25 , P75, P95) for the Triangular model.

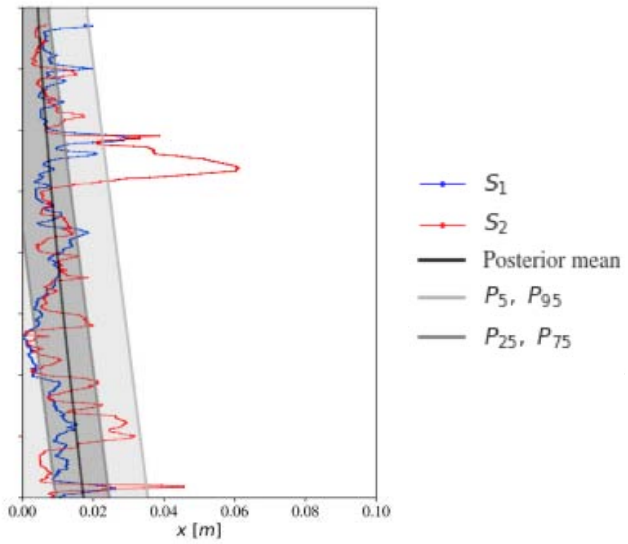


Figure 83: Measured degradation profiles (S1, S2), posterior mean degradation pattern, and confidence intervals (P5, P25 , P75, P95) for the triangular model [3]

Finally, the prediction of the deterioration tren over the next 500 years has been proposed by assuming a constant recession rate over the five centuries of the building [3]. Figure 84 represents the prognosticated average deterioration at different times of the main façade of San Jerónimo Monastery.

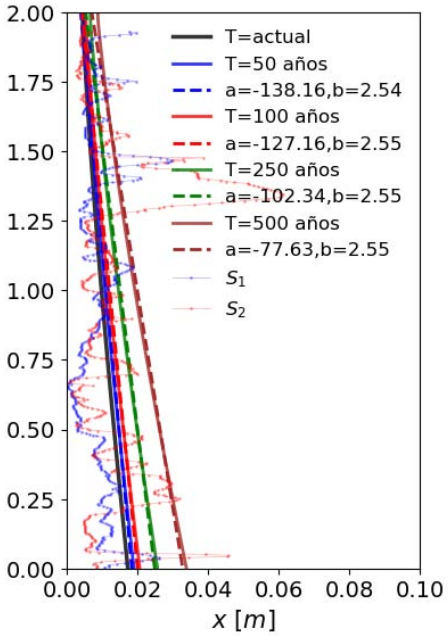


Figure 84: Prognosticated average deterioration behaviour at different times

## *Puerta Elvira*

This CH is a fortress constructed with rammed earth and bricks during different periods starting from the 9$^{th}$ century.

For that, the deterioration profiles of the CH asset are taken from the geometrical 3D data known as Photogrammetric Point Cloud (PPC). Four sections separated by 50

cm each are obtained out of the PPC and are represented as relative distances. Figure 85 represents the PPC and the selected sections.

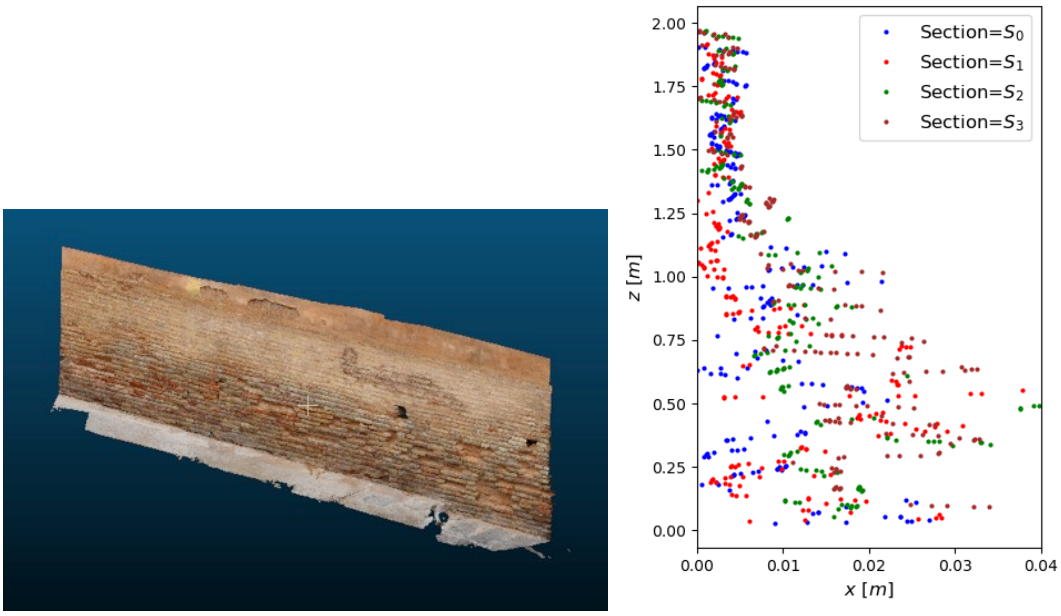


Figure 85: Photogrammetric point cloud (left), sections of Puerta Elvira (right)

As an example, Puerta Elvira is analyzed by adopting a candidate deterioration pattern: Square model. In Figure 86, the measured deterioration profiles (S0, S1, S2, S3), the candidate deterioration pattern and their confidence intervals are presented. The heterogeneity and complexity of the measured degradation profiles are noteworthy.

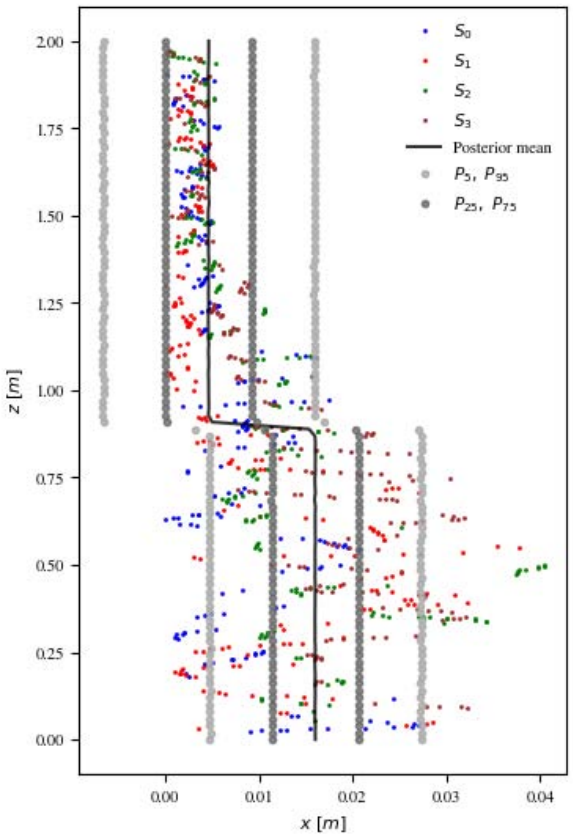


Figure 86: Measured deterioration profiles ($S_0$,$S_1$, $S_2$, $S_3$), posterior average deterioration pattern, and confidence intervals ($P_5$, $P_{25}$ , $P_{75}$, $P_{95}$)

## 4.4. Tønsberg

The exterior side of the building components that is treated with tar was not colonized by mold. In contrast, at the untreated planks of the coating-shed of the Fadum storehouse colonization was observed. As can be seen in Figure 87, the north-oriented side of the coating was the most aggravated. Moreover, fungal growth was detected at the interior of the two buildings. In the Fadum storehouse, brown-rot fungi (*Coniophora puteana*) was detected in the north-oriented side of both the roof and the coating (Figure 88a). The fungus was identified based on its fruiting body. *Coniophora puteana* is a wood-destroying fungus that breaks down the hemicellulose and cellulose. The rotting fungus grew in positions with leaks in which the rainwater had penetrated. The infected building elements were untreated planks. In the Heierstad loft, fungal growth was detected at the inner side of the northeast-oriented wall of the upper level and on the ceiling of the ground floor (Figure 88). The infected surfaces were untreated logs.

Figure 87: At the Fadum storehouse, the growth of biological organisms is more intense on the north façade (left) than on the south façade (right)

Apart from the fungi grown on the building components, samples of airborne fungal spores were also collected. In Figure 89, the position from which the aerosol samples were collected, as well as the fungi colonies grown three days after the samples collection, are shown. As has already been mentioned in Section 2.2, two different growth media were used in the plates. This is because some species of fungi grow favourably on malt agar, while others on DG-18 agar. Moreover, quantitative microbial concentrations were estimated for the culturable fungi colonies as colony forming units per air volume (CFU/$m^3$) (Figure 90). As can be seen in Figure 89 and Figure 90, the smallest fungal concentration was observed outdoors. According to the same figures, in the ground level of the Fadum storehouse, the concentration the airborne fungal spores was at acceptable levels, with values lower than 500 CFU/$m^3$, which is the threshold defined by the World Health Organization (WHO) for noncontaminated indoor air [24]. On the upper level of the Fadum storehouse, on the ground level of the Heierstad loft, and on the upper level of the Heierstad loft, the concentration of the airborne fungal spores was extremely high, exceeding by far the maximum acceptable limit of the WHO (Figure 90).

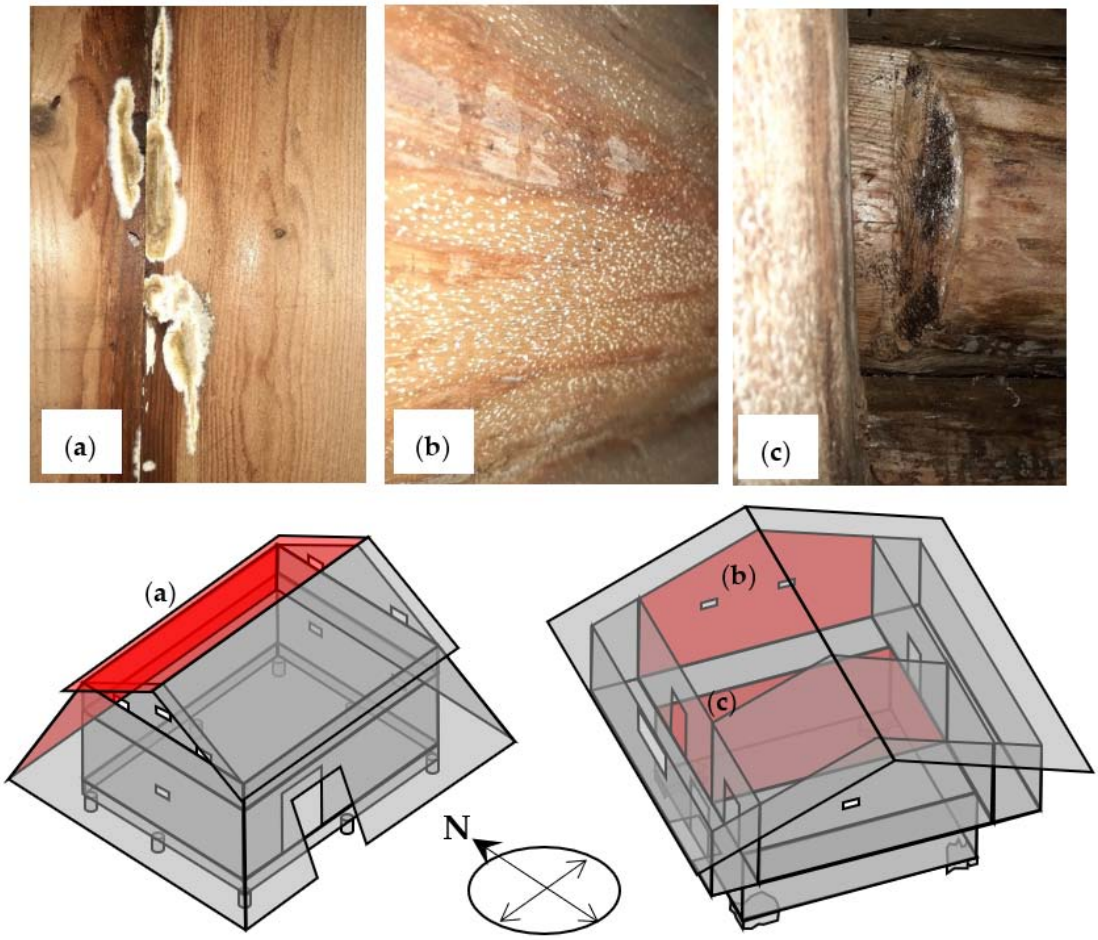


Figure 88: (a) Brown-rot fungi (*Coniophora puteana*) detected at the positions highlighted with red color at the Fadum storehouse. (b) *Scopulariopsis* colonies and (c) *Myxomycetes* detected at the positions highlighted with red color at the Heierstad loft

In addition, identification of microfungi grown on the plates was performed by using optical microscopy (Figure 91). In Table 32, the microfungi species found in each of the two buildings are presented. The identified microfungi (Figure 91 and Table 32) in the concentrations that were found (Figure 90) can cause irritation of the eyes and respiratory tract, headache, drowsiness, skin rash, and itching of the skin, or even allergies and more ad-verse human diseases [25].

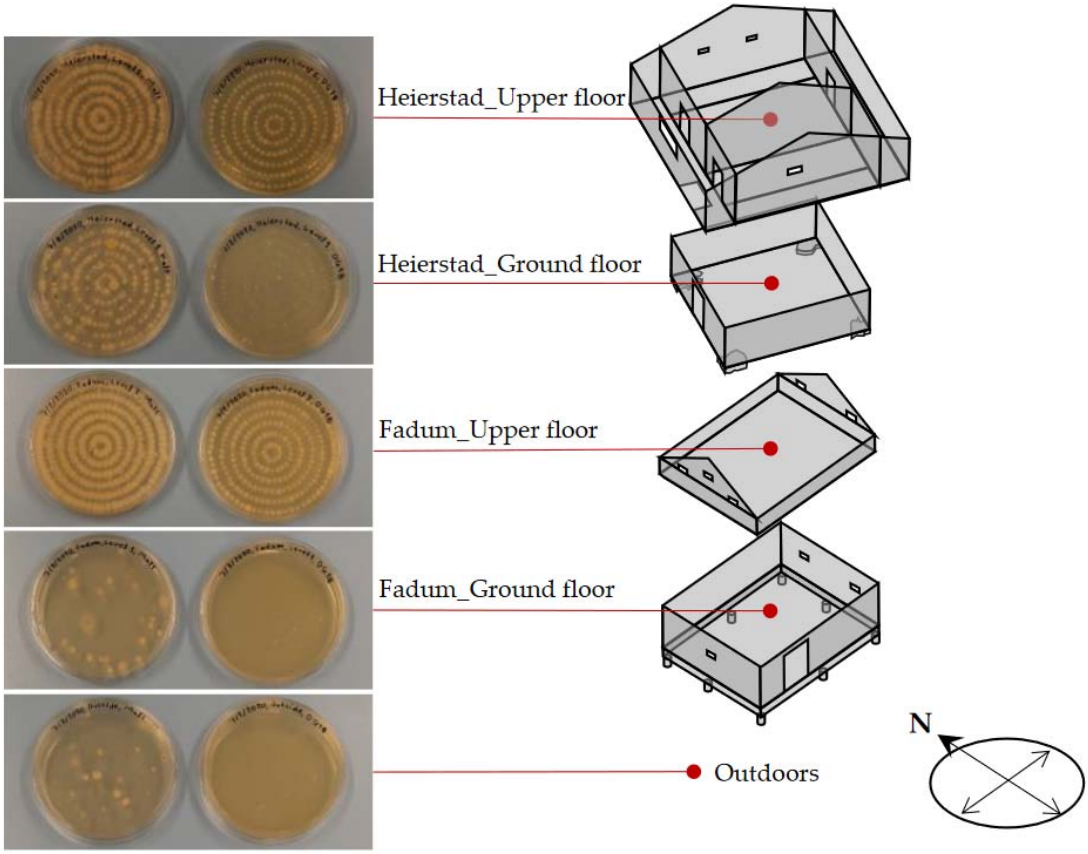


Figure 89: Positions of aerosol sampling and fungi colonies grown after 3 days at 25 °C on malt agar (plates on the left side of the pictures) and on DG-18 agar (plates on the right side of the pictures)

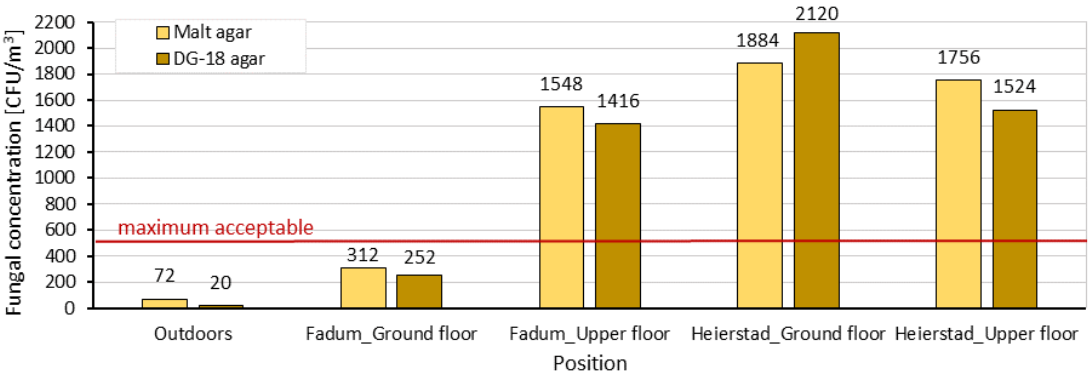


Figure 90: Fungal concentration in the two case studies considering the number of colony forming units found on the plates

The maximum acceptable value of 500 CFU/m3 for noncontaminated indoor environments [43] is highlighted with the red line.

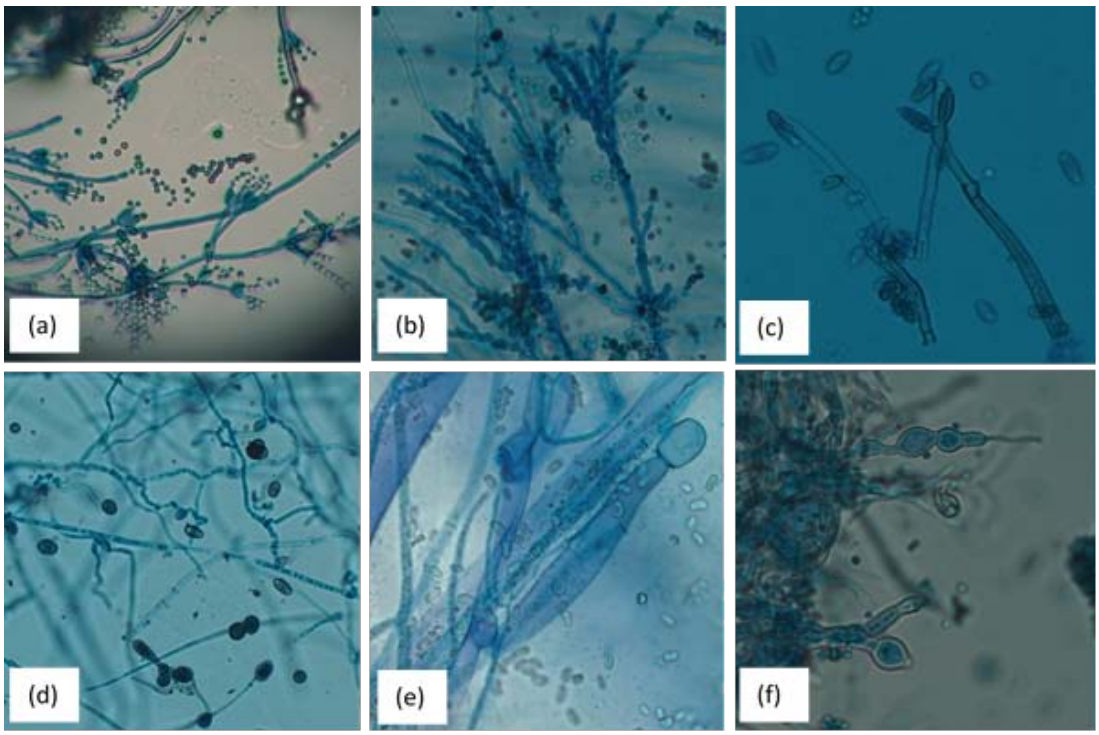


Figure 91: Fungal structures of (a) *Penicillium spp*., (b) *Aureobasidium spp*., (c) *Cladosporium spp*., (d) *Alternaria spp*., (e) *Mucor spp*., and (f) *Scopulariopsis spp*. after methylene blue staining

Table 32: Fungi genera identified from the samples collected from the two case studies

| Fungi Genera | Fadum Storehouse | Heierstad Loft |
|---|---|---|
| ***Penicillium spp.*** | ✓ | ✓ |
| ***Aureobasidium spp.*** | ✓ | ✓ |
| ***Cladosporium spp.*** | ✓ | ✓ |
| ***Alternaria spp.*** | ✓ | ✓ |
| ***Scopulariopsis spp.*** | ✓ | ✓ |
| ***Mucor spp.*** | ✓ | |

# 5. Conclusion

This deliverable contains all the field and laboratory data collected through a detailed analyzing procedure. Data are related to both specific building materials selected for laboratory tests and samples collected on significant architectures (Tier 1 and 2) of the Pilot sites. In this second case, also the deterioration morphologies and products were considered and analytically characterized. Data presented in the current deliverable will be entered into the HYPERION system as a starting point for further analysis and modeling and will implement the integrated HT simulator and the HRAP system

Building materials as well as their deterioration morphologies and products of the Tier 1 and 2 selected buildings were also mapped following different procedures chosen on the basis of significance, typology of materials (i.e. stone, timber, rammed earth) and accessibility of the building itself. The obtained maps, which will be available to the scientific community and all the stakeholders, will become a useful reference tool for further investigations related to the prediction of the evolution of the building materials' decay in relation to climate change.

# 6. REFERENCES

1. Choidis, P., Kraniotis, D., Lehtonen, I., & Hellum, B. (2021). A Modelling Approach for the Assessment of Climate Change Impact on the Fungal Colonization of Historic Timber Structures. *Forests*, *12*(7). https://doi.org/10.3390/f12070819

2. Nimis, P., Monte, M., & Mauro, T. (1987). Flora e Vegetazione Lichenica di Aree Archeologiche del Lazio. *Studia Geobotanica*, *7*, 3–161.

3. Jalón, M. L., Chiachío, J., Gil-Martín, L. M., & Hernández-Montes, E. (2021). Probabilistic identification of surface recession patterns in heritage buildings based on digital photogrammetry. *Journal of Building Engineering*, *34*, 101922. https://doi.org/10.1016/j.jobe.2020.101922

4. Le Maitre, R. W., Streckeisen, A., Zanettin, B., Bas, M. J. L., Bonin, B., & Bateman, P. (2005). *Igneous Rocks: A Classification and Glossary of Terms: Recommendations of the International Union of Geological Sciences Subcommission on the Systematics of Igneous Rocks*. (R. W. Le Maitre, Ed.). Cambridge University Press.

5. Whitney, D. L., & Evans, B. W. (2009). Abbreviations for names of rock-forming minerals. *American Mineralogist*, *95*(1), 185–187. https://doi.org/10.2138/am.2010.3371

6. Fettes, D. J., Desmons, J., Árkai, P., Sciences., I. U. of G., & Rocks., S. on the S. of M. (2011). *Metamorphic rocks : a classification and glossary of terms : recommendations of the International Union of Geological Sciences Subcommission on the Systematics of Metamorphic Rocks*. Cambridge; New York: Cambridge University Press.

7. Folk, R. L. (1962). Spectral Subdivision on Limestone Types, Classification of Carbonate Rocks-A Symposium Mem.

8. Dunham, R. J. (1962). Classification of Carbonate Rocks According to Depositional Texture: in Northern Iraq. *Arabian Gulf, Geology and Productivity. AAPG, Foreign Reprint Series*, (2).

9. Embry, A. F., & Klovan, J. E. (1971). A late Devonian reef tract on northeastern Banks Island, NWT. *Bulletin of Canadian petroleum geology*, *19*(4), 730–781.

10. Navarro, R., Molina, E., & Baltuille, J. M. (2013). The relevance of "Santa Pudia" calcarenite: a natural stone to preserve heritage buildings in Andalusia (Spain). *Geophysical Research Abstracts*, *15*(EGU2013-4297–2).

11. Alcalde Moreno, M., Bello López, M., Martín García, L., & Martín Pérez, A. (1992). Macroscopical morphology of deterioration of the stone used in the cathedral whole of Granada (Spain). *Materiales de construcción, Vol. 42, n$^{o}$ 226, p. 23-30*, *42*.

12. Zuffa, G. (1980). Hybrid Arenites: Their Composition and Classification. *Journal of Sedimentary Research - J SEDIMENT RES*, *50*. https://doi.org/10.1306/212F7950-2B24-11D7-8648000102C1865D

13. Antonelli, F., & Lazzarini, L. (2015). An updated petrographic and isotopic reference database for white marbles used in antiquity. *Rendiconti Lincei*, *26*(4), 399–413. https://doi.org/10.1007/s12210-015-0423-4

14. Cultrone, G., Rodriguez-Navarro, C., Sebastian, E., Cazalla, O., & De La Torre, M. J. (2001). Carbonate and silicate phase reactions during ceramic firing. *European Journal of Mineralogy*, *13*(3), 621–634. https://doi.org/10.1127/0935-1221/2001/0013-0621

15. Maritan, L., Nodari, L., Mazzoli, C., Milano, A., & Russo, U. (2006). Influence of firing conditions on ceramic products: Experimental study on clay rich in organic matter. *Applied Clay Science*, *31*(1–2), 1–15. https://doi.org/10.1016/j.clay.2005.08.007

16. Antonelli, F., Cancelliere, S., & Lazzarini, L. (2002). Minero-petrographic characterisation of historic bricks in the Arsenale, Venice. *Journal of Cultural Heritage*, *3*(1), 59–64. https://doi.org/10.1016/S1296-2074(02)01160-3

17. Schiavon, N., Mazzocchin, G. A., & Baudo, F. (2008). Chemical and mineralogical characterisation of weathered historical bricks from the Venice lagoonal environment. *Environmental Geology*, *56*(3–4), 767–775. https://doi.org/10.1007/s00254-008-1481-z

18. Duminuco, P., Messiga, B., & Riccardi, M. P. (1998). Firing process of natural clays. Some microtextures and related phase compositions. *Thermochimica Acta*, *321*(1–2), 185–190. https://doi.org/10.1016/s0040-6031(98)00458-4

19. Zirkelbach, D., Schmidt, T., Kehrer, M., & Künzel, H. M. (2007). *WUFI® Pro 5 Manual*. Retrieved from https://wufi.de/download/WUFI-Pro-5_Manual.pdf%5Cnhttps://wufi.de/en/wp-content/uploads/sites/11/2014/09/WUFI-Pro-5_Manual.pdf

20. ICOMOS. (2008). *ICOMOS-ISCS: Illustrated glossary on stone deterioration patterns*. (V. Vergès-Belmin, Ed.) (XV.). Paris, France: ICOMOS.

21. Fitzner, B., & Heinrichs, K. (2001). Damage diagnosis at stone monuments - Weathering forms, damage categories and damage indices. *Acta Universitatis Carolinae, Geologica*, *45*(1), 12–13.

22. Tesser, E. (2008). *Funghi meristematici su Pietra d'Istria: prove comparative di pulitura*. Università Ca' Foscari.

23. Nimis, P. (2016). *The Lichens of Italy. A Second Annotated Catalogue*.

24. Heseltine, E., & Rosen, J. (2009). WHO Guidelines for Indoor Air Quality: Dampness and Mould. (L. N. Soldatova, P. Rocca-Serra, M. Dumontier, & N. H. Shah, Eds.)*World Health Organization Regional Office for Europe*, *5*. https://doi.org/10.1186/2041-1480-5-S1-I1

25. Baxi, S. N., Portnoy, J. M., Larenas-Linnemann, D., Phipatanakul, W., behalf of the Environmental Allergens Workgroup, on, Barnes, C., … Brock Williams, P. (2016). Exposure and Health Effects of Fungi on Humans HHS Public Access. *J Allergy Clin Immunol Pract*, *4*(3), 396–404. https://doi.org/10.1016/j.jaip.2016.01.008

# 7. ANNEXES

## Annex 1: Samples lists

**A. Venice Clock Tower**
**B. Santa Maria dei Servi Church**

## Annex 2: Venice Clock Tower lithological map

a. **South façade**
b. **East façade**
c. **West façade**

## Annex 3: Venice Clock Tower decay morphologies maps

**A. Crack & deformation**
   a. South façade
   b. East façade
   c. West façade
**B. Detachment**
   a. South façade
   b. East façade
   c. West façade
**C. Features induced by material loss**
   a. South façade
   b. East façade

   c. West façade

**D. Discoloration & deposit**

   a. South façade
   b. East façade
   c. West façade

**E. Biological colonization**

   a. South façade
   b. East façade
   c. West façade

**F. TDI**

   a. South façade
   b. East façade
   c. West façade

# Annex 4: Rhodes Tier 1 buildings material loss maps

**A. Nailac Pier**

**B. Saint Nikolas lighthouse**

# ANNEX 1A

| List of sample from the Venice Clock Tower | | | | | | | | | | | |
|---|---|---|---|---|---|---|---|---|---|---|---|
| **N.** | **Material** | **Sampling location** | **Sampling image** | **Sample stereomicroscope photos** | **Analyses** | | | | | | |
| | | | | | IC | XRPD | PLOM | FTIR | SEM-EDS | Bio |
| **Mori's Terrace – NORTH Façade** | | | | | | | | | | | |
| **TdO_1N** | Stone | Second step under the Mori |   |  | | **X** | **X** | | | **X** |
| **TdO_2N** | Stone + green and black patinas | First step under the Mori (E side) |  |  | | **X** | **X** | **X** | **X** | |
| **TdO_3N** | Stone | From a small column of the N balustrade of the Mori's terrace |   |  | | **X** | **X** | | | |
| **TdO_4N** | Stone + green patina | First step under the Mori (W side) |   |  | | **X** | **X** | | **X** | |
| **WEST Wing Walkway** | | | | | | | | | | | |
| **TdO_1W** | Stone | Stony shelf at the W end |   |  | | **X** | **X** | | **X** | **X** |

| List of sample from the Venice Clock Tower | | | | | | | | | | | |
|---|---|---|---|---|---|---|---|---|---|---|---|
| **N.** | **Material** | **Sampling location** | **Sampling image** | **Sample stereomicroscope photos** | **Analyses** | | | | | | |
| | | | | | IC | XRPD | PLOM | FTIR | SEM-EDS | Bio |
| **TdO_2W** | Biologic patina | From the S balustrade |   |  | | | | | | **X** |
| **TdO_3W** | Biologic patina | From the N balustrade |   | 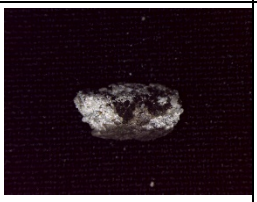 | | | | | | **X** |
| **TdO_4W** | Organic patina (powder) | From the crystalline marble hexagonal mural slab (N side) |  |  | | **X** | | **X** | | |
| **TdO_5W** | Stone | From a small column of the S balustrade | 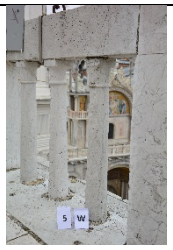 |  | **X** | **X** | **X** | | **X** | |
| **TdO_7W** | Organic patina (powder) | From the crystalline marble hexagonal mural slab (S side) |  |  | | **X** | | **X** | | |
| **TdO_8W** | Stone | From the jamb of the door |  |  | | **X** | **X** | | **X** | |
| **EAST Wing Walkway** | | | | | | | | | | | |

| List of sample from the Venice Clock Tower | | | | | | | | | | | |
|---|---|---|---|---|---|---|---|---|---|---|---|
| N. | Material | Sampling location | Sampling image | Sample stereomicroscope photos | Analyses | | | | | | |
| | | | | | IC | XRPD | PLOM | FTIR | SEM-EDS | Bio |
| **TdO_1E** | Stone | From the stone mural slab (N side) | 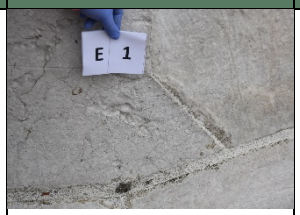  |  | | **X** | **X** | | **X** | |
| **TdO_2E** | Stone | From the crystalline marble hexagonal mural slab (N side) |   |  | | | **X** | | | |
| **TdO_3E** | Stone | From a pillar of the N balustrade, near the door |  |  | | **X** | **X** | | **X** | |
| **TdO_4E** | Stone | From the arch of the doorframe |  |  | | **X** | **X** | | | |
| **TdO_5E** | Stone | From a small column of the S balustrade |   |  | | **X** | **X** | | **X** | |
| **TdO_6E** | Black deposit | From the crystalline marble hexagonal mural slab (S side) |  |  | | **X** | **X** | **X** | | **X** |
| **TdO_7E** | Powder | From a small column of the S balustrade |   |  | **X** | **X** | | | | |

| List of sample from the Venice Clock Tower | | | | | | | | | | | |
|---|---|---|---|---|---|---|---|---|---|---|---|
| N. | Material | Sampling location | Sampling image | Sample stereomicroscope photos | Analyses | | | | | | |
| | | | | | IC | XRPD | PLOM | FTIR | SEM-EDS | Bio | |
| **TdO_8E** | Powder | From a small column of the S balustrade |   |  | **X** | **X** | | | | | |
| **TdO_9E** | Biologic patina | From the top handrail of the S balustrade | 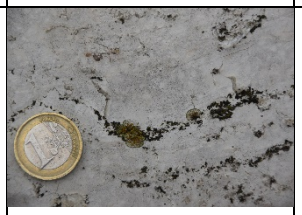 |  | | | | | | **X** | |
| **TdO_10E** | Biologic patina | From the top handrail of the S balustrade |   | 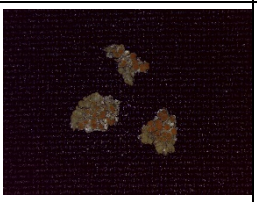 | | | | | | **X** | |
| **TdO_11E** | Biologic patina | From the top handrail of the S balustrade |  | 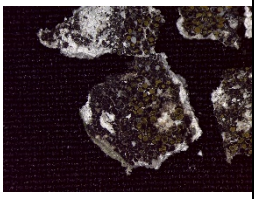 | | | | | | **X** | |
| **TdO_12E** | Biologic material | From the flooring of the walkways |  |  | | | | | | **X** | |
| **SOUTH Façade - Ground Floor** | | | | | | | | | | | |
| **TdO_1S** | Stone + patina | From the E column of the central archway |   |  | | **X** | **X** | **X** | | | |

| List of sample from the Venice Clock Tower | | | | | | | | | | | |
|---|---|---|---|---|---|---|---|---|---|---|---|
| N. | Material | Sampling location | Sampling image | Sample stereomicroscope photos | Analyses | | | | | |
| | | | | | IC | XRPD | PLOM | FTIR | SEM-EDS | Bio |
| **TdO_2S** | Black crust | From the second pillar of the E wing |  | 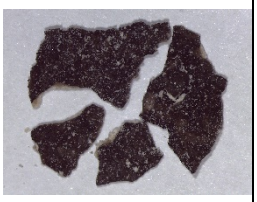 | **X** | **X** | | | **X** | |
| **TdO_3S** | Organic patina | From the third column of the E wing |  |  | | | | **X** | | |
| **TdO_4S** | Black crust | From the Corinthial capital of the second semi-column of the E wing |  | 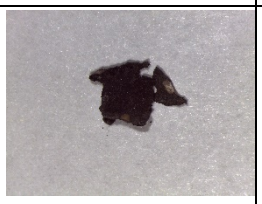 | | **X** | | | **X** | |
| **TdO_5S** | Black crust | From the Corinthial capital of the forth column of the W wing |  |  | **X** | **X** | | | **X** | |

# ANNEX 1B

| List of samples from the main façade of the Santa Maria dei Servi Church | | | |
|---|---|---|---|
| **Labelling** | **Material** | **Color** | **Sample image** |
| A1 | brick | yellow-red |  |
| A2 | brick | yellow-red |  |
| A3 | brick | red |  |
| A4 | brick | yellow-green |  |
| A5 | brick | red |  |
| A6 | brick | red |  |
| A7 | brick | light red-pink |  |
| A8 | brick | yellow-green |  |

| List of samples from the main façade of the Santa Maria dei Servi Church | | | |
|---|---|---|---|
| **Labelling** | **Material** | **Color** | **Sample image** |
| A9 | brick | light red-pink |  |
| A10 | brick | yellow |  |
| A11 | brick | yellow-green |  |
| A13 | brick | light red |  |
| B2 | brick | yellow-green |  |
| B3 | brick | red |  |
| B5 | brick | red |  |
| B6 | brick | yellow |  |

| List of samples from the main façade of the Santa Maria dei Servi Church | | | |
|---|---|---|---|
| **Labelling** | **Material** | **Color** | **Sample image** |
| B7 | brick | Red |  |
| B8 | brick | red-light red |  |
| B9 | brick | pink |  |
| B10 | brick | light red |  |
| B11 | brick | yellow-green + black crust |  |
| C2 | brick | yellow-green |  |
| C3 | brick | red |  |

EAST FAÇADE

SOUTH FAÇADE

WEST FAÇADE

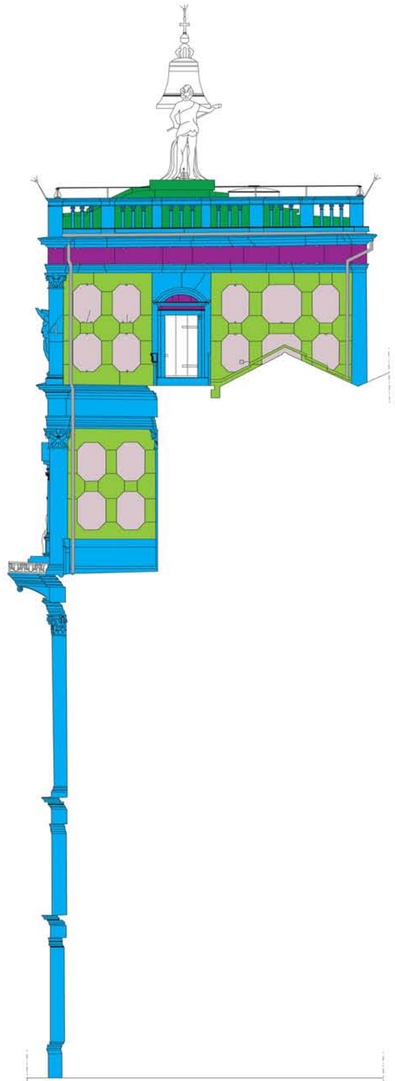

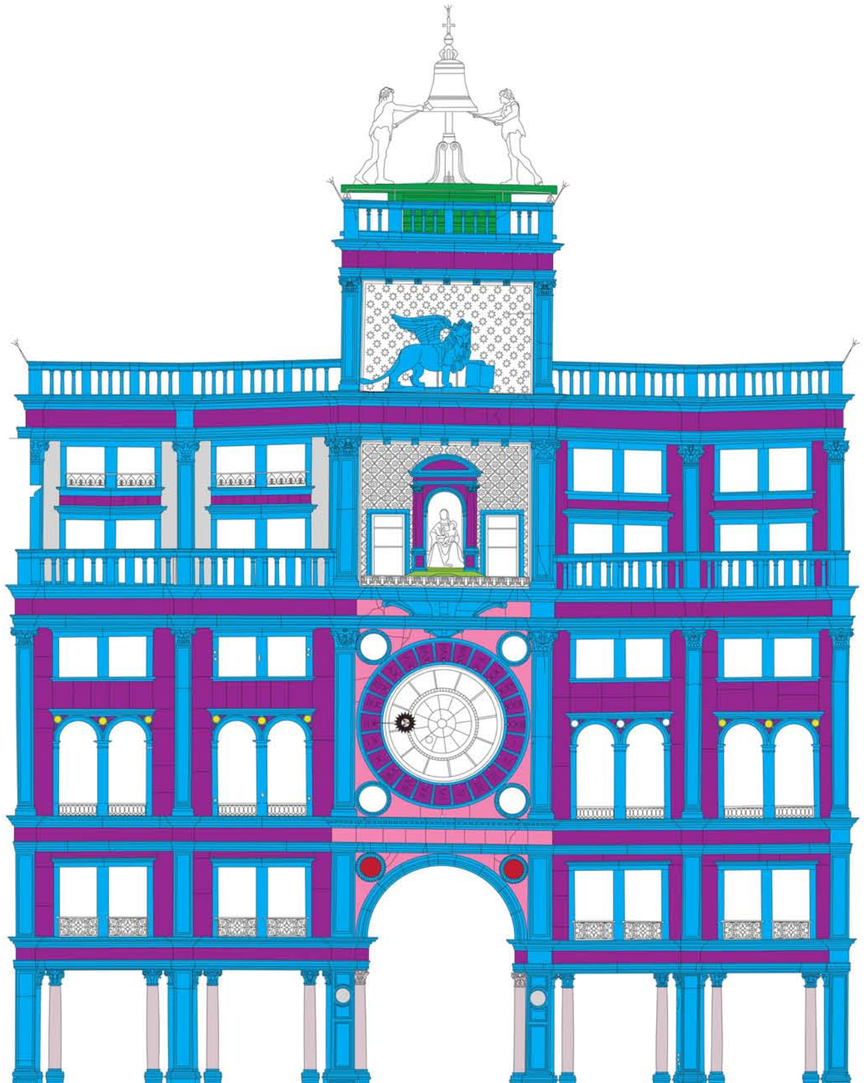

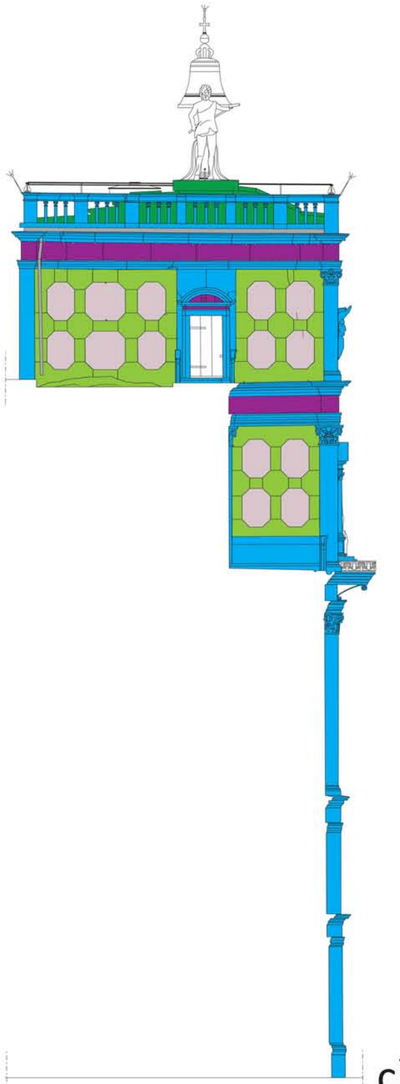

b)

a)

c)

**Rock Type Legend:**

- Red Verona Limestone
- *Pietra di Prun (Scaglia Rossa)*
- Istria Stone
- Proconnesian Marble
- Carrara Marble
- *Pavonazzetto Toscano* Marble
- Hematitic cataclastic limestone
- *Porfido Rosso Antico* - Imperial Porphyry
- Mortar-based materials

## EAST FAÇADE

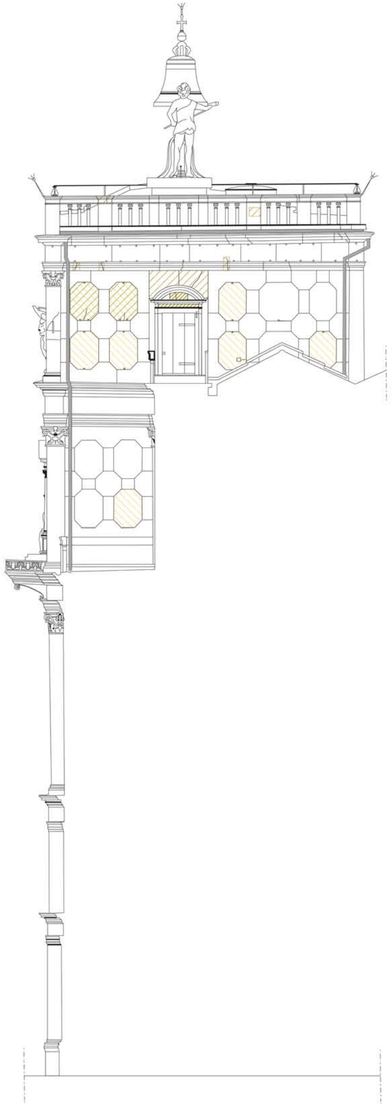

b)

## SOUTH FAÇADE

a)

## WEST FAÇADE

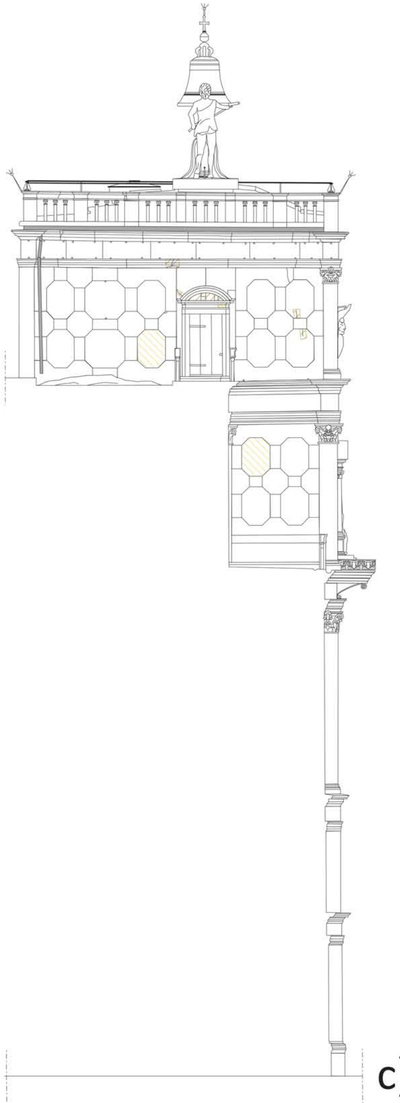

c)

**Crack & Deformation Legend:**

- Crack intesity 1 very slight (pag. 10)
- Crack intesity 2 slight (pag. 10)
- Crack intesity 3 moderate (pag. 10)
- Crack intesity 4 severe (pag. 10)
- Crack intesity 5 very severe (pag. 10)
- Deformation intesity 1 very slight (pag. 12)
- Deformation intesity 2 slight (pag. 12)
- Deformation intesity 3 moderate (pag. 12)
- Deformation intesity 4 severe (pag. 12)
- Deformation intesity 5 very severe (pag. 12)

## EAST FAÇADE

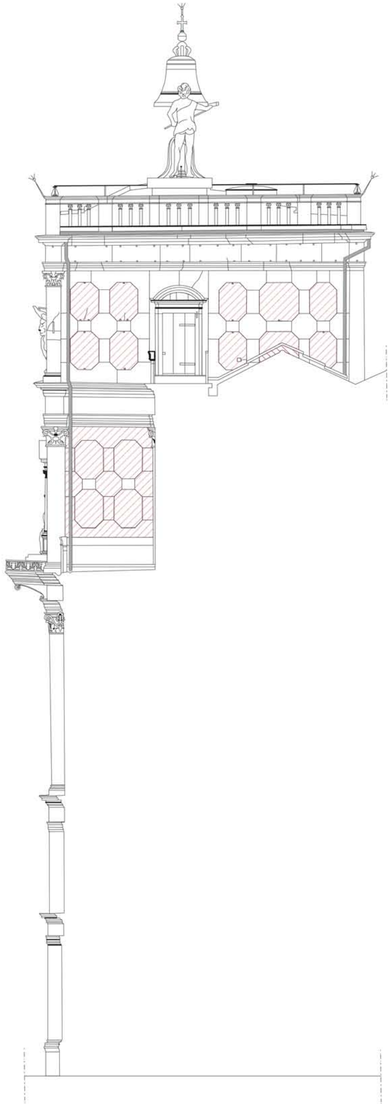

b)

## SOUTH FAÇADE

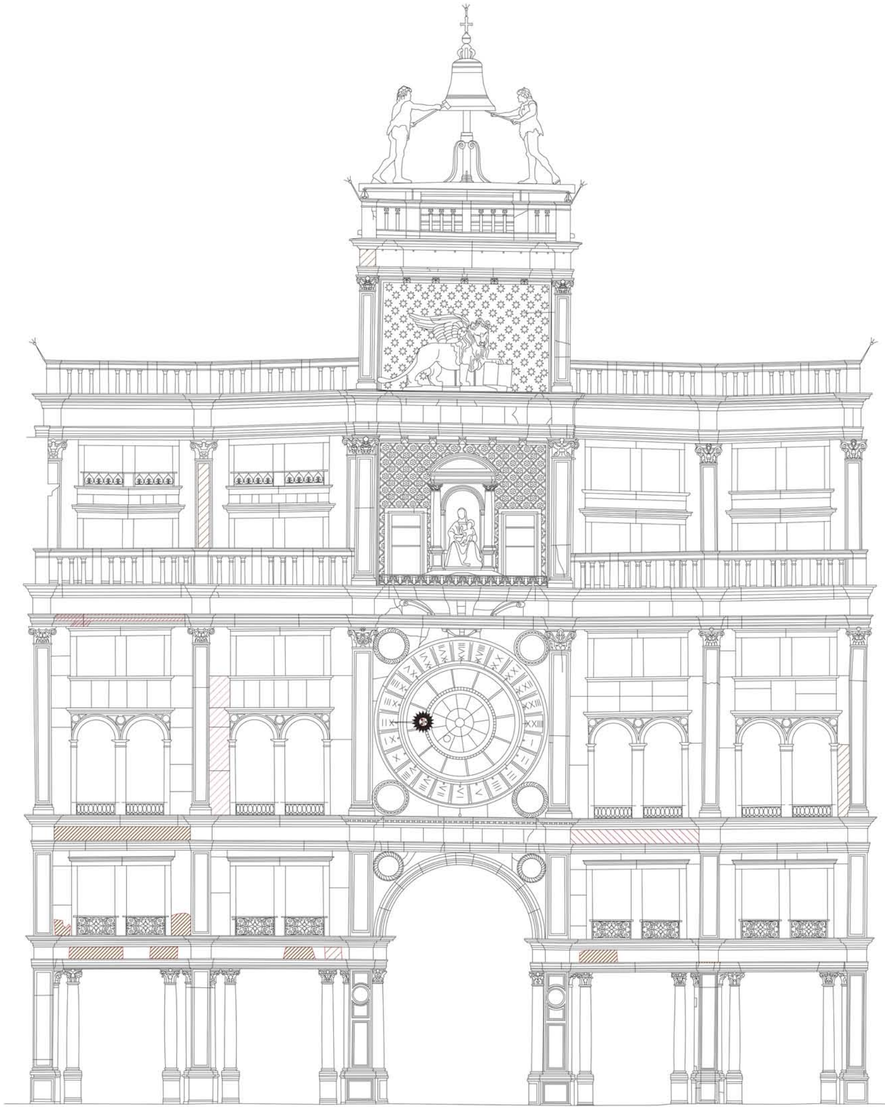

a)

## WEST FAÇADE

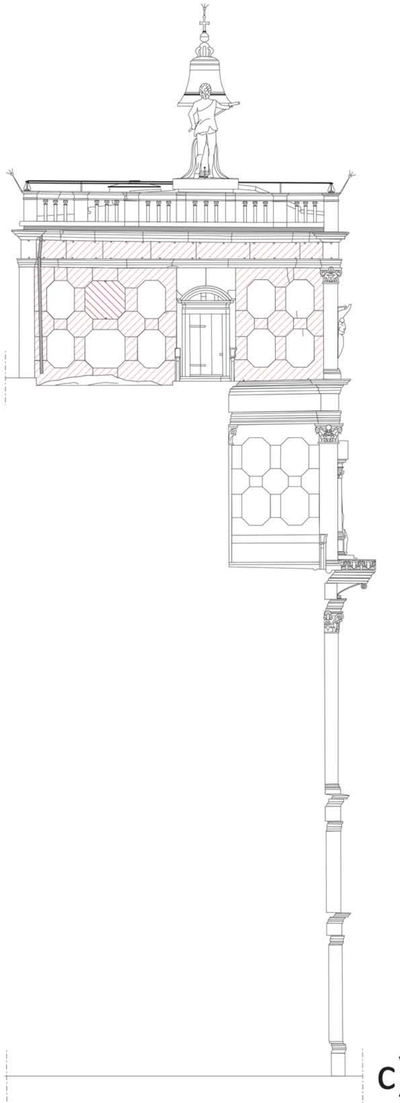

c)

**Detachment Legend:**

- Blistering intesity 1 very slight (pag. 14)
- Blistering intesity 2 slight (pag. 14)
- Blistering intesity 3 moderate (pag. 14)
- Blistering intesity 4 severe (pag. 14)
- Blistering intesity 5 very severe (pag. 14)
- Disintegration intesity 1 very slight (pag. 20)
- Disintegration intesity 2 slight (pag. 20)
- Disintegration intesity 3 moderate (pag. 20)
- Disintegration intesity 4 severe (pag. 20)
- Disintegration intesity 5 very severe (pag. 20)
- Peeling intesity 1 very slight (pag. 24)
- Peeling intesity 2 slight (pag. 24)
- Peeling intesity 3 moderate (pag. 24)
- Peeling intesity 4 severe (pag. 24)
- Peeling intesity 5 very severe (pag. 24)

## EAST FAÇADE

## SOUTH FAÇADE

## WEST FAÇADE

**Material Loss Legend:**

- Alveolization intesity 1 very slight (pag. 28)
- Alveolization intesity 2 slight (pag. 28)
- Alveolization intesity 3 moderate (pag. 28)
- Alveolization intesity 4 severe (pag. 28)
- Alveolization intesity 5 very severe (pag. 28)

- Erosion intesity 1 very slight (pag. 30)
- Erosion intesity 2 slight (pag. 30)
- Erosion intesity 3 moderate (pag. 30)
- Erosion intesity 4 severe (pag. 30)
- Erosion intesity 5 very severe (pag. 30)

- Mechanical damage intesity 1 very slight (pag. 32)
- Mechanical damage intesity 2 slight (pag. 32)
- Mechanical damage intesity 3 moderate (pag. 32)
- Mechanical damage intesity 4 severe (pag. 32)
- Mechanical damage intesity 5 very severe (pag. 32)

- Microkarst intesity 1 very slight (pag. 34)
- Microkarst intesity 2 slight (pag. 34)
- Microkarst intesity 3 moderate (pag. 34)
- Microkarst intesity 4 severe (pag. 34)
- Microkarst intesity 5 very severe (pag. 34)

- Missing part intesity 1 very slight (pag. 36)
- Missing part intesity 2 slight (pag. 36)
- Missing part intesity 3 moderate (pag. 36)
- Missing part intesity 4 severe (pag. 36)
- Missing part intesity 5 very severe (pag. 36)

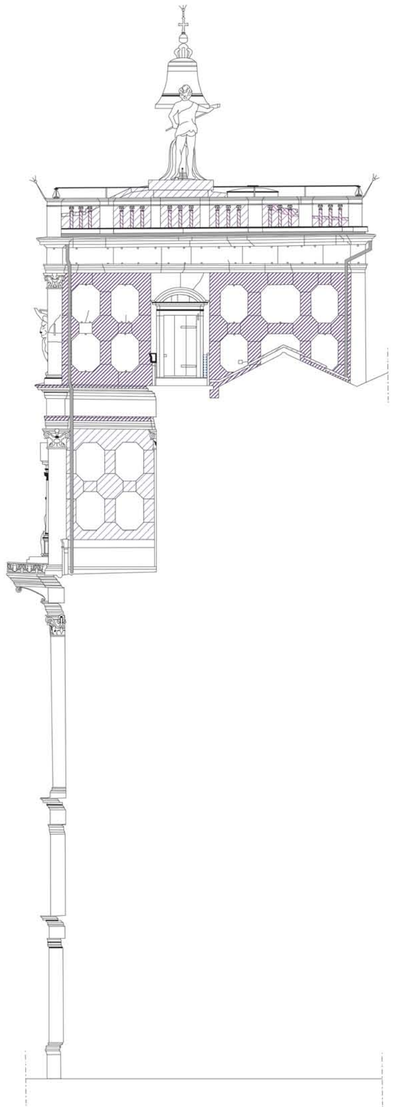

b)

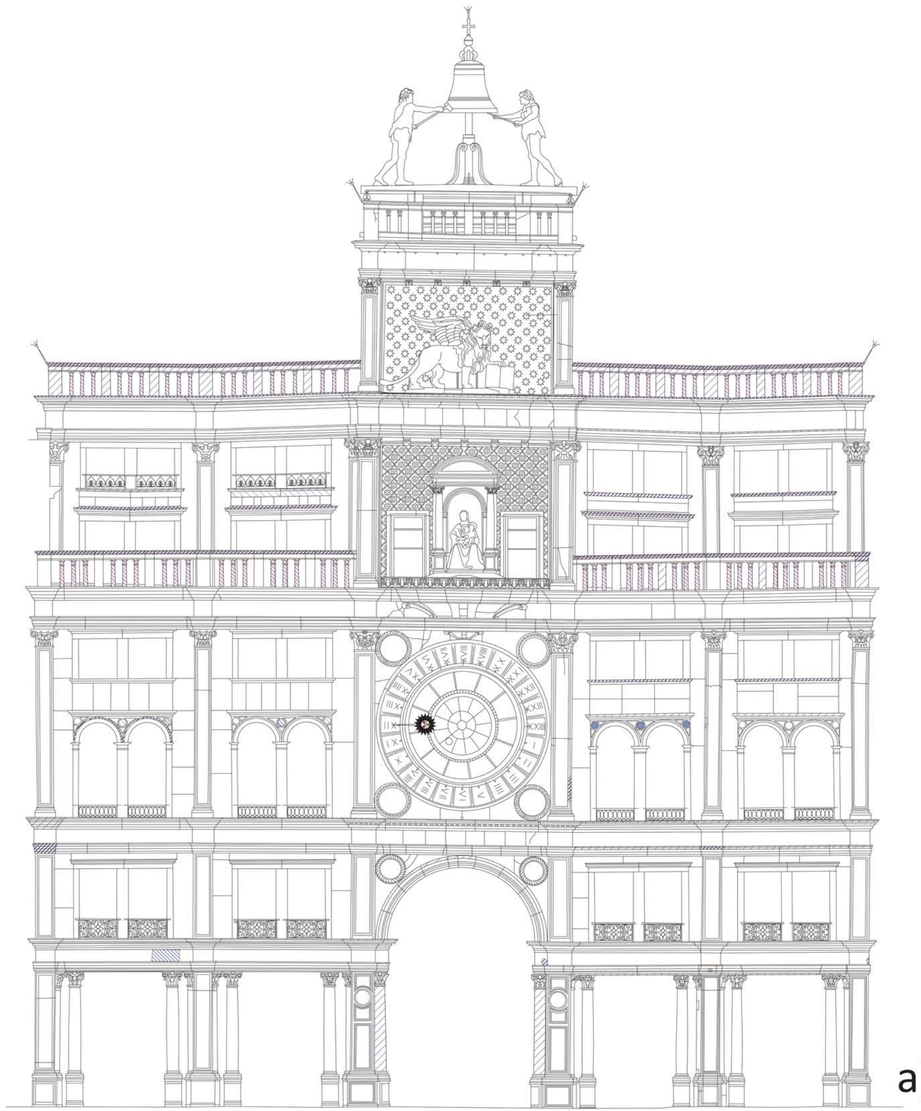

a)

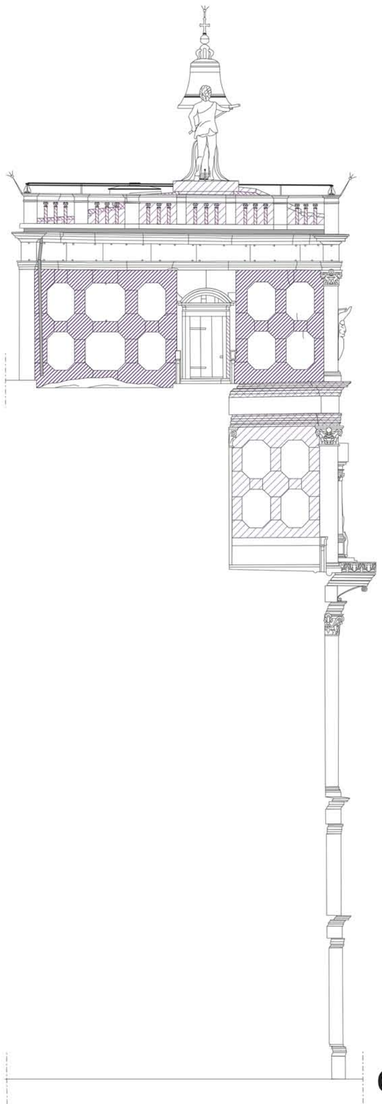

c)

**Discoloration & Deposit Legend:**

- Crust intesity 1 very slight (pag. 42)
- Crust intesity 2 slight (pag. 42)
- Crust intesity 3 moderate (pag. 42)
- Crust intesity 4 severe (pag. 42)
- Crust intesity 5 very severe (pag. 42)

- Bleaching intesity 1 very slight (pag. 46)
- Bleaching intesity 2 slight (pag. 46)
- Bleaching intesity 3 moderate (pag. 46)
- Bleaching intesity 4 severe (pag. 46)
- Bleaching intesity 5 very severe (pag. 46)

- Staining intesity 1 very slight (pag. 47)
- Staining intesity 2 slight (pag. 47)
- Staining intesity 3 moderate (pag. 47)
- Staining intesity 4 severe (pag. 47)
- Staining intesity 5 very severe (pag. 47)

- Efflorescence intesity 1 very slight (pag. 48)
- Efflorescence intesity 2 slight (pag. 48)
- Efflorescence intesity 3 moderate (pag. 48)
- Efflorescence intesity 4 severe (pag. 48)
- Efflorescence intesity 5 very severe (pag. 48)

- Graffiti intesity 1 very slight (pag. 56)
- Graffiti intesity 2 slight (pag. 56)
- Graffiti intesity 3 moderate (pag. 56)
- Graffiti intesity 4 severe (pag. 56)
- Graffiti intesity 5 very severe (pag. 56)

- Patina intesity 1 very slight (pag. 58)
- Patina intesity 2 slight (pag. 58)
- Patina intesity 3 moderate (pag. 58)
- Patina intesity 4 severe (pag. 58)
- Patina intesity 5 very severe (pag. 58)

- Soiling intesity 1 very slight (pag. 60)
- Soiling  intesity 2 slight (pag. 60)
- Soiling intesity 3 moderate (pag. 60)
- Soiling intesity 4 severe (pag. 60)
- Soiling intesity 5 very severe (pag. 60)

## EAST FAÇADE

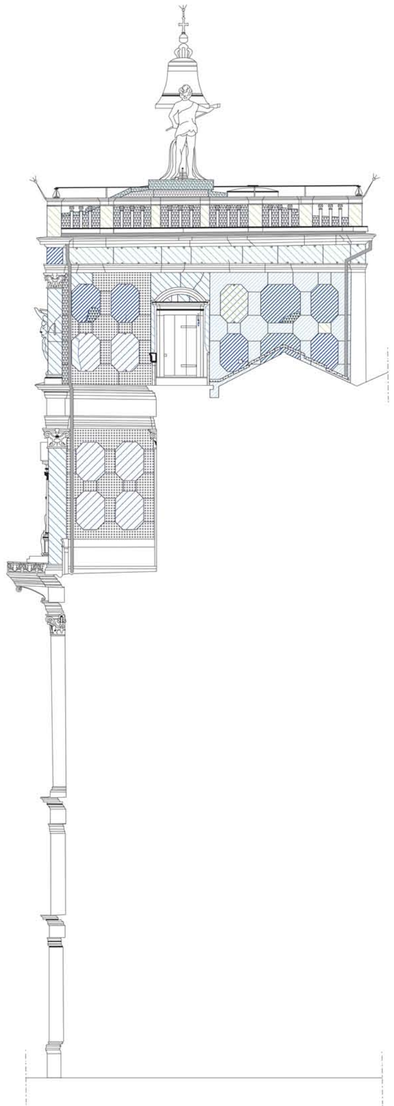

b)

## SOUTH FAÇADE

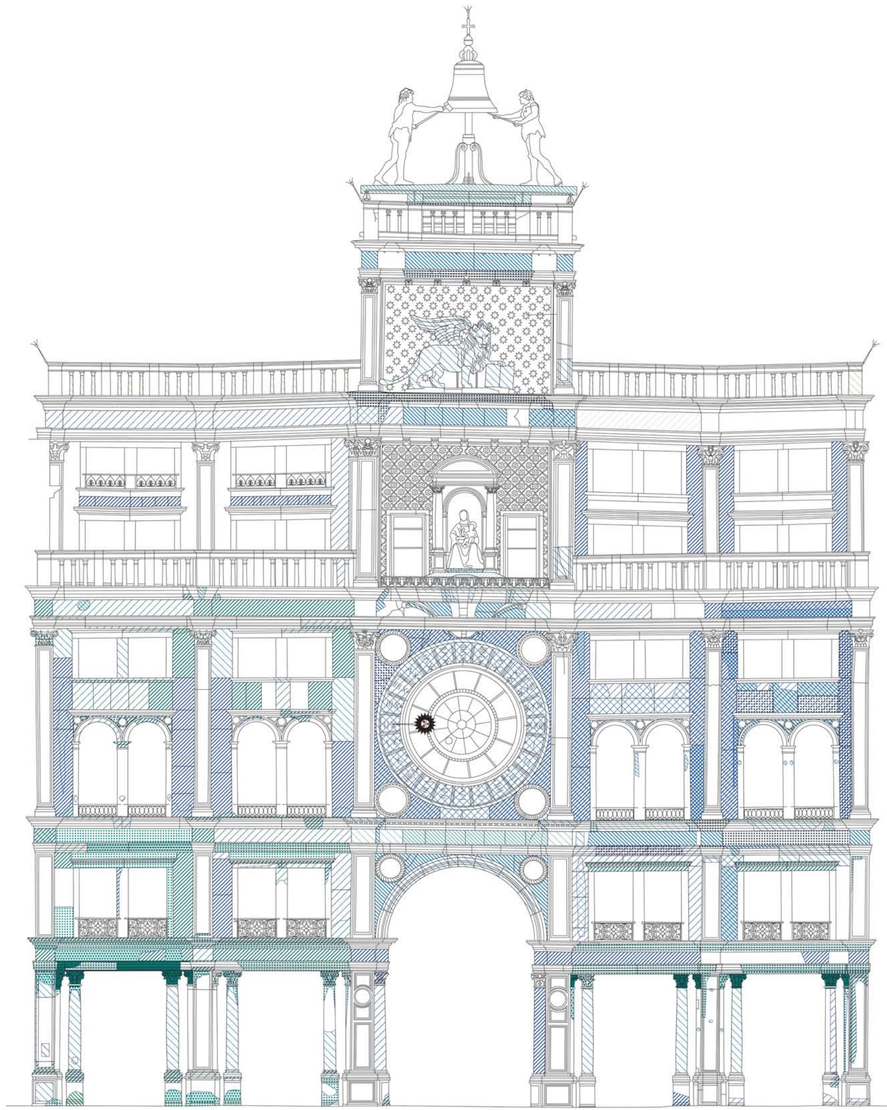

a)

## WEST FAÇADE

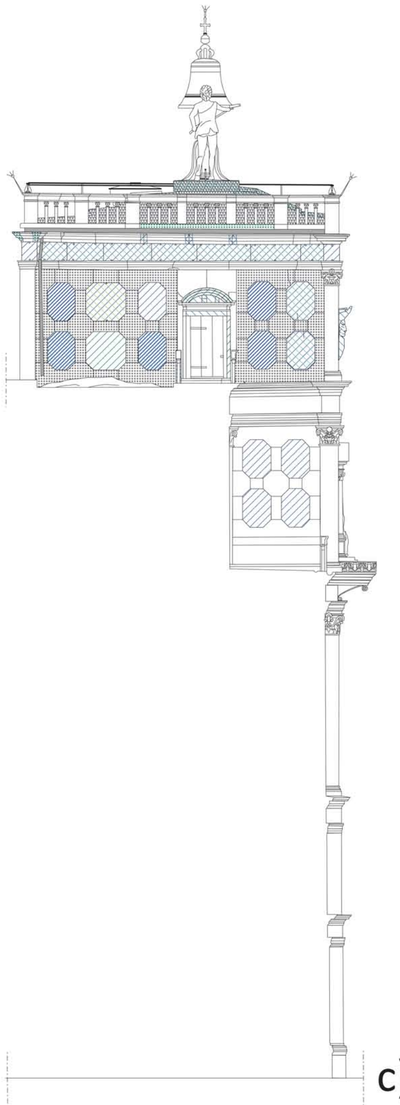

c)

**Biological Colonization Legend:**

- Fungi intesity 1 very slight (pag. 64)
- Fungi intesity 2 slight (pag. 64)
- Fungi intesity 3 moderate (pag. 64)
- Fungi intesity 4 severe (pag. 64)
- Fungi intesity 5 very severe (pag. 64)
- Lichen intesity 1 very slight (pag. 68)
- Lichen intesity 2 slight (pag. 68)
- Lichen intesity 3 moderate (pag. 68)
- Lichen intesity 4 severe (pag. 68)
- Lichen intesity 5 very severe (pag. 68)
- Moss intesity 1 very slight (pag. 70)
- Moss intesity 2 slight (pag. 70)
- Moss intesity 3 moderate (pag. 70)
- Moss intesity 4 severe (pag. 70)
- Moss intesity 5 very severe (pag. 70)
- Plant intesity 1 very slight (pag. 74)
- Plant intesity 2 slight (pag. 74)
- Plant intesity 3 moderate (pag. 74)
- Plant intesity 4 severe (pag. 74)
- Plant intesity 5 very severe (pag. 74)

## EAST FAÇADE

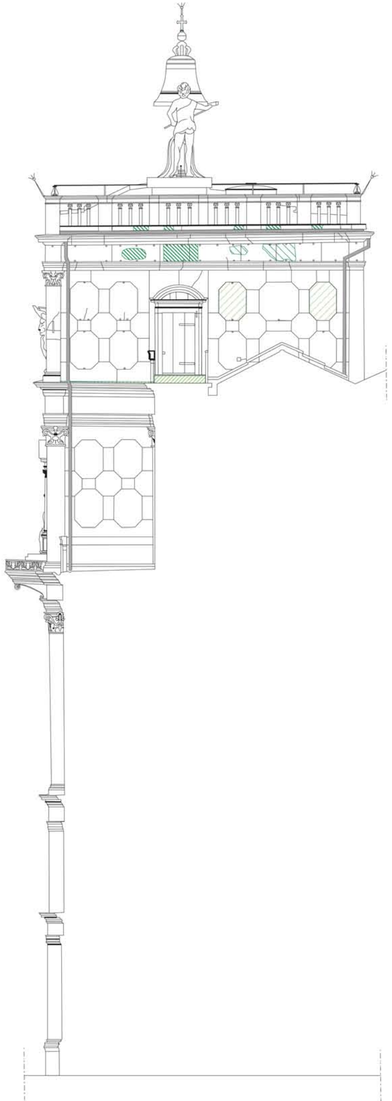

b)

## SOUTH FAÇADE

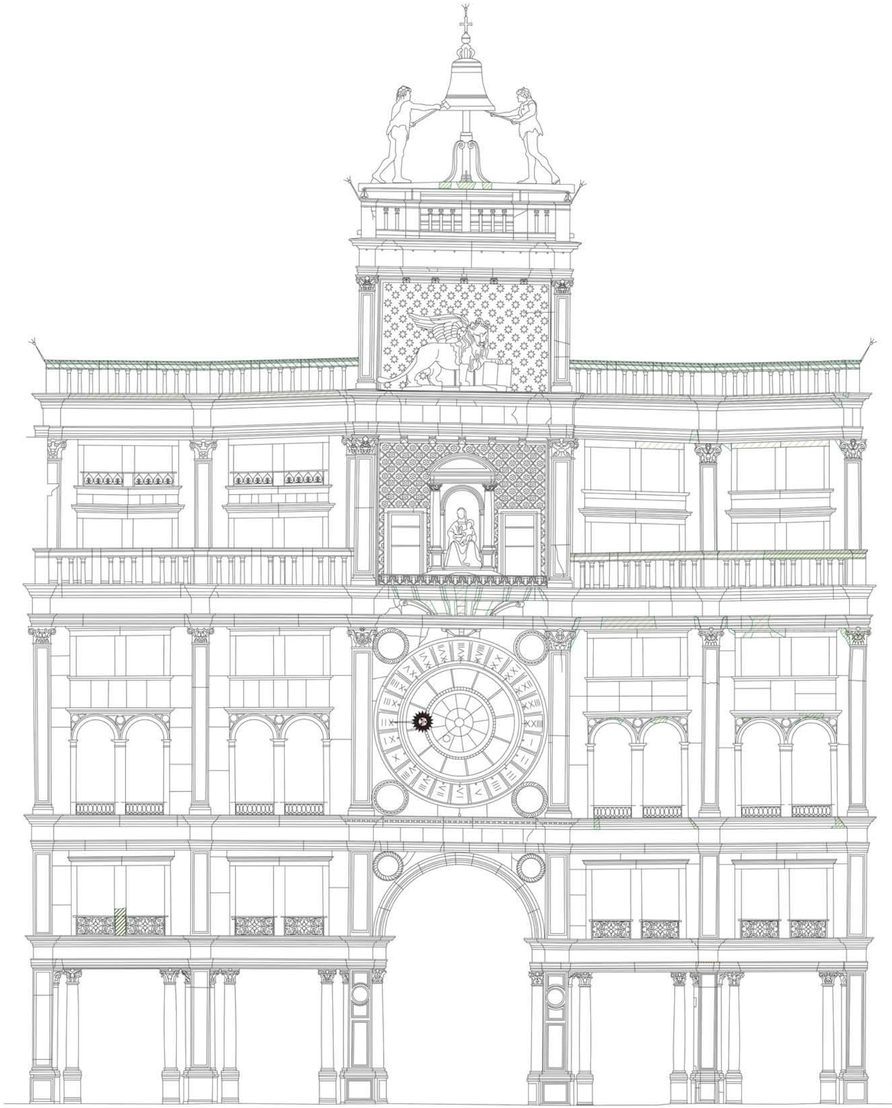

a)

## WEST FAÇADE

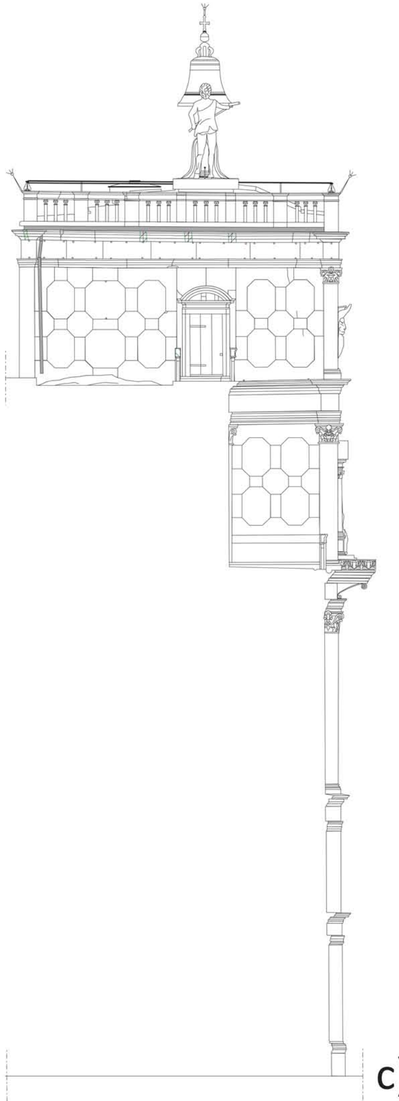

c)

## EAST FAÇADE

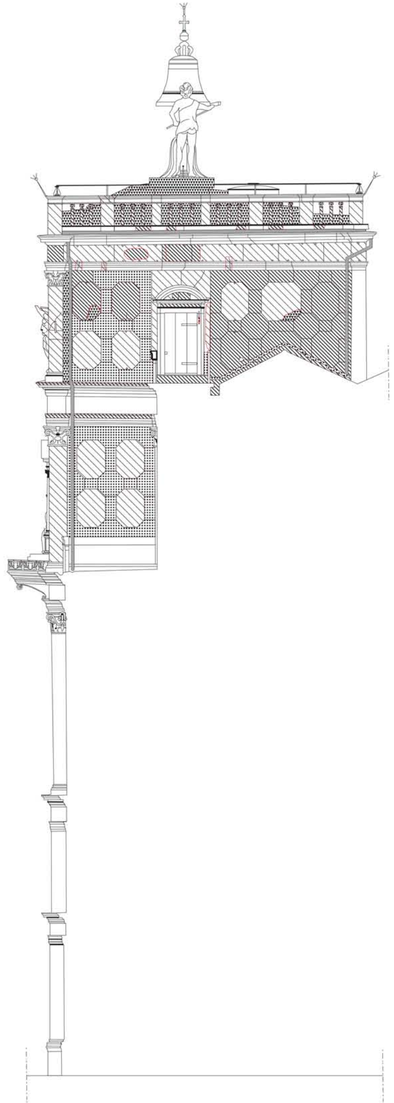

b)

## SOUTH FAÇADE

a)

## WEST FAÇADE

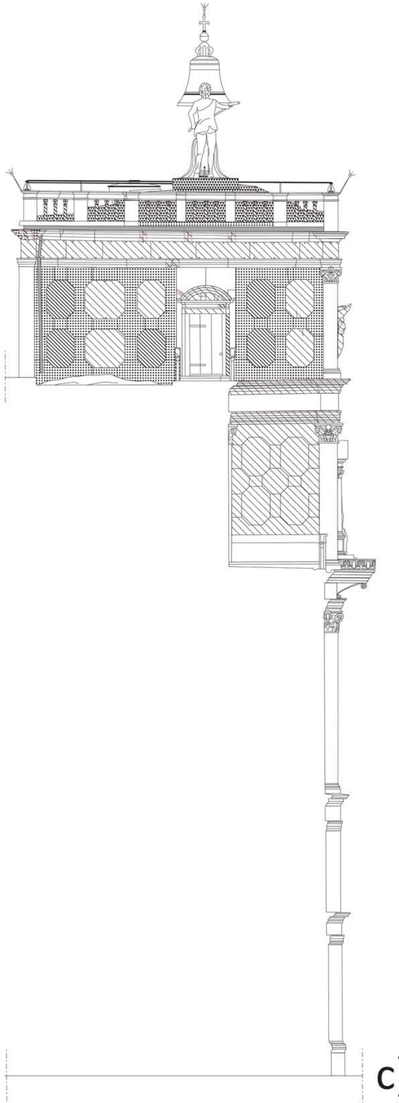

c)

**Total Decay Index (TDI) Legend:**

- Alveolization intesity 1 very slight (pag. 28)
- Alveolization intesity 2 slight (pag. 28)
- Alveolization intesity 3 moderate (pag. 28)
- Alveolization intesity 4 severe (pag. 28)
- Alveolization intesity 5 very severe (pag. 28)

# Nailac Pier

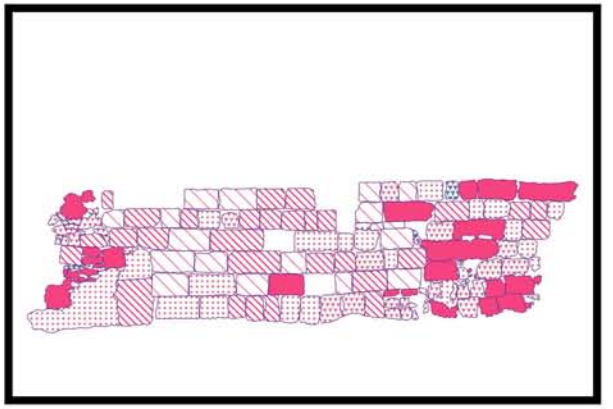

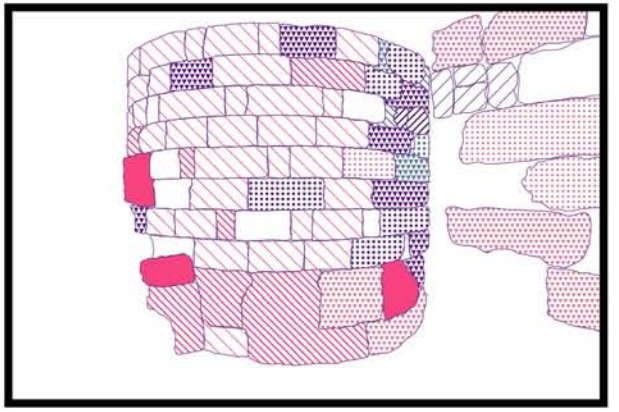

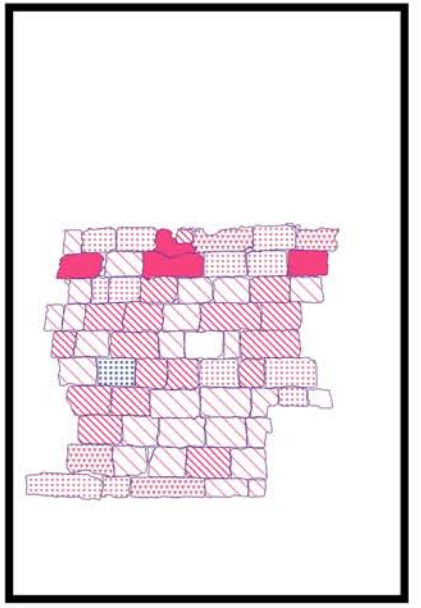

**Legend Material Loss:**

- Alveolization intesity 1 very slight (pag. 28)
- Alveolization intesity 2 slight (pag. 28)
- Alveolization intesity 3 moderate (pag. 28)
- Alveolization intesity 4 severe (pag. 28)
- Alveolization intesity 5 very severe (pag. 28)
- Erosion intesity 1 very slight (pag. 30)
- Erosion intesity 2 slight (pag. 30)
- Erosion intesity 3 moderate (pag. 30)
- Erosion intesity 4 severe (pag. 30)
- Erosion intesity 5 very severe (pag. 30)
- Mechanical damage intesity 1 very slight (pag. 32)
- Mechanical damage intesity 2 slight (pag. 32)
- Mechanical damage intesity 3 moderate (pag. 32)
- Mechanical damage intesity 4 severe (pag. 32)
- Mechanical damage intesity 5 very severe (pag. 32)
- Microkarst intesity 1 very slight (pag. 34)
- Microkarst intesity 2 slight (pag. 34)
- Microkarst intesity 3 moderate (pag. 34)
- Microkarst intesity 4 severe (pag. 34)
- Microkarst intesity 5 very severe (pag. 34)
- Missing part intesity 1 very slight (pag. 36)
- Missing part intesity 2 slight (pag. 36)
- Missing part intesity 3 moderate (pag. 36)
- Missing part intesity 4 severe (pag. 36)
- Missing part intesity 5 very severe (pag. 36)

# Saint Nikolas lighthouse

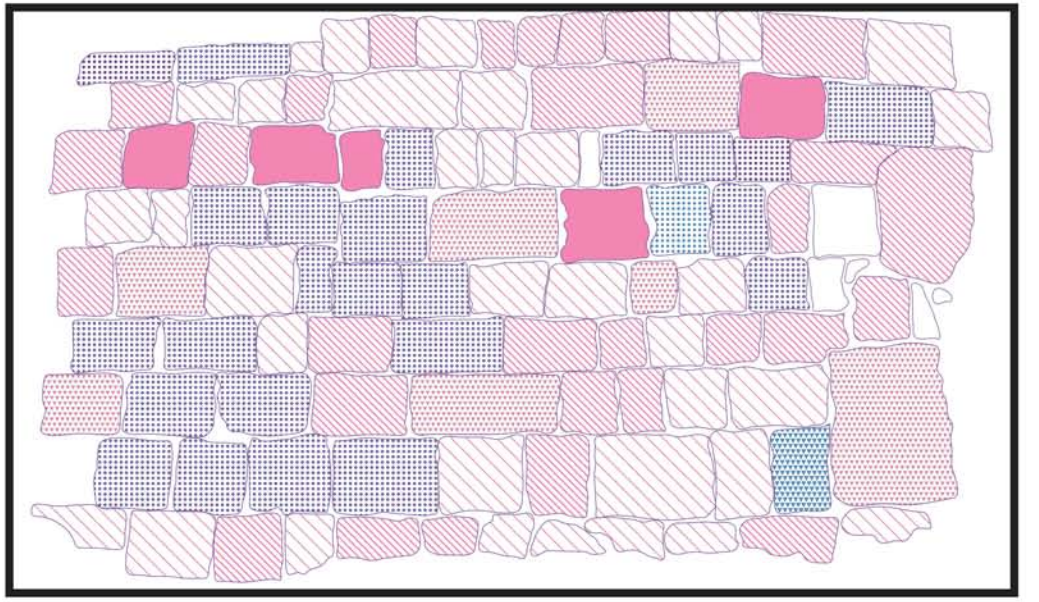

**Legend Material Loss:**

- Alveolization intesity 1 very slight (pag. 28)
- Alveolization intesity 2 slight (pag. 28)
- Alveolization intesity 3 moderate (pag. 28)
- Alveolization intesity 4 severe (pag. 28)
- Alveolization intesity 5 very severe (pag. 28)
- Erosion intesity 1 very slight (pag. 30)
- Erosion intesity 2 slight (pag. 30)
- Erosion intesity 3 moderate (pag. 30)
- Erosion intesity 4 severe (pag. 30)
- Erosion intesity 5 very severe (pag. 30)
- Mechanical damage intesity 1 very slight (pag. 32)
- Mechanical damage intesity 2 slight (pag. 32)
- Mechanical damage intesity 3 moderate (pag. 32)
- Mechanical damage intesity 4 severe (pag. 32)
- Mechanical damage intesity 5 very severe (pag. 32)
- Microkarst intesity 1 very slight (pag. 34)
- Microkarst intesity 2 slight (pag. 34)
- Microkarst intesity 3 moderate (pag. 34)
- Microkarst intesity 4 severe (pag. 34)
- Microkarst intesity 5 very severe (pag. 34)
- Missing part intesity 1 very slight (pag. 36)
- Missing part intesity 2 slight (pag. 36)
- Missing part intesity 3 moderate (pag. 36)
- Missing part intesity 4 severe (pag. 36)
- Missing part intesity 5 very severe (pag. 36)